THE INTERACTIONS BETWEEN COMPATIBILISER ACTIVITY UNDER MELT PROCESSING CONDITIONS AND THE MORPHOLOGY AND MECHANICAL PROPERTIES OF POLYAMIDE 6/POLYPROPYLENE BLENDS

ADISAKDI CHATATHANOM

A THESIS SUBMITTED IN PARTIAL FULFILLMENT
OF THE REQUIREMENTS FOR
THE DEGREE OF MASTER OF SCIENCE
(POLYMER SCIENCE)
FACULTY OF GRADUATE STUDIES
MAHIDOL UNIVERSITY

2000

ISBN 974-665-032-7

Thesis
entitled

THE INTERACTIONS BETWEEN COMPATIBILISER ACTIVITY UNDER MELT PROCESSING CONDITIONS AND THE MORPHOLOGY AND MECHANICAL PROPERTIES OF POLYAMIDE 6/POLYPROPYLENE BLENDS

.....A. Chatathanom.....
Mr.Adisakdi Chatathanom
Candidate

.....
Asst.Prof.Richard A Venables, Ph.D.
Major-advisor

.....
Asst.Prof.Krisda Suchiva, Ph.D.
Co-advisor

.....A. Tabtiang.....
Asst.Prof.Arunee Tabtiang, Ph.D.
Co-advisor

.....
Prof.Liangchai Limlomwongse,
Ph.D.
Dean
Faculty of Graduate Studies

.....
Asst.Prof.Krisda Suchiva,
Ph.D.
Chairman
Master of Science Programme
in Polymer Science
Faculty of Science

Thesis
entitled

THE INTERACTIONS BETWEEN COMPATIBILISER ACTIVITY UNDER MELT PROCESSING CONDITIONS AND THE MORPHOLOGY AND MECHANICAL PROPERTIES OF POLYAMIDE 6/POLYPROPYLENE BLENDS

was submitted to the Faculty of Graduate Studies, Mahidol University
for the degree of Master of Science (Polymer Science)
on
November 6, 2000

A. Chatathanom
.....
Mr.Adisakdi Chatathanom
Candidate

.....
Asst.Prof.Richard A Venables, Ph.D.
Chairman

.....
Asst.Prof.Krisda Suchiva, Ph.D.
Member

Pongdhorn Saeoui
.....
Dr. Pongdhorn Sae-Oui, Ph.D.
Member

A. Tabtiang
.....
Asst.Prof.Arunee Tabtiang, Ph.D.
Member

.....
Prof.Liangchai Limlomwongse,
Ph.D.
Dean
Faculty of Graduate Studies
Mahidol University

.....
Prof.Amaret Bhumiratana,
Ph.D.
Dean
Faculty of Science
Mahidol University

ACKNOWLEDGEMENTS

The deepest appreciation of the author is expressed to many people who tried very hard to make the publication of this thesis possible to meet the deadline. Before all, I would so much like to give the sincere gratitude to Dr. Richard A Venables whose worthy advice, patience, and understanding were demonstrated throughout the process of correction and bringing the thesis into print. In comparable, the sincere gratitude also goes to Dr. Krisda Suchiva, Dr. Arunee Tabtaing, and Dr. Pongdhorn Sae-Oui for their editorial work, comments and interest on the process to complete this thesis. Grateful acknowledges are heartily given to Faculty of Graduate studies and Faculty of Science, Mahidol University for the financial support and the partial scholarship during the study.

A special word of thanks goes as well to the National Metal and Materials Technology Center (MTEC), and the electron microscopy and cell biology laboratory, Mahidol University, for the assistance with TGA facility and SEM observations, respectively. For the lecturers, friends, and teammates in my football club, I am also greatly indebted many thanks for their helpful suggestion, care, and laughter.

This thesis is lovingly delicated to my parents both of whom hugged me tight and means the most to me. Nothing could compare to what they have done for me so far. I just want one thing. To live long enough to pay back in some way they undeserved and overwhelming generosity.

Adisakdi Chatathanom

4036462 SCPO/M : MAJOR: POLYMER SCIENCE; M.Sc. (POLYMER SCIENCE)
KEY WORDS : POLYAMIDE 6/ POLYPROPYLENE/ MORPHOLOGY/ INDEPENDENT VARIABLES/ POLYMER BLENDS

ADISAKDI CHATATHANOM: THE INTERACTIONS BETWEEN COMPATIBILISER ACTIVITY UNDER MELT PROCESSING CONDITIONS AND THE MORPHOLOGY AND MECHANICAL PROPERTIES OF POLYAMIDE 6/POLYPROPYLENE BLENDS. THESIS ADVISERS: RICHARD A VENABLES, Ph.D., KRISDA SUCHIVA, Ph.D., ARUNEE TABTIANG, Ph.D., 147 p. ISBN 974-665-032-7

In this study, the activity of an *in-situ* formed block copolymer in a polyamide 6/polypropylene (PA6/PP) blend was investigated under melt processing conditions through the use of a factorial screening experiment. The independent variables selected were twin screw extruder screw configuration, screw speed, and compatibiliser concentration. The level of dispersion of the minor component in the blend and the dispersion stability were quantified through analysis of extruded and injection moulded specimens. It was found that for compatibiliser contents greater than 2.4 vol% and average stresses during compounding above 100 MPa that the ratio of the specific interfacial area between the PA6 and PP phases reached a constant value of around 90 μm^{-1}. This value corresponded to an average interfacial thickness of 11 nm.

The radius of gyration of the PP block in the *in-situ* formed PP-block-PA6 was estimated to be 12.9 nm, and hence was of comparable size to the interfacial thickness. It was inferred that the mixing was principally controlled by the quantity of *in-situ* formed PP-block-PA6 at the higher mixing stresses. During injection moulding a plasticisation energy of 7.5 MJm^{-3} at a channel shear rate of 52 s^{-1} was used; the nozzle shear rate was around 6,500 s^{-1}. Under these conditions, it was found that the largest domains produced during extrusion underwent the greatest change during injection moudling. For the highest compatibiliser content employed; i.e., 3.8 vol%, at average extrusion stresses greater than 100 MPa, the domain morphology was largely stable under the injection moulding conditions.

4036462 SCPO/M : สาขาวิชา: วิทยาศาสตร์พอลิเมอร์; วท.ม. (วิทยาศาสตร์พอลิเมอร์)

อดิศักดิ์ ชตาถนอม: การศึกษาความสัมพันธ์ระหว่างความสำคัญของสารช่วยผสมภายใต้สภาวะการผสมแบบหลอมเหลวกับโครงสร้างสัณฐาน และ คุณสมบัติเชิงกลของพอลิเมอร์ผสมพอลิเอไมด์6 และพอลิพรอพิลีน (THE INTERACTIONS BETWEEN COMPATIBILISER ACTIVITY UNDER MELT PROCESSING CONDITIONS AND THE MORPHOLOGY AND MECHANICAL PROPERTIES OF POLYAMIDE6/POLYPROPYLENE BLENDS). คณะกรรมการควบคุมวิทยานิพนธ์: Richard A. Venables, Ph.D., กฤษฎา สุชีวะ, Ph.D., อรุณี ทับเที่ยง, Ph.D. 147 หน้า. ISBN 974-665-032-7

งานวิจัยนี้เป็นการศึกษาความสำคัญของบล็อคโคพอลิเมอร์ที่เกิดขึ้นในกระบวนการผสมแบบหลอมเหลวของพอลิเมอร์ผสมพอลิเอไมด์และพอลิพรอพิลีน โดยวิธีการทดลองแบบแฟคทอเรียลสกรีนนิ่ง (factorial screening experiment) ค่าตัวแปรอิสระที่เลือกศึกษาในครั้งนี้ประกอบด้วย แบบของการจัดเรียงเกลียวหนอนคู่ในเครื่องอัดรีด, ความเร็วรอบของเกลียวหนอนคู่และความเข้มข้นของสารช่วยผสม วิธีการที่ใช้ศึกษาระดับการกระจายตัวของส่วนประกอบรอง (minor component) ในพอลิเมอร์ผสม คือการวิเคราะห์ตัวอย่างที่ผ่านการอัดรีดและตัวอย่างที่ผ่านการฉีดขึ้นรูป จากการวิเคราะห์พบว่าความเข้มข้นของสารช่วยผสมปริมาณมากกว่า 2.4 เปอร์เซนต์โดยปริมาตร ที่ค่าความเค้นเฉลี่ยขณะผสมมากกว่า 100 MPa ค่าอัตราส่วนของพื้นที่ผิวประจันจำเพาะ (specific interfacial area) ระหว่างวัฏภาคพอลิเอไมด์และพอลิพรอพิลีนมีค่าคงที่ประมาณ 90 μm^{-1} และค่าความหนาของผิวประจันโดยเฉลี่ยเท่ากับ 11 nm.

ค่ารัศมีไจเรชั่น (radius of gyration) ของพอลิเมอร์ส่วนที่เป็นพอลิพรอพิลีนใน พอลิพรอพิลีน-บล็อก-พอลิเอไมด์โคพอลิเมอร์ที่เกิดขึ้น มีค่าเท่ากับ 12.9 nm ซึ่งมีขนาดอยู่ในช่วงความหนาของพื้นที่ผิวประจัน ที่ค่าความเค้นสูงๆ พบว่าชนิดการผสมที่ใช้เตรียมพอลิเมอร์ผสม จะควบคุมปริมาณของบล็อคโคพอลิเมอร์ที่เกิดขึ้น เครื่องฉีดขึ้นรูปที่มีค่าพลังงานการหลอมเหลว (plasticisation energy) เท่ากับ 7.5 MJm^{-3} ที่ค่าอัตราเฉือนในช่องเท่ากับ 52 s^{-1} และค่าอัตราการเฉือนที่น็อซเซิล (nozzle) มีค่าประมาณ 6500 s^{-1} พบว่าภายในสภาวะการผสมเช่นนี้ ขนาดของวัฏภาคกระจายที่มีขนาดใหญ่ที่เกิดขึ้นขณะผ่านการอัดรีด จะมีการเปลี่ยนแปลงขนาดอย่างมากขณะที่ผ่านเครื่องฉีดขึ้นรูป สารตัวอย่างที่เติมสารช่วยผสมที่มีปริมาณสูงสุดที่ใช้ในงานวิจัยครั้งนี้ กล่าวคือมีค่า 3.8 เปอร์เซนต์โดยปริมาตร ที่ค่าความเค้นเฉลี่ยระหว่างอัดรีดมากกว่า 100 MPa ขนาดของวัฏภาคกระจายในตัวอย่างดังกล่าวมีความเสถียรมาก ภายใต้สภาวะของเครื่องฉีดขึ้นรูปตามที่กล่าวมา

CONTENTS

CONTENTS (cont.)

CONTENTS (cont.)

CONTENTS (cont.)

CONTENTS (cont.)

CONTENTS (cont.)

LIST OF TABLES

LIST OF TABLES (cont.)

LIST OF TABLES (cont.)

LIST OF FIGURES

LIST OF FIGURES (cont.)

LIST OF FIGURES (cont.)

LIST OF FIGURES (cont.)

LIST OF FIGURES (cont.)

LIST OF FIGURES (cont.)

LIST OF FIGURES (cont.)

LIST OF ABBREVIATIONS

ABS	=	Poly(acrylonitrile-*co*-butadiene-*co*-styrene)
AN	=	Acrylonitrile
BP	=	Benzoyl peroxide
C	=	Compatibiliser content
CMC	=	Critical micelles concentration
DDRM	=	Deformed drop-retraction method
DSC	=	Differential scanning calorimetry
EMA	=	Poly(ethylene-*co*-methyl acrylate)
EPR	=	Poly(ethylene-*co*-propylene) rubber
FTIR	=	Fourier transform infrared spectroscopy
HAC	=	High anhydride content
HIPS	=	High impact polystyrene
LAC	=	Low anhydride content
LCPs	=	Liquid crystalline polymers
LDPE-g-MAH	=	Maleic anhydride grafted low-density polyethylene
LDPE-g-PA6	=	Polyamide-6 grafted low-density polyethylene
LLDPE	=	Linear low-density polyethylene
MWD	=	Molecular weight distribution
N	=	Extruder screw speed

LIST OF ABBREVIATIONS (cont.)

N(mould)	=	Injection moulder screw speed
PA(s)	=	Polyamide(s)
PA6	=	Polyamide6
PA12	=	Polyamide12
Par	=	Polyarylate
PBT	=	Poly(butylene terephthalate)
PC	=	Polycarbonate
PC-LLDPE	=	Post-consumer linear low-density polyethylene
PC-HDPE	=	Post-consumer high-density polyethylene
PE	=	Polyethylene
PEI	=	Poly(ether imide)
PEST(s)	=	Polyester(s)
PET	=	Poly(ethylene terephthalate)
P(HB-b-I-S)	=	Hydrogenated poly(butadiene-*b*-isoprene-*b*-styrene)
PO	=	Polyolefin
POE	=	Polyolefin elastomer
POM	=	Polyoxymethylene
POP	=	Polyolefin plastomer
PP	=	Polypropylene
PPE	=	Polyphenylenether
PP-g-GMA	=	Glycidyl methacrylic grafted polypropylene

LIST OF ABBREVIATIONS (cont.)

PP-g-MAH	=	Maleic anhydride grafted polypropylene
PP-HBP	=	Hyperbranched polymers grafted Polypropylene
PPO	=	Poly(phenylene oxide)
P(S-b-BMA)	=	Poly(styrene-*b*-butyl methacrylate)
P(S-b-MMA)	=	Poly(styrene-*b*-methyl methacrylate)
PSMA	=	Poly(styrene-*co*-maleic anhydride)
PS-OX	=	Polystyrene with oxazoline groups
PVC	=	Poly(vinyl chloride)
S	=	Extruder screw configuration
SAN	=	Poly(styrene-*co*-acrylonitrile)
SB	=	Poly(styrene-*co*-butadiene)
SEM	=	Scanning electron microscopy
SEBS	=	Poly(styrene-*co*-ethylene-*co*-butene-*co*-styrene)tri block copolymer
SIS	=	Poly(styrene-*co*-isoprene-*co*-styrene)tri block copolymer
SME	=	Specific mechanical energy
SSE	=	Single screw extrusion
TEM	=	Transmission electron microscopy
TWE	=	Twin screw extrusion

CHAPTER I

INTRODUCTION

1.1 General introduction and literature review

Polymer blends are mixtures of at least two macromolecules. For the practical reasons, the name blend is given to a system only when the minor component content exceeds 2 wt% [1]. The polymer/polymer miscibility is always limited to a range of independent variables, such as composition, molecular weight, temperature, pressure, etc. [1] Most polymer blends are either partially miscible or immiscible, because of their small combinatorial entropy of mixing and the mostly positive enthalpy of mixing [2]. Morphology of immiscible blends depends heavily on, for example, constituents of polymer blends [3], the interfacial tension [4], the viscosity ratio [4,5], the time of mixing, and mixing temperature [6]. At high dilutions and low flow rates the morphology of polymer blends is controlled by the three micro-rheological dimensionless parameters [1]: (I) the viscosity ratio, $\eta_r = \frac{\eta_1}{\eta_2}$, where η_1 is the viscosity of the dispersed liquid and η_2 is that of matrix; (II) the capillary number, $\kappa = \frac{\sigma_{12}}{\nu_{12}} d$ where σ_{12}, d, and ν_{12} are respectively the shear stress, the initial drop diameter, and the interfacial tension coefficient; and (III) the reduced time, $t^* = \frac{t\dot{\gamma}}{\kappa}$, where $\dot{\gamma}$ is the deformation rate, and t is its duration. Thus, for binary systems the

interfacial and rheological properties are the keys for the morphology development in polymer blends, thus to their performance.

To obtain high performance of immiscible blends, usually compatibiliser needs to be added. It is widely known that there are at least three aspects of compatibilisation [7-8]:

(1) Reduction of the interfacial tension, which facilitates dispersion;
(2) Stabilisation of the morphology against changes during the following processing steps; and
(3) Enhancement of adhesion between the phases, facilitating the stress transfer, hence improving the mechanical properties of the product.

Two basic strategies of compatibilisation are being used: (I) addition of a copolymer compatibiliser [9-11], and (II) reactive compatibilisation [12-13]. Within the first category one may distinguish addition of a small quantity (0.5 to 2 wt%) of well-tailored copolymer, and that of a large quantity (up to 35 wt%) of a multicomponent ingredient [1]. Usually, the first copolymer is specifically designed to have one part miscible with polymeric phase and the other with the other. Furthermore, to ascertain stabilisation effects on the generated morphology, the central part of copolymer is usually a random copolymer that creates a thicker interphase for better protection of the dispersed phase from coalescing [9,11].

The second type of additive is usually a general-purpose compatibiliser and impact modifier. Most often, this is either a core-shell [14] or multilayered copolymer containing reactive groups attached to either an elastomeric or rigid part [12-13].

These materials are commonly based on acrylics and vinyls [1,13-14], thus in blend with an engineering and specialty resin they may not have adequate thermal stability. The reactive compatibilisation is designed to *in-situ* generate the desired quantity of either block or graft copolymer, that forms chemical bonds across the interface.

It is to be expected that different compatibilisation strategies generate different morphologies, hence different sets of physical properties. For example, addition of block copolymer may decrease the interfacial tension and the growth of the phase domains on thermal annealing in the melt [10]. Addition of a core-shell copolymer compatibilises and toughens the blends [14].

Processing parameters are found to play a remarkable role on the morphology development of polymer blends, which ultimately result in their final properties. It is found that the morphological development under mixing was reported to take place at a very short of time [6]. The additional processing time had little effect on morphological change [6,15]. The evolution of morphology is a process involving the competition between drop breakup and coalescence for both non-reactive and reactive blends [16-17].

Some of the same factors that are intuitively believed to increase the efficiency of mixing in polymer blends could have the opposite effect on reactively compatibilised systems where the dispersed phase is more finely dispersed. More intensive mixing can lead to coalescence of the dispersed phase particles to form significantly larger domains [17].

Wu [4] investigated blends of Nylon and poly(ethylene terephtalate) with poly (ethylene-*co*-propylene-*co*-diene monomer) processed by twin screw extrusion with the constancy of average shear rate and dispersed phase volume percent. It was found

that the deformation and breakup of droplets during mixing could be enhanced by small interfacial tension, large shear rate, and high matrix viscosity. Moreover, for the same processing conditions and composition, the minimum size could be reached when the components viscosity ratio was unity [4].

In order to achieve an acceptable levels of dispersion, Valsamis and Canedo [18] used a *polygon-type configured screws*, see Figure 1.1, in a twin screw extruder. These elements provided higher throughput rates and were less susceptible to wear than the conventional kneading-block technology.

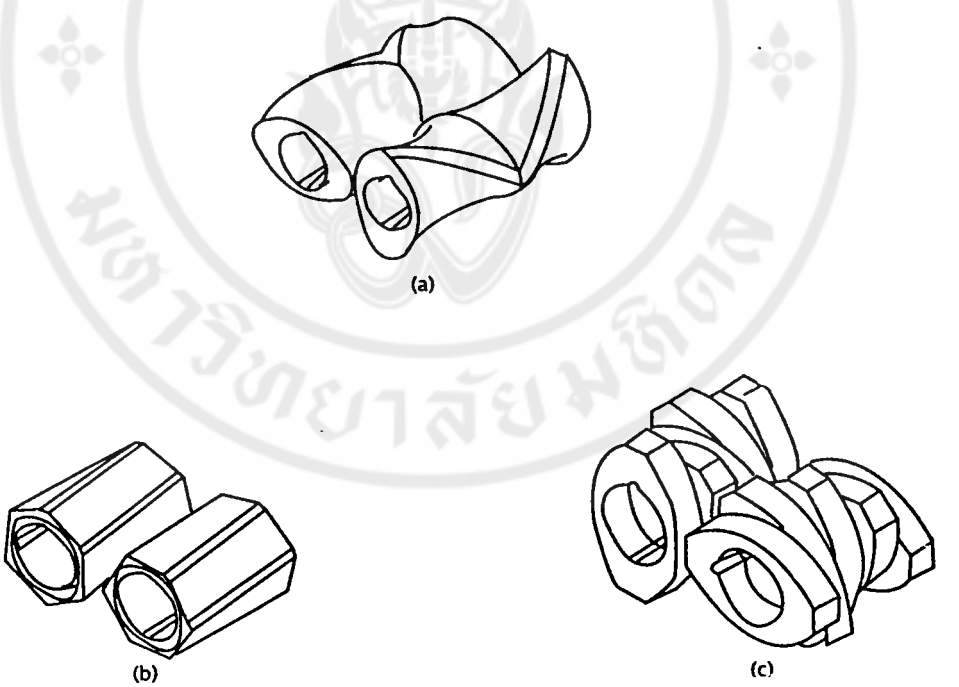

Figure 1.1 Intensive mixing technologies used: (a) continuous mixing elements; (b) polygon-type elements; and (c) conventional kneading blocks (adapted from Valsamis and Canedo [18])

1.2 Basic principles

The attempts to quantify drop breakup and coalescence in multiphase fluid systems can be traced back to the first half of this century and have been pursued by numerous efforts over the last three decades to understand the factors that control morphology in multifluid systems. Most of the initial works dealt with simple Newtonian systems. Over the last two decades viscoelastic systems have come to the forefront of the research activity owing to wide spread interest in the control of morphology in multi phase polymer systems as a means to manipulate the properties of these materials [17].

1.2.1 Newtonian drop breakup

In 1932, Taylor [5,17,19] first published his work on the breakup of the single Newtonian drop in a simple shear field. He modeled drop size using viscosity ratio, $\eta_r = \eta_d / \eta_m$, and capillary number, Ca:

$$\text{Ca} = \frac{\dot{\gamma}\eta_m D}{2\Gamma}, \qquad (1.1)$$

where $\dot{\gamma}$ is the shear rate, η_m is the matrix phase viscosity, η_d is the disperse phase viscosity, D is the diameter of the drop, and Γ is the interfacial tension. For simple shear flow, Taylor balanced the interfacial forces and the shear flow forces and obtained a relation for the maximum drop size that would be stable:

$$D = \frac{4\Gamma(\eta_r + 1)}{\dot{\gamma}\eta_m(\frac{19}{4}\eta_r + 4)} \quad ;\eta_r < 2.5 \qquad (1.2)$$

This relation is valid for small deformations in Newtonian fluids. Taylor predicted that no drop breakup occurs when $\eta_r < 2.5$. Serpe *et al.* [16] reported that in simple shear experiments there is a critical value of Weber number below which particle deformation will no longer occur, and therefore there is a critical particle size determined by the rheological effects.

For extensional flow, both experiments and theory indicate that the critical capillary number, which can be thought of as an effective shear rate, is lower than that in the case of simple shear flow. The flow in mixers used for polymer blending is a mixture of simple shear flow and extensional flow. Thus, the critical capillary number for simple shear flow would predict the upper limit of drop size for break up in a dilute Newtonian system [19].

There has been a monumental work performed on breakup of Newtonian drops in both simple shear flow and extensional flow. These results are illustrated in Figure 1.2. As can be seen, the breakup is possible in pure extensional flow at all viscosity ratios but is impossible in simple shear flow above $\eta_r = 4$.

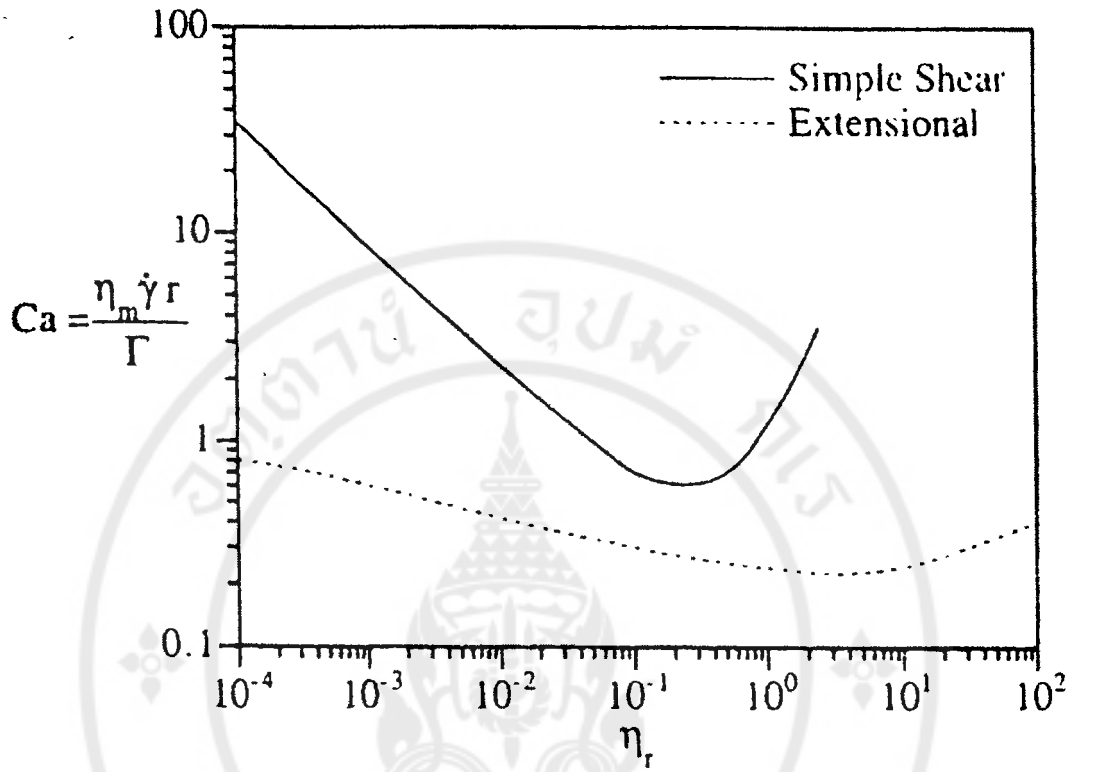

Figure 1.2 Plot for Newtonian drop breakup. The experiments show that planar extensional flow is more effective at breaking drops than simple shear flow (adapted from Sundararaj and Macosko [19])

1.2.2 Drop breakup in polymer blends

The effect of viscosity ratio on drop size in melt blends has been investigated. Wu [4] has expressed a correlation between droplet size, capillary number, and viscosity ratio in extruded polymer blends. A relation for the final particle diameter was given as:

$$D = \frac{4\Gamma \eta_r^{\pm 0.84}}{\dot{\gamma} \eta_m} \qquad (1.3)$$

Where the plus (+) sign in the exponent applies for $\eta_r > 1$ and the minus (-) sign in the exponent applies for $\eta_r < 1$. In all blends used for the correlation, the dispersed phase concentration was 15 wt% and the effective shear rate was arbitrarily chosen as 100 s^{-1}. This relation obviously is not appropriate to the Taylor limit or to work on breakup of a single drop in a matrix.

Favis and Chalifoux [5] have summarised their conclusions that the viscosity ratio (λ) has a marked effect on the morphology of the dispersed phase with the phase size increasing by a factor of 3 to 4 times from λ = 4.5 to λ = 17.3. The minimum dispersed phase size can be achieved at λ = 0.15. This indicated that the deformation of the dispersed phase becomes difficult at the upper and lower limits of λ. This was shown to be similar in some respects to the behaviour of Newtonian fluids in shear flow.

1.2.3 Newtonian coalescence

The most frequently published depiction concerning the coalescence in binary Newtonian liquid mixtures is shown schematically in Figure 1.3 [6,19-20]. It was found that the contact time required for drop coalescence increases when the drop diameter increases, the matrix viscosity increases, and the density difference between the drop and matrix phases increases. Flow-induced coalescence of two Newtonian liquid drops can be modeled as a three-step mechanism as shown in Figure 1.3.

First of all, two drops come close to each other and the pair rotates in the shear field. The film of the matrix phase between the two drops drains, thus the film thickness decreases to the critical value, and rupture of the interface occurs, resulting in coalescence. Unlike gravity-induced coalescence, where the drops have time to

equilibrate, contact times in shearing flow are even smaller. The film can, therefore, drain quite quickly for a drop pair to coalesce.

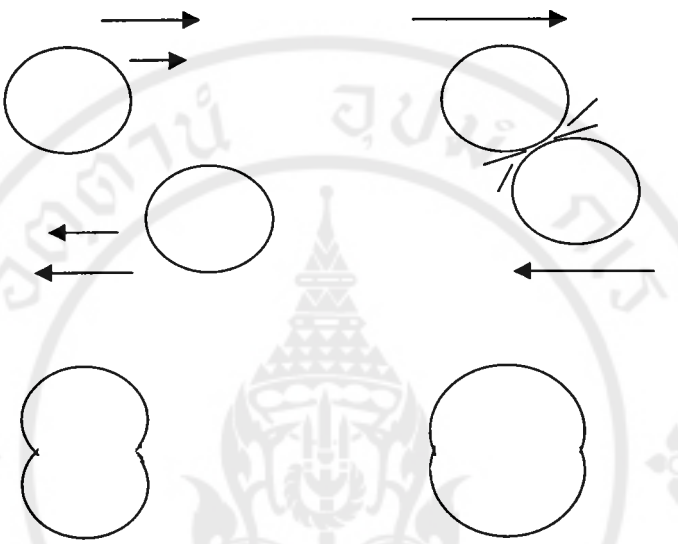

Figure 1.3 Idealised depiction of shear-induced coalescence of dispersed Newtonian droplets. The shear field brings the drops close to each other and then the matrix film between the drops thins until the interface ruptures and coalescence occurs (adapted from refs 6,19-20)

1.2.4 Coalescence in polymer blends

Most coalescence studies in polymer blends have not often used mechanical mixing because of its difficulty to sample [19]. However, it is currently found that a state-of-art mechanical mixer can offer the sampling points along its length, which makes this task easier [17]. Instead, studies have relied frequently on solvent-cast blends [11] or, melts blends [15,21] under quiescent conditions. Coalescence after mixing plays a crucial role since manufactured polymer products are annealed and

coalescence is believed to take place during annealing. Coalescence in molten polymer blends without the influence of mechanical stress has previously been modeled by Fortenlý and Kovář, then recently by Sundararaj and Macosko [19]. They found that the amount of coalescence in blends decreases significantly if the matrix phase viscosity is above a critical value and if the dispersed phase volume fraction is below a critical value. For a typical dispersed particle size encountered in polymer blends of about 1 μm at 0.25 dispersed phase volume fraction, the model predicts that very little coalescence will occur above a critical maximum matrix viscosity of 496 Pa s. However, Sundararaj and Macosko [19] found significant coalescence within 10 minutes in an uncompatibilised polymer blend with a lower dispersed volume fraction of about 0.2 and a much higher matrix phase viscosity of 9500 Pa s. The result is shown in Figure 1.4.

Sundararaj and Macosko [19] also demonstrated the power of using interfacial reaction to stabilize morphology during processing. The particle size at 20 wt% for non-reactive PA6,6/PSMA systems were stable during processing throughout the concentration range studied, this was the case for both 1.5 wt% MAH functionality and 17 wt% MAH functionality. Thus, very little reaction is required to produce a significant effect on the morphology stabilisation.

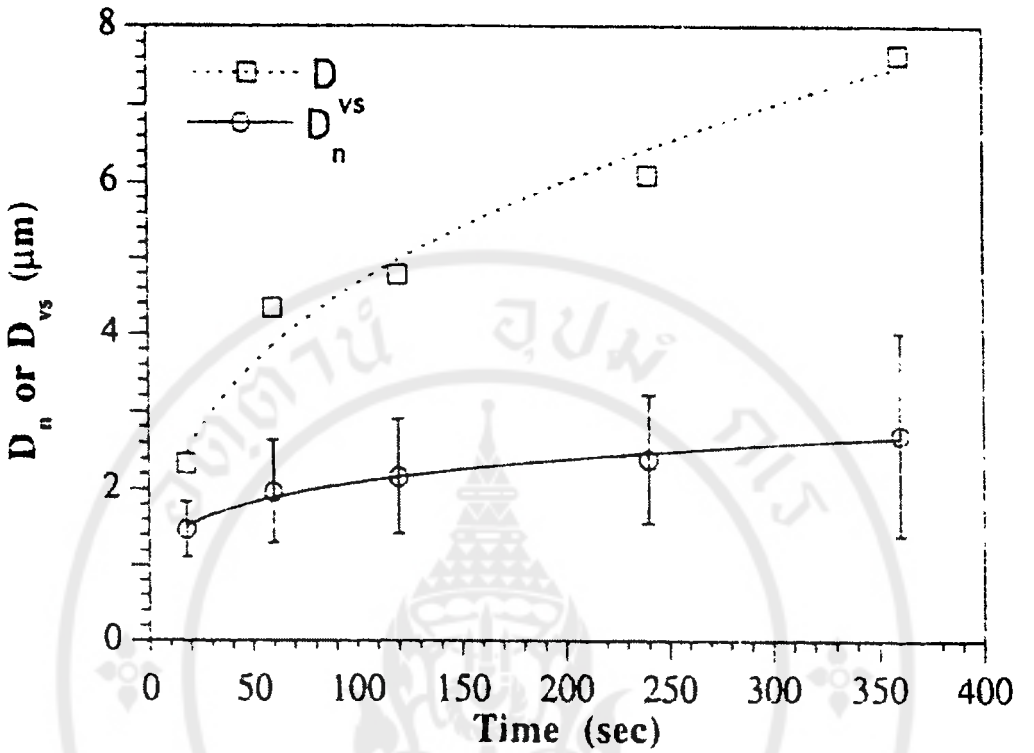

Figure 1.4 Quiescent coalescence in a polystyrene/polypropylene (80/20 wt%) system. The annealing temperature was 180 ^{0}C. The zero shear rate viscosities were: $\eta_{m,0}$ = 9500 Pa·s, $\eta_{d,0}$ = 6000 Pa·s. D_n is the number-average diameter, and D_{vs} is the volume-to-surface average diameter (taken from [19])

Angola *et al.* [22] showed that at 15 wt% functionality, a minimum particle size (< 1 μm) was achieved for Nylon6/(SAN+SMA-15) blends through the *in-situ* formation of SMA-Nylon6 graft copolymer during mechanical mixing. Guégan *et al.* [23] also revealed that they could provide effective morphology stabilisation even for end-functional material where there is only a low level of block copolymer formed *in-situ*. They also included in the report that a dense block copolymer monolayer at the interface, estimated at 0.3 chain/nm^2, will completely cover the surface of each particle and it was found that only 0.1 chain/nm^2 was sufficient to prevent

coalescence. The reactive groups go to the interface and form sufficient copolymer so that even at high dispersed phase concentrations, the dispersed phase domains act like isolated droplets in an infinite medium. When surfactants are used in Newtonian emulsions, there is an increase in the energy required for coalescence partly due to steric interactions of adsorbed layers at the liquid-liquid interface. The stabilization against coalescence for compatibilised polymer blends is similar in nature and is depicted schematically in Figure 1.5 [19].

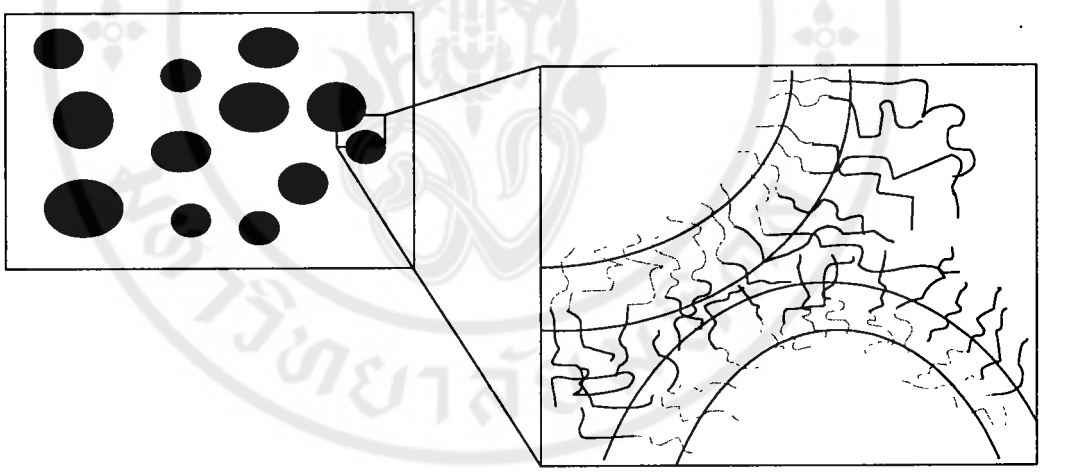

Figure 1.5 Suppression of coalescence. Two drops, which have a layer of di-block or graft copolymer at the interface, are less likely to coalesce since copolymer molecules form shells around the drops (adapted from Sundararaj and Macosko [19])

The interface consists of a layer (or layers) of copolymers. The block segment of the matrix phase polymer is located on the outside of the drop since it is incompatible with the drop. Therefore, one can imagine the dispersed phase drop with a shell of polymer, with an outside consisting of matrix phase block segments. When the matrix fluid tries to drain as the drops come together, the copolymers at the interface do not allow the dispersed phase in the two drops to meet and the drops recoil. In order for the two drops to meet, the copolymers must be moved out of the contact area. Since the interfacial viscosity increases upon adding a compatibiliser [2], it will be difficult to move the copolymers thus the coalescence is retarded. If there is enough copolymer at the interface, then it may form an interface which must be overcome for coalescence to occur. However, the interface does not necessarily need to be saturated with di-block or graft copolymer to be effective. It is only required that amount of copolymer, which will provide enough steric interactions to prevent droplets from coalescing.

1.3 Copolymer background

1.3.1 Interface in copolymers

Block copolymers are polymers constituted of at least two different monomers specifically polymerised such that they can be di-block, tri-block, multi-block, linear, star-shaped, etc. For compatibilisation studies, mainly di-block copolymers have been used.

In 1980, Leibler [24] created a system to study the microphase separation in block copolymers, the simplest system comprising a molten A-B di-block copolymer

was used. Since A blocks from different polymer molecules can aggregate with each other and, separately, B blocks from different polymer molecules can also aggregate with each other, therefore block copolymers tend to be phase separated [25]. As the blocks in each polymer molecule are chemically bonded together complete segregation cannot lead to a macroscopic phase separation as in mixtures of two homopolymers. Although in the case of a sufficiently strong incompatibility, microphase separation only occurs: micro domains rich in A, and domain rich in B are formed, instead of being macrophases.

In 1986, de la Cruz co-worked with Sanchez [26] to calculate phase stability criteria and a static structure factor of AB graft copolymers and additionally star copolymers with equal numbers of A and B arms. They offered the representation of four types of copolymer, as Figure 1.6 shows.

In addition, de la Cruz and his colleague [26] reported that the phase separation in copolymers could only occur on a microscopic level. The constraint that the A and B chains are chemically connected forces the phase separation to occur on size scales of the order of the radius of gyration (Rg) of the copolymer. Although each phase (one rich in A and the other rich in B) is disordered, the phases themselves are arranged in a periodic ordered structure (a meso phase). Three possible structures have been predicted so far: namely body-centered cubic, hexagonal, and lamellar.

The size of these micro-domains is controlled by the molecular weights of the blocks, the copolymer composition, and temperature. The ordered structure that is formed must be the one that minimises the free energy. Since the type of morphology depends on the concentration as well as on the transition temperatures of the

individual phases, the phase diagram of block copolymers shows comparable complexity to those of homopolymer mixtures or metallic alloys [1,26].

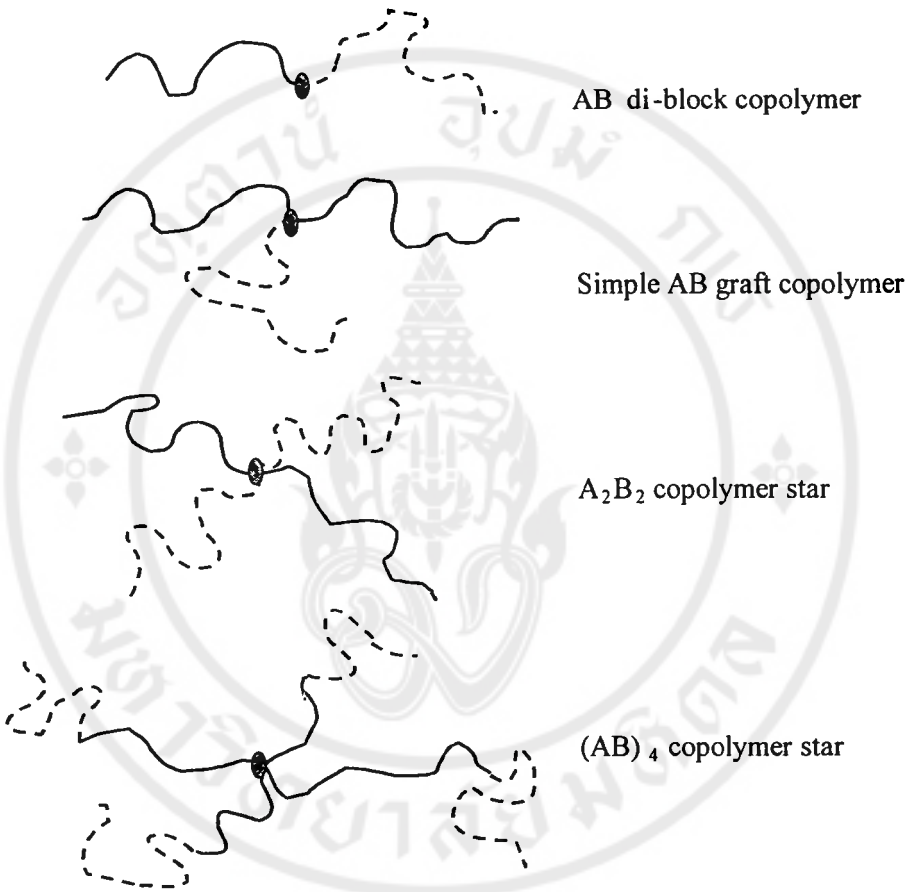

Figure 1.6 Schematic representation of four types of copolymer (adapted from de la Cruz and Sanchez [26])

The phase diagram of block copolymers is characterised by the presence of an upper critical solution temperature (UCST) [1], also well known as an order-disorder transition (ODT) [27], or perhaps called a microphase separation temperature (MST) [24]. Above UCST the copolymer's blocks form an isotropic melt, while below it they are phase separated. Upon further cooling the more rigid block turns either into glass

or a semicrystalline solid. Then, in order to avoid degradation or at least to minimise it, the block copolymers are usually processed within the micro-domain separated molten state; e.g., at T_g (rigid) < T < UCST. The copolymer should be in the ordered-separated state at the temperature employed [1,26]. The schematic presentation order-disordered transition is illustrated in Figure 1.7.

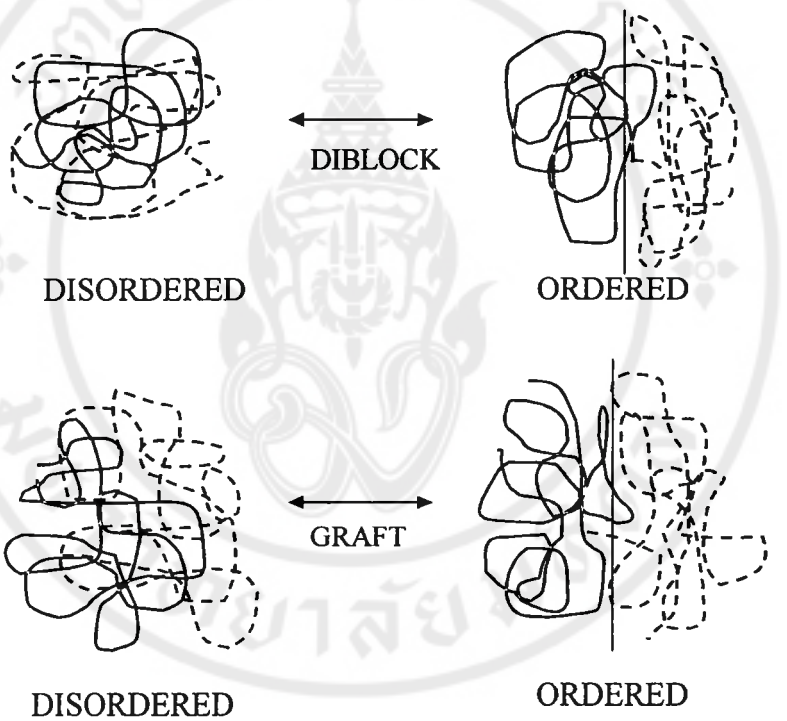

Figure 1.7 Schematic of the effect of the disorder-to-order transition on the configurational properties of di-block and graft copolymers (adapted from de la Cruz and Sanchez [26])

The domain size, shape, and the interfacial thickness of block copolymers depend on three factors: (I) magnitude of the repulsive interactions between A and B blocks, χ_{AB}; (II) the conformational entropy loss necessary to maintain constant segment density; and (III) the localisation entropy loss that causes the chemical links to be present at the interface. These mutually compensating factors (I vs. II + III) depend on the MW of each block and χ_{AB}. Theoretically, the derived interfacial thickness of block copolymer was [1]:

$$\Delta l = 2[(\beta_A^2 + \beta_B^2)/2\ \chi_{AB}]^{1/2} \qquad (1.4)$$

$$\beta_i^2 = \rho_{oi} < R_i^2 > /6Z_i$$

Where Z_i is the degree of polymerisation, ρ_{oi} is the density and $< R_i^2 >$ is the radius of gyration of the block i. This equation is valid in the limit of immiscible blocks having MW $\rightarrow \infty$.

1.3.2 Interfaces in copolymer/homopolymer blends

Green and Russel [28] monitored closely the effect of addition of a low molecular weight symmetric block copolymer of P(S-b-MMA) on the interfacial tension in blends comprising high molecular weight homopolymers, namely PS and PMMA. The theory predicted that the reduction in interfacial tension could be calculated to be:

$$v_{12} = v_{12,0} - k_B T[a\ \phi_c\ \rho \exp(\chi_{AB} Z_c)]/Z_c \qquad (1.5)$$

Where a is a statistical segment length, ϕ_c is the volume fraction of the copolymer, ρ is the density of the copolymer chains at the interface, k_B is the Boltzman constant, T is absolute temperature, χ_{AB} is the Flory-Huggins interaction parameter, and Zc is the degree of polymerisation of the block copolymer. At the concentrations studied, the excess number of copolymer chains per unit area at the interface of the homopolymers varied linearly with the volume fraction of copolymer chains in the bulk. The solubility of the copolymer chains was found to be slightly higher in the PMMA phase than in the PS phase. The theory indicates that the efficiency of block copolymer to lower the interfacial tension increases with its MW. This statement agrees well with the data lately published by Hermes and Higgins [9].

There are only a few papers dealing with systems comprising a graft copolymer and a homopolymer. For example, blends of graft A-B copolymer with homopolymer A (identical with the backbone of the A-block in the copolymer), were found to have unusual morphologies. The most common of these were spherical structures (named onion) consisting of alternating concentric layers of A and B components. The conclusion was that the onions had their origin in the immiscibility of the copolymer with the homopolymer even when molecular weights of the chemically identical block were comparable [1].

1.3.3 Interfaces in blends containing a copolymer with two homopolymers

Ternary blends that consist of two immiscible homopolymers and a copolymer are of a particular interest. Not only do they represent an ideal model for studying

compatibilisation of polymer blends, but also have found direct commercial applications. From the compatibilisation point of view, three theoretical indications are of importance: the best configuration of copolymer chain, the optimum copolymer composition, and the amount of a copolymer one should add to achieve the desired effect [1].

In 1980, Hong and Noolandi [29] developed a theory for the investigation of the interfacial density profile in three components systems that comprised two immiscible homopolymers (polydimethylsiloxane and polystyrene) in the presence of a solvent (benzene). The limit of infinite molecular weight for the polymer and a small compressibility were considered. The interfacial tension and density profiles for typical values of the interaction parameters were reported. The calculation of the interfacial properties as a function of benzene concentration was also revealed.

However, the important question remained unsolved as to whether the same effect can be found in the system in which two homopolymers are relatively compatible. A few years later, Leiber [30] formulated a theory to study the interfacial properties of nearly compatible mixtures of two homopolymers, A and B, and a copolymer A-B. The interfacial composition profile and interfacial tension were calculated analytically, as well as the interfacial activity of copolymer additives.

1.3.4 Composition of copolymer chain

Copolymers are constituted of at least two different monomers arranged in a specific manner. They can be random, alternating, di-block, tri-block, multi-block, star-shaped, graft, comb, etc. The composition of a copolymer depends on the nature and the amount of constituents, this is controlled by the polymerisation mechanism

(anionic, radical, etc.) and conditions (temperature, pressure, etc.). The composition is usually expressed as a molar fraction; e.g., f_A is the mole fraction of constituent A in a block copolymer. Thus, a symmetric AB block copolymer has: $f_A = f_B = 0.5$

For the compatibilisation of blends by the addition of copolymers, mostly di-block and/or tri-block copolymers have been used. Block copolymers can also be *in-situ* generated during the reactive compatibilisation of condensation polymers, particularly polyesters (PESTs) and polyamides (PAs). On the other hand, reactive compatibilisation of addition polymer, e.g., polyolefins, poly-vinyls, and styrenics, usually leads to graft copolymers. In the following discussion, the reviews will be focused on the compatibilisation through the addition of block copolymers; reactive compatibilisation will later be addressed.

1.3.5 Configuration and conformation of block copolymer chain

The configuration, which is the permanent microstructure that results from the polymerisation reaction (organisation of atoms in a macromolecule), and in turn conformation, which is shape of polymer chain that results from rotation of the bonds (arrangements of macromolecules in space), of a block copolymer greatly influence its compatibilising efficiency. The configuration of a block copolymer is required to match that of the polymer and the respective block that it is supposed to dissolve into. Similar argument can also be made regarding the other aspects of chain configuration such as head-to-tail, cis-trans isomerism, and branching. Conformation is governed by, for example, the repulsive interactions between the two blocks, the conformational entropy loss, and the localisation entropy loss resulting from placing the chemical links between blocks at the interface [1]. Fine balance between these effects forces the

polymeric chains to adopt different conformations when the conditions change so one might notice the transformation of a disordered to one of many ordered structures (e.g., spherical, cylindrical, lamellar, and more complex three-dimensional entities). In addition to a block copolymer, either a single homopolymer or a two-polymer mixture (or vice versa: adding block copolymer to a homopolymer or a blend), will induce changes of its conformation. Based on experiments, it is believed that there are three possible places for a copolymer to position itself, the copolymer chain can be located at the interface [2,11], dissolved in one or both phases [2,31], or it can form micelles in one or both polymeric phases [2,31].

In terms of the compatibilisation efficiency, morphological analyses showed that di-block copolymers have higher interfacial activity than tri-block or graft copolymers [30]. It is due to the di-block copolymer interacting more readily with the two homopolymer phases, forming appropriate entanglements that result in a decrease of the interfacial coefficient, and enhanced interfacial adhesion in the solid state. Experimentally, a comparative study of the morphology and the mechanical behaviour of modified low-density polyethylene/polystyrene blends have been demonstrated by Fayt and co-workers. They showed that a tapered di-block is more efficient than a pure di-block with the same composition and molecular weight [32]. These observations were confirmed by measuring the mechanical properties. However, there are also reports that indicate better mechanical performance in blends comprising a three-block copolymer than these with di-block ones even when the tri-block was relatively inefficient to reduce the interfacial coefficient [1].

1.3.6 The critical micelles concentration, CMC

Banaszak and Whitemore [33] concentrated on the phase diagrams of ternary homopolymer/copolymer blends, A/B/A-B, for a perfectly symmetric copolymer mixed with two homopolymers, both having the same degree of polymerisation, $Z_A = Z_B = Z_H$. The computed phase diagrams were quite complex, depending upon the temperature, χ_{AB}, degree of polymerisation, DP = Z_i, as well as their chain length ratio, viz Z_H/Z_C. For high copolymer content, there was a competition between the Huggins-Flory contribution to the free energy of mixing that tended to induce a macroscopic phase separation, and the micro phase free energy contribution that tended to stabilise the microphase. A decrease of temperature, T, causes the formation of a region where segregated domains of the two homopolymers coexisted. By increasing the relative DP of the homopolymer to $Z_H/Z_C = \frac{1}{4}$, for a specified value of Z_C, a meso phase was formed. By adding an equal amount of A and B homopolymers to A-b-B block copolymer, the composition changed in the following sequence:

M(mesophase) → H(homogeneous) → M → macro-phase separation

Neutron scattering studies of P(S-b-MMA) showed that the thermodynamic binary interaction parameter depends on temperature: $\chi_{AB} = 0.028 + 3.9/T$ [1]. For symmetric block copolymers, the lamellar microphase separation occurs when $\chi_{AB} Z_c = 10.5$ [24]. By combining these two relations, one can approximate the variations of the microphase separation temperature with DP: $T_c = 3.9/[(10.5/ Z_c) - 0.028]$. The

dependence has limited applicability to low molecular weight blocks with $Z_c < 375$ [1].

Park and Roe [11] studied the critical micelle concentration, CMC. Examined with X-ray scattering at a fixed angle 2θ of 0.26^0 and a specified temperature they found that a doubling of the molecular length causes a reduction in CMC by more than 1 order of magnitude.

1.3.7 Compatibilisation by addition of copolymer

There are two methods for the compatibilisation of the blends. The first one involves addition of a third component capable of lowering the interfacial energy, stabilising the dispersion, and providing interfacial adhesion in the solid state. Its effect on the behaviour of polymer blends will be discussed briefly in the next section. The second method is known as reactive compatibilisation, blending, or processing will also be discussed.

1.3.8 Interfacial characteristics

The efficiency of compatibiliser is determined by its preferential diffusion onto and sustainable location at the interface. From the point of view of the equilibrium thermodynamics, this is accompanied by dissolution of the compatibiliser in both polymeric phases, then at higher concentration, formation of micelles [11,34]. At still higher concentrations, the explanation how and under which conditions that compatibilisers with regular structure just like block copolymers may form meso-phases is provided theoretically [24]. The compatibilisation process is kinetic in nature, dependent on the diffusion rate. Consequently, the compatibiliser should be

designed by taking thermodynamic and kinetic parameters into account. A report of an elegant method of identification of the polymer location in LDPE/PS blends involved the use of hydrogenated poly(butadiene-b-isoprene-b-styrene), P(HB-b-I-S), copolymer that could be stained prior to TEM (Transmission electron microscopy) observations, it was shown that indeed, the block copolymer was located at the interface [32].

To gain its top efficiency, compatibilisation of binary polymer blends by addition of a copolymer must reduce the dispersed particles' size [35] and lower the interfacial tension coefficient [36-37]. At constant stress, the ratio of dispersed phase size to interfacial tension is supposed to be: d/ν_{12} = constant, thus these two parameters are expected to be inversely proportional to each other [1].

Compatibilisation is similar to the emulsification of classical colloids. The effect is best described by the emulsification curve that characterises the efficiency of the surfactant. It is worth noting, however, that the shape of the curve depends on the type of emulsifier and the emulsification process as well. The general emulsification curve is started by a sharply decreased curve in interfacial tension, directly related to a reduction in dispersed phase size as emulsification curves given in Figure 1.8, with the addition of small amounts of emulsifier. Then followed by a leveling off as the emulsifier concentration is increased above the apparent critical micelle concentration, CMC [36-37]. The amount of the emulsifier to saturate the interface depends on the mixing time, mixing equipment, the affinity of the emulsifier to the dispersed phase, the size of the dispersion, the orientation of the emulsifier at the interface and its ability to stabilise the interface against flocculation or coalescence [1].

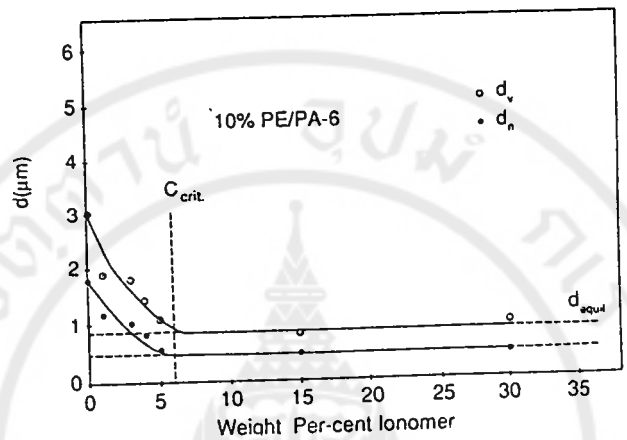

Figure 1.8 Emulsification curves show the influence of the interfacial modifier concentration on the dispersed phase size for 10% polyethylene dispersed in polymaide-6 (adapted from [37])

Addition of a block copolymer not only reduces the interfacial tension coefficient, but it alters the molecular structure of the interface as well. As shown by scattering methods, placement of block copolymer at the interface broadens the segmental density profile. Significant penetration of the block copolymer into the homopolymer phase was also observed. The penetration in turn, improves adhesion between the phases, and hence upgrades mechanical behaviour [38-40].

1.3.9 Interfacial thickness

The improvement of homopolymer blends with the incorporation of block copolymers can be demonstrated basically by the enhancement of their physical and mechanical properties. Russell and his colleagues made their effort to measure the interfacial thickness [40]; the PS/PMMA blend was studied. With the assistance of neutron reflectivity and small angle X-ray scattering, the interfacial thickness values (Δl) between PS and PMMA were found to be from 5 to almost 8.5 nm upon addition of P(S-b-MMA). Further addition of copolymer chains to the interface resulted in a marked increase in an ordering of the copolymer chains at the interface or an increase in the curvature of the interface.

Interfacial thickness data for a bi-layer specimens of PMMA with PS as well as poly(styrene-*ran*-acrylonitrile) (SAN) was measured by two dissimilar methods, namely ellipsometry and transmission electron microscopy (TEM) [41]. The replacement of PS in PS/PMMA with SAN offered a thicker interface from about 50 nm to a thick interface of 265-325 nm and a comparison between two methods was made and was found to be in good agreement. However, these observations do not agree well with the previous report published by Tanaka and Hashimoto [1] that upon addition of a *homopolymer* Δl remained constant.

Yukioda worked with Inoue [42] to investigate the interfacial properties between two unlike polymers, namely PMMA/SAN, by ellipsometry. The interfacial thickness between PMMA (substrate 0.5 mm) and SAN (thin film 400 nm) layers with annealing above T_g was reported. By changing the acrylonitrile (AN) content of SAN, the system can either be immiscible or miscible. It was observed that the interfacial

thickness increases from nearly 20 nm up to 60 nm for immiscible and miscible systems, respectively.

The stabilisation mechanism of morphology has not been clearly identified and so has not the stabilisation mechanism of interfacial thickness. In principle, the copolymer at the interface should form a barrier against the thermal and flow coalescence [23], the latter being more important. The copolymers' migration to the particle's surface is controlled by a function of, for example, temperature, degree of polymerisation (Z_c), the composition of one block in the copolymer, molecular architecture (such as the number of arms *n* in the star-shaped block copolymers) [43], and the morphology of the blend [1]. One can postulate that the shear coalescence occurs in three stages [6]. Firstly, deforming the dispersed phase that increases the interfacial area and thins the interphase, secondly, bringing the adjacent dispersed entities into a close proximity for sufficient long time, and finally "pinching" the two interphases to form a single entity. This mechanism suggests that the following aspects of compatibilisation are important for the stabilisation of morphology: (I) fine dispersion, (II) rigidity of the interphase, thus (III) the appropriate thickness of the interphase can finally be achieved [1].

1.3.10 Morphology

Several methods have been used to characterise morphology of polymer blends. In the pioneering works, the transparency of solution-cast films was used as a measurement of the emulsifying agent efficiency [11,40,43-44]. Following studies have focused on observation of the phase size reduction, using either the scanning or transmission electron microscopy; (SEM or TEM) [38,41,44-46]. The blend

morphology depends on the compatibiliser type: (I) co-solvent, (II) copolymer with inherent morphology, and (III) copolymer with irregular morphology.

The prepared block copolymer has inherent morphology that is defined by its MW and the composition of block, also depending on its selective environment [47]. Blends of homopolymers and block copolymers truly produce complex morphologies featuring instable macrophases as well as stable microphases, for example, in blends of PMMA/PS with P(S-b-MMA), quite a variety of morphologies can be formed at different copolymer contents [44]. Similarly, when PPO was added to poly(styrene-*block*-butylmethacrylate), P(S-b-BMA), the original cylinders turned into spheres. Further addition provided multilayer vesicles, or if still the further amounts of PPO were added, lamellae were eventually obtained. In blends having small amount of P(S-b-BMA); i.e., < 5 wt% , P(S-b-BMA) micelles dotted in PPO were observed [47].

PE blends were modified by addition of high-molecular-weight block copolymers, either linear (SB and SIS), or a star-block [48]. In the first case co-continuous, elongated structures were observed, whereas in the second the morphology was dispersed. The latter structure was attributed to the low molecular weight of branches that did not engender a sufficient number of entanglements.

Srinivasan and Gupta [49] have improved the tensile and flexural properties of rubber-toughened polymer systems, and incorporated the study on the effects of SEBS addition to PP/PC blends. The observations of the morphology and measurements of mechanical properties were carried out. A correlation of morphology and the properties was also discussed. For 10 to 20 wt% PC in PP/SEBS ratios varying from 95/5 to 90/10 blends, PP was the matrix, in which droplets of SEBS and PC were dispersed with SEBS forming an interphase, SEBS being the outer envelope around

PC. Thus, in this case the SEBS content was too low for imposition of a structure. It is worth emphasising herein that the introduction of block copolymer greatly affects the blend's morphology.

1.3.11 Crystallisation

Addition of a block copolymer in order to compatibilise the blends which comprise semi-crystalline polymers may affect the crystalline morphology and total crystallinity. For example, in PE/PP blends four separate phases may coexist: PE-crystalline phase, PP-crystalline phase, PE amorphous phase and PP amorphous phase [1]. Poly(ether imide) and poly(ethylene terephthalate) (PEI/PET) were solution-blended using two different solvents [50]. The miscibility and crystallisation pattern were observed as the annealing time and the amount of PEI were altered. The approximately constant crystallinity was the result only for weight fractions of PEI less than 0.4. Where the miscible melt became demixed into the PET-enriched phase and the PEI-rich phase. The crystallisation was assumed to take place at the domain interfaces. The situation can be more complex if the polymorphism of constituent polymers is taken into account. Processing conditions, material characteristics, compatibilisation, the cooling rate, and annealing history, all influence the crystallinity, spherulite size, the lamellar thickness, and perfection of the crystallinities, and affect the final morphology and thus performance. Note that the discussion on miscibility and compatibilisation is restricted to the non-crystalline part of the polymer blends.

The maximum rate of crystallisation is mid-way between the melting point, T_m, and the glass transition temperature, T_g; i.e., $T_c = \frac{T_m + T_g}{2}$. In miscible blends, T_g is a monotonic function of composition, thus T_c depends on composition. Different crystallisation mechanisms usually lead to different morphology; i.e., separated when the crystallisation ranges overlap, nucleated when minor phase polymer crystallises first, nucleating crystallisation of the major phase, increasing its T_c and the crystallisation rate, and rather seldom found epitaxial crystallisation and co-crystallisation.

There is suggestion that the ultimate properties are enhanced by co-crystallisation [51]. The recent development of Dow's INSITE™ constrained geometry catalyst and process technology has made available copolymers of ethylene with α-olefins that differ significantly from conventional LLDPEs in having narrow molecular weight distribution, and homogeneous long chain branching structure [52]. Blends of homogeneous ethylene-octene copolymer, researched by DOW's INSITE™, have recently been produced and there was an explanation from the second heating thermogram that two components, however, crystallised as separate crystal populations in all the blends [51].

1.4 Reactive compatibilisation

1.4.1 General methods

A reactive group can be grafted onto a homopolymer by means of a solution, melt, and even a solid-state route with, mostly, the incorporation of peroxide initiator [53]. Its use as compatibiliser can therefore be applied into blend systems as, it is hoped, it can react with the end groups of the blend constituents, thus *in-situ* generate block or graft copolymers that can diffuse readily toward the interface between limited miscible blend constituents. Ultimately, the improvement of interfacial adhesion between phases could be successfully achieved. A very recent preparation of funtionalised low-density polyethylene by Kelar and Jurkowski [54] has been published. Maleic anhydride (MAH) was grafted onto LDPE through reactive extrusion in a single screw brabender extruder, equipped with a static or dynamic mixer in the presence of the free radical initiator benzoyl peroxide (BP). It was found experimentally that the highest grafting efficiency was for the dynamic mixer, next the static mixer, and the lowest was for shaping extruder's head. Here, the grafting process was concluded to be accompanied by cross-linking side reactions of the polyethylene chains.

Polypropylene (PP) was lightly maleated by solid-state graft polymerisation and further neutralised to prepare semicrystalline ionomers, H^+-, Na^+-, Ca^{2+}-, and Mn^{2+}-form maleated PP (mPP) [55]. Solvents such as xylene and decaline were used to swell the polymer and also to provide a medium for the delivery of monomer and free radical initiator to the reactor. The size of the polymer powder was found to influence

the graft level; the smaller the size, the higher the graft level because of the higher specific surface area. In reactive compatibilisation, the interfacial agent is produced *in-situ*, with segments each from compatibiliser and homopolymer. From the economic, as well as the performance points of view, the technique is more interesting than addition of a block copolymer for one of many reasons that the system provides larger polymer-polymer interface [56].

During the reactive blending, the copolymer should be formed through an inter-chain reaction. The process may be defined as a reaction between two or more polymers to form a block copolymer. The five chemical processes by which interchain copolymer can be *in-situ* formed, are listed in Table 1.1 [1].

Reactive processing is an integration of polymer chemistry with polymer processing. It combines chemical kinetics with flow and heat balance, integrating them into a mathematical model. Since there is strong interrelation between processing, morphology, and performance, the development of mathematical models is being pursued vigorously. The model must be able to predict and therefore lead to control the morphology evolution during compounding or processing steps.

Table 1.1 Chemical processes for interchain copolymer formation in extruder reactors (adapted from [1])

Type of chemical reaction	Type of resulting copolymer
Chain cleavage and recombination resulting in either block and random copolymers	AAAAABBBBB + AABBBBBAAA + AABBAAABBB, etc.
Reaction between end-groups	AAAAABBBBB
End-group of 1st polymer reacting with pendant functionality of 2nd polymer resulting in a graft copolymer	u A-BBBBB u A-BBBBB u
Reaction either between pendant groups or main chains of two polymers	Graft copolymer or crosslinked network
Ionic bond formation	Usually graft, frequently crosslinked system

In 1994, Scott and Macosko [57] modeled bilayer film extrusion to study the interfacial reaction between a poly(stryrene-co-maleic anhydride) copolymer with two amine terminated polymers, namely a poly(butadiene-co-acrylonitrile) copolymer and Nylon11. The way that they confirmed the occurrence of cyclic imide formed when anhydride end groups react with amine groups of two polymers was Fourier transform infrared spectroscopy (FTIR). The kinetics of reaction were found to depend greatly on the molecular weight as well as temperature. Higher temperatures and lower molecular weights led to faster kinetics and greater amounts of reaction. For example,

at approximately constant temperatures, Nylons 11 possessing higher molecular weight used in the study lowered a depth of penetration from 2 μm to 0.3μm. Because of reactive processing, many commercial blends can be prepared. Super tough polyamides, PO/PA, and PPE/PA blends, or PC/PA are but a few examples. The technology makes it possible to develop blends with new sets of properties. Although a lot of research on reactive compatibilisation has been carried out, the actual mechanism has not been totally understood yet. Many efforts are being made and the basic requirements for efficient reactive compatibilisation are:

(I) Sufficient mixing to achieve the desired dispersed morphology of one polymer in another.

(II) Presence of reactive functionality for covalent or ionic bond formation.

(III) Sufficient chemical activity to react across the phase boundary.

(IV) High reactivity, to complete the reaction within the residence time of the extruder.

(V) The formed bonds to remain stable in subsequent processing steps.

In the majority of cases, the interchain copolymer formation involves combination of reactive groups of one polymer with reactive groups of the second polymer. These form graft or block copolymers with molecular weight roughly equal to the sum of those of the two homopolymers. Because of the residence time limitations in the extruder, high conversion rates are required. These can be achieved either by using relatively high concentration of the reactive groups; e.g., high concentration of chain ends, highly reactive functional groups, or efficient catalysts.

The majority of commercial polymers that are used to form copolymers have nucleophilic end groups such as carboxylic acid, amine, and hydroxyl. These can form covalent bonds with suitable electrophilic functionalities; e.g., cyclic anhydride, epoxide, oxazoline, isocyanate, and carbodiimide.

1.4.2 The interface and morphology in reactive blends

It has been reported that reactive blends show a thicker polymer-polymer interface than blends with or without the addition of copolymer (see Table 1.2). Yukioka and Inoue used time-resolved ellipsometric analysis to measure Δl between amorphous Nylon and styrenic copolymers (SMA or SAN) as a function of the annealing time [56]. The styrenic copolymers were neat poly(styrene-co-maleic anhydride) (SMA) and single-phase mixtures of SMA with poly(styrene-co-acrylonitrile) (SAN). The measurement indicated that Δl increased with time to a plateau whose level depended on the temperature and net concentration of reactive sites, Δl = 10 to 50 nm. It was postulated that if flow is present during the reactive compatibilisation, the interface can possibly become undulated, composed of heterogeneous copolymeric species. It has been published that polymer-polymer interfaces depend greatly on the applications and conditions under which the polymer blends have been processed as tabulated in Table 1.2.

Table 1.2 Polymer-polymer interface thickness (adapted from refs 1,56)

Type of blend	Thickness (nm)
Immiscible	2
Block copolymer	4 to 6
Polymer/copolymer	30
Reactive compatibilisation	30 to 60

In 1992, Sundararaj co-worked with Macosko [58] to study the morphology development in non-reactive polymer blends. The two systems studied were 80:20 polystyrene/amorphous polyamide and 80:20 polystyrene/polypropylene. The remarkable morphological changes took place during the initial softening stage and changed less after the polymers were completely melted. Several unstable shapes were also present.

In the following years, Scott and Mocosko [59] studied the morphology development during reactive and non-reactive blending of an EPR with either PS-OX or amorphous, semi-aromatic PA. A rapid reduction of the dispersed phase size was found to occur in the "melting" region. For example, in the case of reactive PA/EPR blending, the volume average particle diameter of the dispersed phase was reduced from 4 mm (pellet size) to 1 μm within the first 90 s of mixing. The interfacial chemical reaction between the phases reduced the size of the dispersed phase and narrowed the size distribution. Another work by the same authors was published [60] in which a model experiment was developed that allows the matrix to be dissolved away so that the dispersed phase could be observed directly using a scanning electron

microscopy (SEM). The initial mechanism of morphology development was found to be intimately connected with the melting or softening process. The intermediate morphologies have been demonstrated to be quite complex. These model experiments reveal the primary modes of particle deformation and the nature of the morphologies at short mixing times.

1.4.3 Reaction between functional groups

Block copolymers can be *in-situ* formed in reaction between functionalised end groups of two different polymers. Since the probability of two end groups reacting within the extruder residence time is low, highly reactive funtionality is necessary and sometimes lower MW polymers are required.

Fellahi *et al.* [61] recently have investigated injection-moulded high-density polyethylene/polyamide-6 (25:75 vol%) blends with and without compatibiliser. Their interest was in both the bulk of the sample and in the weldline region. With reactive compatibilisation, ethylene-methacrylic acid-isobutyl acrylate ionomer was added as the interfacial modifier. The chemical bonding was believed to occur at the interface through amide formation between the carbonyl group of the ionomer and the terminal amine of polyamide. The dispersed phase size, skin thickness, and the width of the weldline were considerably reduced. Less coalescence and a more stable morphology were also observed.

This observation agrees very well with a study of polyethylene/polyamide-6 blends recently made by Kelar and Jurkowski [54]; LDPE-g-MAH, as the compatibiliser was synthesised, and was introduced at the 5 wt% level into LDPE/PA6 blend by using the dynamic mixer. An *in-situ* formed graft copolymer

(LDPE-g-PA6) was created both because of reaction of the end amine groups in PA6 with carbonyl groups in MAH and also because of the recombination of macro-radicals generated under the action of shearing stresses. Good stability of the phase structure during reprocessing and heating and good mechanical properties of the blend were obtained.

Enhancement of the interfacial adhesion between immiscible amorphous polyamide (PA) and polystyrene (PS), by *in-situ* copolymer formation at the interface was investigated [62], using styrene maleic anhydride (SMA) as the reactive compatibiliser. The fracture toughness remarkably increased as the amount of SMA in the deposited layer and the annealing temperature was increased. The improvement originated in the copolymer *in-situ* formed at the interface in reaction between the amine end group of PA and MA of SMA.

1.4.4 Trans-reactions: tranesterification and ester-amide exchange

Transesterification during polyester blending takes place in blends that comprise at least two components from between: PEST, PC, PAr, LCPs, and polymers with side-chain ester groups. Transesterification in blends of wholly aromatic thermotropic copolyesters was highlighted by McCullagh and his co-workers [63]. The data provide a unique method to study transesterification between copolyesters with different monomer ratios. Transesterification may also involve chain cleavage followed by recombination of the end groups to change MWD and randomise the monomeric sequences in the polymer. The latter process may result in reduction of

crystallinity and poorer performance [64]. Transesterification is catalysted by metal compounds, e.g. organo-tins.

Compatibilisation of the blends of PET with PBT depends on the extent of transesterification. The materials were reported to show good crystallinity without a need to use nucleation. They were toughened by addition of either an acrylic elastomer or EVAc. At $T \geq 200\ ^{o}C$, PC/PET blends showed coarse, phase separated morphology whereas at $T = 220\ ^{o}C$, the blend was homogeneous. The morphology depended on the relative rates of phase separation and transesterification. However, slow transesterification was observed at $T \leq 200\ ^{o}C$ [65].

PC with PAr was extruded using either a single-screw, SSE, or a twin screw extruder, TSE. Blends prepared in SSE (as well as those prepared by solution casting) show two Tg's, whereas those prepared in TSE showed a single Tg, suggesting greater extent of transesterification. The latter blend has poor tensile and impact strength. The extend of reaction could be controlled by addition of a phosphite, carbodiimide, or hindered phenols [66].

1.5 Compatibilisation effects

Blending is one of the most available, rapid and effective technological ways of modifying the properties of polymers that could hardly be succeeded by any means of chemical synthesis. In addition to the difficulty, very often the chemical synthesis also requires relatively costly approach. The components of a blend are generally incompatible. The incorporation of interfacial or modifying agent is therefore needed. According to numerous publications, however, the properties of compatibilised blends

both when melted and when solid depend on many factors. They include the chemical nature of the polymers, the composition of the blends, the level of rheological action and the influence of additives making the components compatible [67].

1.5.1 Compatibilisation effects on rheology

The rheological property consequences of compatibilisation can be predicted from emulsion models. Making the interface more rigid increases the intrinsic viscosity that in turn causes the emulsion viscosity to increase. Similarly, increasing the volume fraction of the dispersed phase increases the viscosity. Finally, the increased interactions between the phases enhance the formation of associative net work that may lead to a yield stress. In short, compatibilisation is expected to increase melt viscosity, elasticity, and the yield stress. However, there are other mechanisms that may invalidate this prediction [68]:

(I) Added copolymer may prefer to from micelles inside the polymeric phases instead of locating at the interphase, e.g., as in PE/PS blends "compattibilised" by addition of SEBS.

(II) Addition of compatibilisers may affect the free volume (evidenced by reduced melt density).

The rheological properties of PE/PS blends remained virtually unchanged upon addition of SEBS [68]. Linear low-density polyethylene (LLDPE) was blended with an ethylene methyl acrylate (EMA) copolymer containing a diol [13]. In the study, it

was assumed that the Cox-Merz rule is valid for both phases. Since the viscosity was a function of both frequency and the reaction time, the viscosity as a function of time at a given frequency and temperature was obtained. For 160, 180, and 200 ^{0}C, the viscosity was found to increase as temperature and reaction time increase. At 140 ^{0}C, however, no viscosity change could be observed until up to 60 min reaction time.

Without compatibiliser, the investigation of rheological properties of blends of two immiscible polymers, namely linear low-density polyethylene (LLDPE) and polyamide12 (PA12), having almost the same viscosity but different elasticity, over a wide range of composition has been reported [69]. Zero shear rate viscosity η_0 and first normal stress difference N_1 increase gradually at low and moderate volume fraction of the dispersed phase but remain almost constant in the phase inversion region. In PS/SAN blends, addition of P(S-b-MMA) reduced the average size of PS drops from diameter of 0.4 μm to micellar dimensions, with diameters of 0.12 μm. Using Choi & Schowalter's modified emulsion model, correlation between d and v_{12} was established. It was found that that reduction of diameter and v_{12} took place at different concentration of block copolymer [2].

1.5.2 Compatibilisation effects on mechanical and impact properties

The most important properties of polymer blends are tensile and impact strength. Blending is often used to improve the toughness of PS, PVC, PMMA, PET, and PA. When more complex mixtures of polymers started to be involved, the impact modification was progressively changed into compatibilisation. However, even today,

many blends profit from the simultaneous compatibilisation and impact modification by addition of multicomponent modifiers.

It is widely accepted that mechanical properties of engineering thermoplastic polymers can be improved by blending two or more in miscible polymers. The mechanical blending of miscible polymers results in a homogeneous morphology that exhibits a single glass transition. However, the mechanical blending of immiscible but compatible components, such as polycarbonate with poly(acrylonitrile-co-butadiene-co-styrene) [1] gives multiphase morphology with efficient dispersion of the minor component and good interfacial adhesion between the unmodified components. Two types of mechanical tests have been used: the low rate of deformation tests; i.e., in tensile, compressive, or blending mode; and high speed impact tests. Immiscibilty of polymers is reflected in both. For example, in tensile tests the maximum elongation and the maximum strength can be dramatically reduced by poor adhesion between the phases. Similarly, the lack of adhesion is responsible for low values of impact strength.

Polymeric systems can be classified as either brittle or pseudo-ductile [70]. The first type tends to fail by the crazing mechanism, and has low crack initiation as well as propagation energy. Typical examples include high impact polystyrene (HIPS) and numerous grades of acrylonitrile-butadiene-styrene polymers (ABS). The second type tends to fail by yielding, having high crack initiation energy and low crack propagation energy. Typical examples are impact modified polyamide (PA) and impact modified polypropylene (PP). As usual, there are some polymers that show and intermediate behaviour; e.g., POM and PVC. The transition from brittle to ductile

depends on the material characteristics as well as on external variables, such as test temperature, rate of testing, geometry, loading mode, etc.

Interfacially compatibilised immiscible blends with an isotactic polypropylene matrix (PP) and dispersed polyamide-6,6 (PA6,6) phase were produced through extrusion with two anhydride-grafted isotactic PP compatibilisers, one of high-anhydride content (HAC, 2.7 wt% grafted maleic anhydride) and one of low-anhydride content (LAC, 0.2 wt% anhydride) [71]. Both of the compatibilisers were found to be equally efficient. Both compatibilisers imparted similar tensile strength improvements compared to an uncompatibilised blend. Kudva and co-workers [72] investigated blends of Nylon6 and polyethylene over a wide range of compositions. The polyethylenes used were grafted with maleic anhydride varying from 0-0.9 wt% maleic anhydride. Higher viscosity maleated polyethylenes were found to be able to produce blends with high impact strength and excellent low temperature toughness over a range of compositions. It was also demonstrated that polyethylene materials containing a very low degree of anhydride functionality could also generate blends with satisfactory impact properties.

1.6 Commercial blends

Most commercial polymer blends are multiphase or compatibilised systems. In commercial blends, it has always been important to control size and shape of the individual phases, which is perhaps best known as phase morphology of the blend. There is a relationship between phase morphology and properties of the blend and therefore the properties of the blend could also be controlled. The properties of the

individual of the polymers, the quantities of the polymer, or even the interactions between the phases in the blend are also factors that affect properties.

1.6.1 Interesting blends

Bani-hani [73] compounded post-consumer linear low-density or high-density polyethylene (PC-LLDPE or PC-HDPE) with calcium carbonate and a polyolefin plastomer (POP). Compounded POP blends were later compared with those of a PVC-calcium carbonate formulation to see if they can replace it for flooring applications. Some of compounded POP blends possess synergistic properties. Even for higher amounts of PC-LLDPE and PC-HDPE (at the ratio of 50/50), blended with POP are found to retain satisfactory elongation and impact properties.

Bensason and his co-workers [51] investigated blends of homogeneous ethylene-octene copolymers with different comonomer contents (mol%). Polymer designation was derived into 4 groups, namely type I base, type I, type II, and type III with their densities consisted of, respectively, 0.865,0.887,0.901, and 0.913 gcm^{-3}. The lowest density copolymer (0.865 gcm^{-3}) was combined separately with three other copolymers of increasing densities (0.887, 0.901, and 0.913 gcm^{-3}) at varying compositions. The conclusion was blends of type I base-I appeared to form a single non-crystalline phase, whereas the non-crystalline regions of blends that combined a type II and III copolymers appeared favorably to be phase separated which was strengthened by DSC thermograms.

Blends of polyethylenes and their families have attracted great interest. The morphology of HDPE/LDPE blends with different thermal histories was observed [74] and it was found that the addition of LDPE disrupts the higher order of the

HDPE. It was assumed that the blends can form a co-crystalline phase in the solid, but experimentally they did not because of the non-linearity of the LDPE. High-density polyethylene homopolymer (HDPE) with a low resistance to slow crack growth was blended with a linear low-density polyethylene (LLDPE) with a high resistance to slow crack growth [75]. The two resistances to slow crack growth differed by a factor of 10^6. The resistance to slow crack growth increased as the amount of the strong component increases. The results were concluded to be from a network which consisted of crystals joined together by tie molecules, which contain short-chain branches from the LLDPE. The strength increases greatly when the network becomes continuous phase.

1.6.2 Polyolefins/polyamides blends

When incompatible thermoplastic polymers like polyolefines and polyamides are mixed, the interfacial adhesion is known to be relatively weak, which ultimately results in inferior mechanical properties and poor dispersion of the components. These blends require a compatibilising agent to achieve satisfactory interfacial adhesion and better interfacial stress transfer between the phases. One approach to polymer blend compatibilisation is to manipulate the interactions at the interface by the addition of "compatibiliser" that facilitates graft reaction.

Polyamides (PAs) are polymers of great industrial importance, but they have several limitations in their end-use because of their (I) low impact strength, particularly below the glass transition temperature, (II) poor dimensional stability due to high moisture absorption, and (III) high costs. Blending with polyolefins such as polypropylene (PP) or polyethylene (PE) can overcome these drawbacks because

polyolefins have better resistance to organic solvents, negligible water absorption, and are relatively inexpensive. Numerous attempts have been made to investigate polyolefins-polyamides blends [72,76-82]. Polyolefins-polyamides blends are incompatible due mainly to the differences of polarity between the components. Polymers possessing reactive groups are very often introduced into polyolefins-polyamides blends. Those reactive groups are usually maleic anhydride [72,76-78,81], acrylic acid [79-80], or glycidyl methacrylate [82]. The reactive group-containing component is expected to form specific interactions or chemical reactions with the blend constituents, thus copolymers are chemically created.

Recent experiments [83] have shown the compatibilising effect of hyperbranched polymers grafted onto polypropylene (PP-HBP) on the interfacial tension of polypropylene (PP)/polyamide-6 (PA6) blends, through the use of the deformed drop-retraction method (DDRM). This was shown to be a more effective compatibiliser in decreasing the interfacial tension than the commonly used maleic anhydride-grafted polypropylene (PP-g-MAH). This experiment included the measurement of the average particle size diameters of dispersed particle; the sizes were found to be 0.63 and 0.55 μm for the 2.5 wt% PP-g-MAH and 2.5 wt% PP-HBP compatibilised PP/PA6 blends, respectively. Although several pieces of evidence have been built to support the compatibilising effect through the lowering of the interfacial tension and reduction of the average particle size diameter, investigations relating to the effect of its compatibilising effect on the mechanical properties of compatibilised PP/PA6 blends is lacking.

1.7 Scope of the thesis

The objective of this work was to investigate the relationships between the activity of the compatibiliser under the range of melt processing conditions found during twin screw extrusion and injection moulding and its effect upon the morphology and properties of a reactively compatibilised blend. The constituent PA6/PP/PP-g-MAH system was chosen due to its commercial importance and the availability of relevant literature on which to draw. The commercial PA6/PP blends comprise a PA6 matrix with a high concentration of dispersed PP, and hence a formulation of this type was chosen in this work; i.e., a blend comprising the PA6/PP composition.

In the first part of the work, a screening experimental design was used to determine the influence of twin screw extruder configuration, screw speed, and compatibiliser content and their interactions upon the morphology and mechanical properties of the PA6/PP blend. Barrel temperature was fixed at 230 °C, that is approximately equal to the melting point of the PA6, since this is the near universally used compounding temperature of compounds containing PA6. Higher temperatures enhance degradation and reduce melt viscosities thereby leading to poorer mixes. The stability of the morphology produced through twin-screw extrusion was quantified through the difference in phase dimensions between the moulded samples and the extrudates. The performance of the compatibiliser was related to the molecular dimensions of the *in-situ* formed PP-b-PA6 copolymer.

In the second part, the influences of extruder screw speed and a series of compatibiliser content on the properties of the PA6/PP blend were studied during

twin-screw extrusion. Upon injection moulding, the injection moulder screw speed was varied. Two types of conditioning prior to the mechanical test, namely dry and wet conditions, were used to quantify the effect of water absorbed into PA6 matrix phase upon mechanical properties. In order to analyse the dispersed phase stability, the annealing was performed at 230 ^{0}C for 10 minutes under quiescent conditions.

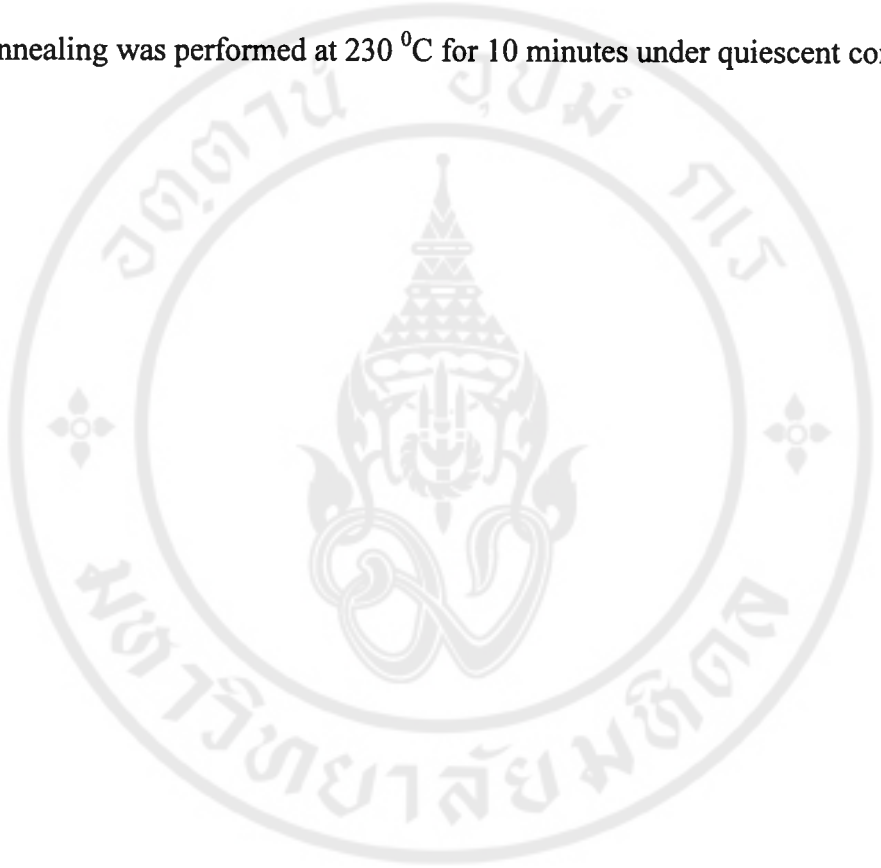

CHAPTER II

EXPERIMENTAL

This chapter is separated into 3 parts, namely chemical reagents and instruments, procedures, and characterisation.

2.1 Chemical reagents and instruments

2.1.1 Chemical reagents and materials

The chemical reagents and materials used in this study are given in Table 2.1.

Table 2.1 Trade name/grade and manufacturers of chemical reagents/materials used in this study

Chemical reagents/Materials	Trade name/Grade	Manufacturer
Polypropylene	P600F	TPE Co., Ltd.
Polyamide 6	1013NB	UBE Co., Ltd.
PP-g-MAH[a]	MZ109D	Du Pont
Xylene	AR	J.T. Baker
Absolute ethanol	AR	Merck
Benzyl alcohol	AR	Carlo Erla Reagenti

Table 2.1 (continued)

Chemical reagents/Materials	Trade name/Grade	Manufacturer
Phenol	AR	BDH Chemicals
Phenolphthalein	AR	BDH Chemicals
Conc. hydrochloric acid	AR	J.T. Baker
Phosphotungstic acid hydrate	AR	Aldrich

[a] MAH content 0.45 % by weight

2.1.2 Instruments

The instruments and suppliers of the instruments utilised in this study are listed in Table 2.2.

Table 2.2 Instruments and suppliers utilised in this study

Instruments	Suppliers
Co-rotating twin screw extruder	Prism TSE 16TC
Injection moulder	DR Boy 22S
Universal tester	Instron 4301
Pendulum impact tester	Zwick 5102
Thermal gravimetric analyser	Perkin Elmer TGA7
Scanning electron microscope	Hitachi S-2500
Vacuum oven	Shel lab
Circulating pump	Neslab RTE111

2.2 Procedures

The preparation of the PP/PA6 blends was divided into 2 parts. In the first part, an experimental design was used. The influences of extruder screw configuration, extruder screw speed, and compatibiliser content as well as the interactions between these factors on the phase morphology and properties of the blends were investigated. In the second part, the effects of extruder screw speed, injection moulder screw speed, compatibiliser content, and wet and dry specimen conditions upon the properties of the blends were investigated.

In general, all materials used in this study were firstly ground in order to gain better mixing. The PA6 and PP-g-MAH were dehydrated under vacuum at 80 ^{0}C for 3 hours. All the components were dry blended manually before feeding into a co-rotating twin screw extruder from a single screw hopper. The temperatures along the barrel were set at 210, 230, 230, 230, and 230 ^{0}C from feeding zone to the die. The melt temperature was directly measured with a thermocouple at the end of the die. The processing parameters of particular interest during melt blending were recorded; i.e., torque, die pressure, and melt temperature at die. The specific mechanical energy (SME) was calculated and is defined to be the energy consumed to process the materials per unit weight, as expressed in equation 2.1.

$$SME = \frac{Screw\,speed(rpm)\,X\,Torque\,X\,Drive\,power(kW)}{\max.Screw\,speed\,X\,\max.Torque\,X\,out\,put\,rate(kg/hr)} \quad (2.1)$$

Solidification of the extrudate after it had exited from the die was performed in cooling bath, after which it was pelletised. The compounded pellets were dehydrated under vacuum at 80 ^{0}C for 3 hours to minimise hydrolytic degradation during injection moulding. Afterwards, the compounded pellets were injection moulded using a DR BOY 22S injection moulder. Injection moulding conditions were varied in the second part. The hopper temperature was fixed at 90 ^{0}C and the mould temperature was 80 ^{0}C . The compounds were finally shaped into two impact test bars and one tensile test bar. These specimens were kept under desiccation before the mechanical tests and characterisation were carried out.

2.2.1 Part I: Compatibilised PP/PA6 blends

The properties of polymer blends can be affected substantially by the conditions under which they have been compounded. A special type of *experimental design* was used to investigate more than one variable at a time. The dependent variables are defined to be the responses to the independent variables. The response to any variable observed under different conditions indicates whether the variables act on the experimental units independently of one another. Interaction between factors occurs when they do not act independently of one another.

Table 2.3 Formulations of the blends prepared in the first part

Run	Weight of constituent resins (g)		
	PP	**PA6**	**PP-g-MAH**
1	362.27	684.29	9.05
2	362.29	684.92	9.05
3	362.37	684.12	9.05
4	362.87	684.09	9.05
5	362.00	684.25	36.27
6	362.00	684.04	36.20
7	362.34	684.47	36.20
8	362.14	684.75	36.20
9	362.53	684.07	22.60
10	362.66	684.12	22.60
11	362.94	684.68	22.60
12	362.53	684.53	22.60

The density of solid resins for PP, PA6, and PPMA are 0.905, 1.14, and 0.905 gcm^{-3}, respectively.

In this part, the blends were coded as follows: A and B mean, respectively, low and high intensity twin screw configuration; 1, 0, and -1 are codes representing, respectively, the maximum, centre point, and minimum value of the variables used in melt blending; i.e., 3.8, 2.4, and 1.0 vol% for compatibiliser content and 200, 150, and 100 rpm for screw speed. For example, in Run 1, a blend was prepared with the low

intensity twin screw configuration, A, while compatibiliser content and the extrusion screw speed were 1.0 vol% and 100 rpm, respectively. The experiment unit was screened throughout the varying of the independent variables, therefore this can be called a "*screening design*". The compound formulations are detailed in Table 2.3. The experimental design is detailed in Table 2.4 and Figure 2.1. The experimental design, given in Table 2.4, consists of a total 2^n factorial design, where n is the number of independent variable; i.e., extruder screw configuration, extruder screw speed, and compatibiliser content, giving n = 3, provides eight treatments. An additional four treatments for centre point samples; i.e., Run 9, 10, 11, and 12, were prepared as samples to determine the experimental error or reproducibility.

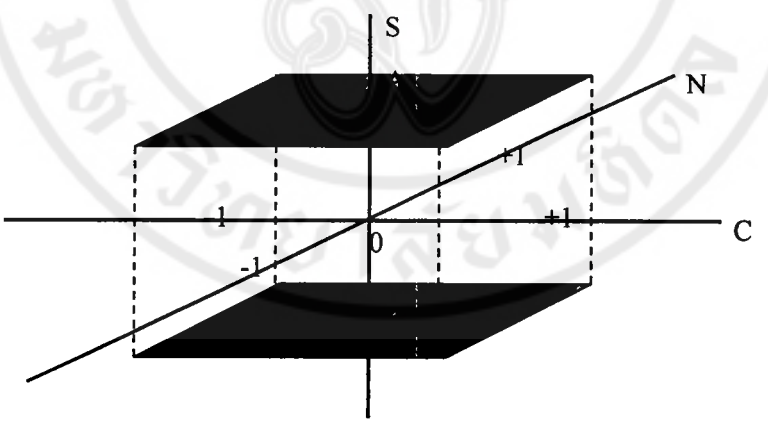

Figure 2.1 The diagram displays how the varying of the independent variables affects the experiment unit. S, C, N stand for extruder twin screw configuration, compatibiliser content, and the extruder screw speed, respectively. These abbreviations will be used throughout this thesis.

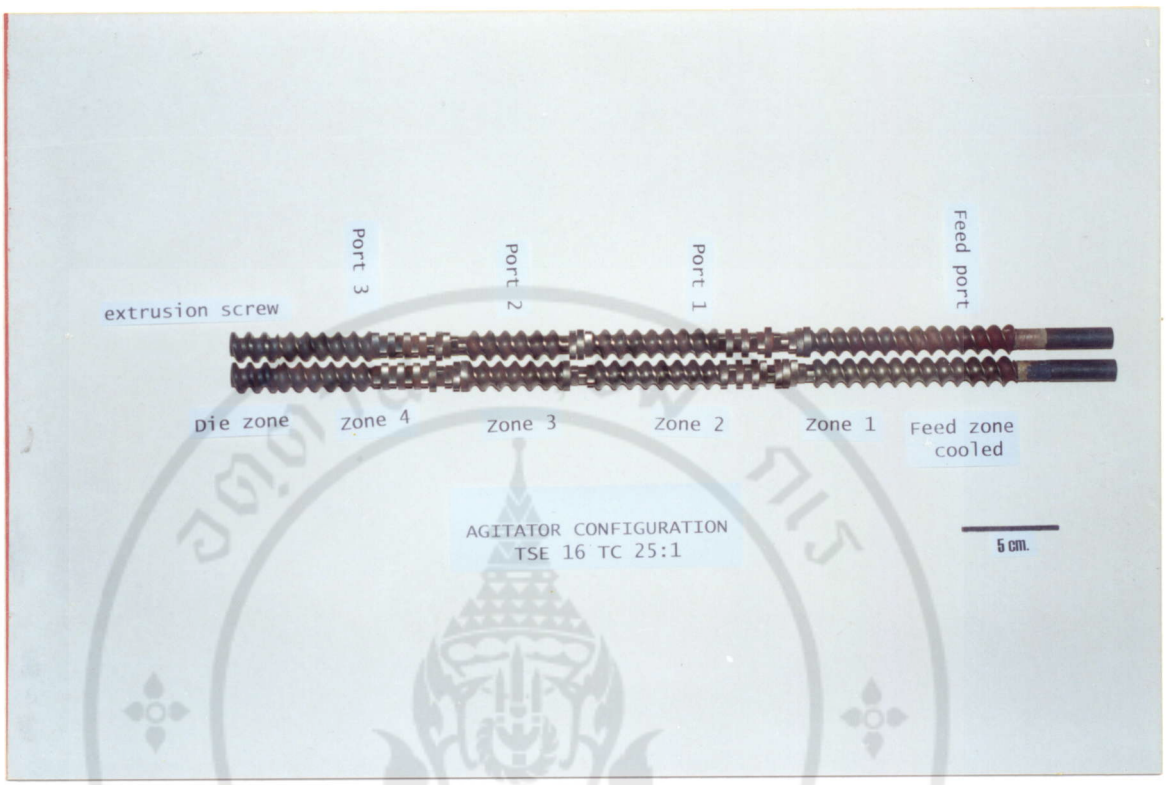

Figure 2.2 The agitator extruder screw configuration C installed in twin screw extruder (TSE 16 TC 25:1)

2.2.1.1 Screw configuration

A twin screw extruder, Prism TSE 16 TC, with a L/D ratio of 25/1 was used to produce the blends throughout the study. Agitator configuration C, see Figure 2.2, was only used in the second part. From the midway of zones 1 and 2, the configuration was; F30° (forwarding) conveying screw section, followed by A90° (neutral) kneading piece, then F60° conveying screw section at the beginning of zone 3, and from zone 3 to die zone between which was F60°, then A90° kneading section.

Figure 2.3 The low intensity extruder screw configuration A installed in twin screw extruder (TSE 16 TC 25:1)

Screws with configuration A and B were used to prepare the blends in the first part of the work. Configuration A, see Figure 2.3, is a low intensity configuration equipped with conveying screws throughout feed zone to zone 3; a kneading section at the beginning of zone 4 was the only sequence containing mixing paddles. Configuration B, see Figure 2.4, is a high intensity configuration with a half reverse feed screw in zone 2.

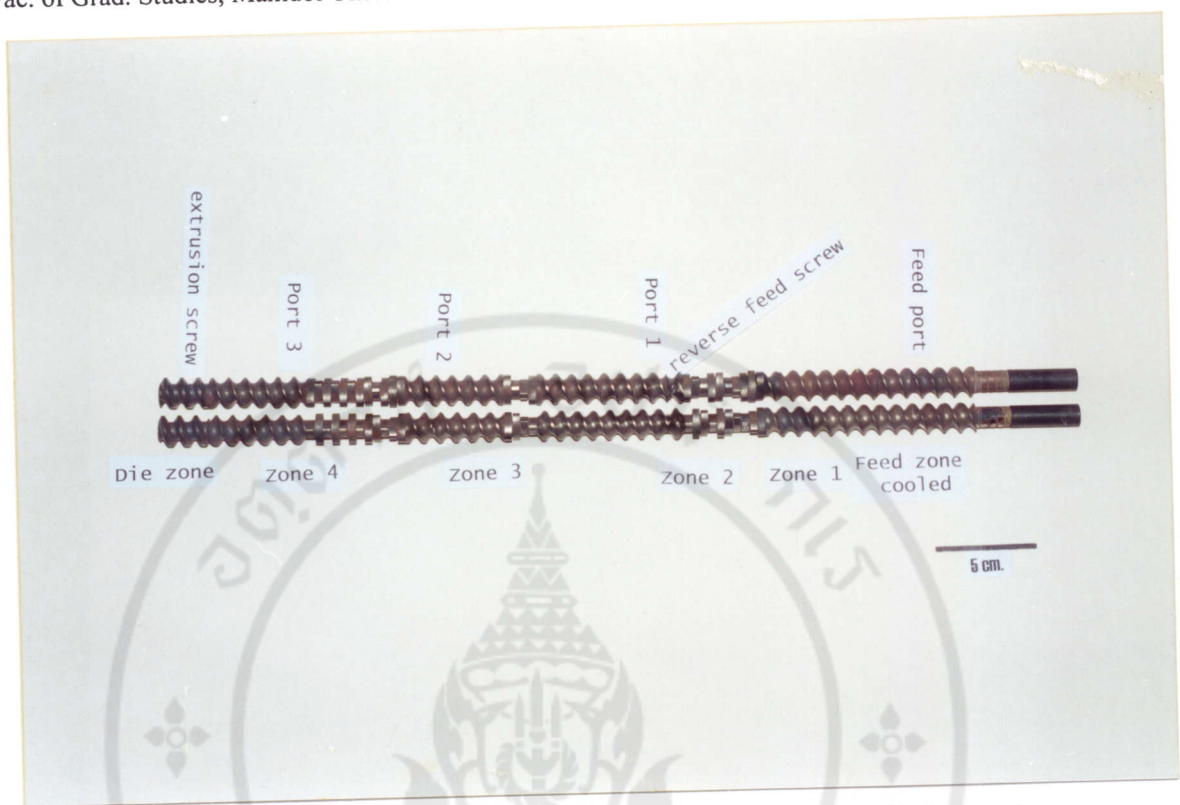

Figure 2.4 The high intensity extruder screw configuration B installed in twin screw extruder (TSE 16 TC 25:1)

Table 2.4 Experimental design

Run	S	C	N
1	A	-1	-1
2	B	-1	-1
3	A	-1	1
4	B	-1	1
5	A	1	-1
6	B	1	-1
7	A	1	1
8	B	1	1
9	A	0	0
10	B	0	0
11	A	0	0
12	B	0	0

In brief, a flow chart describing the sequence of experiments is given in Figure 2.5.

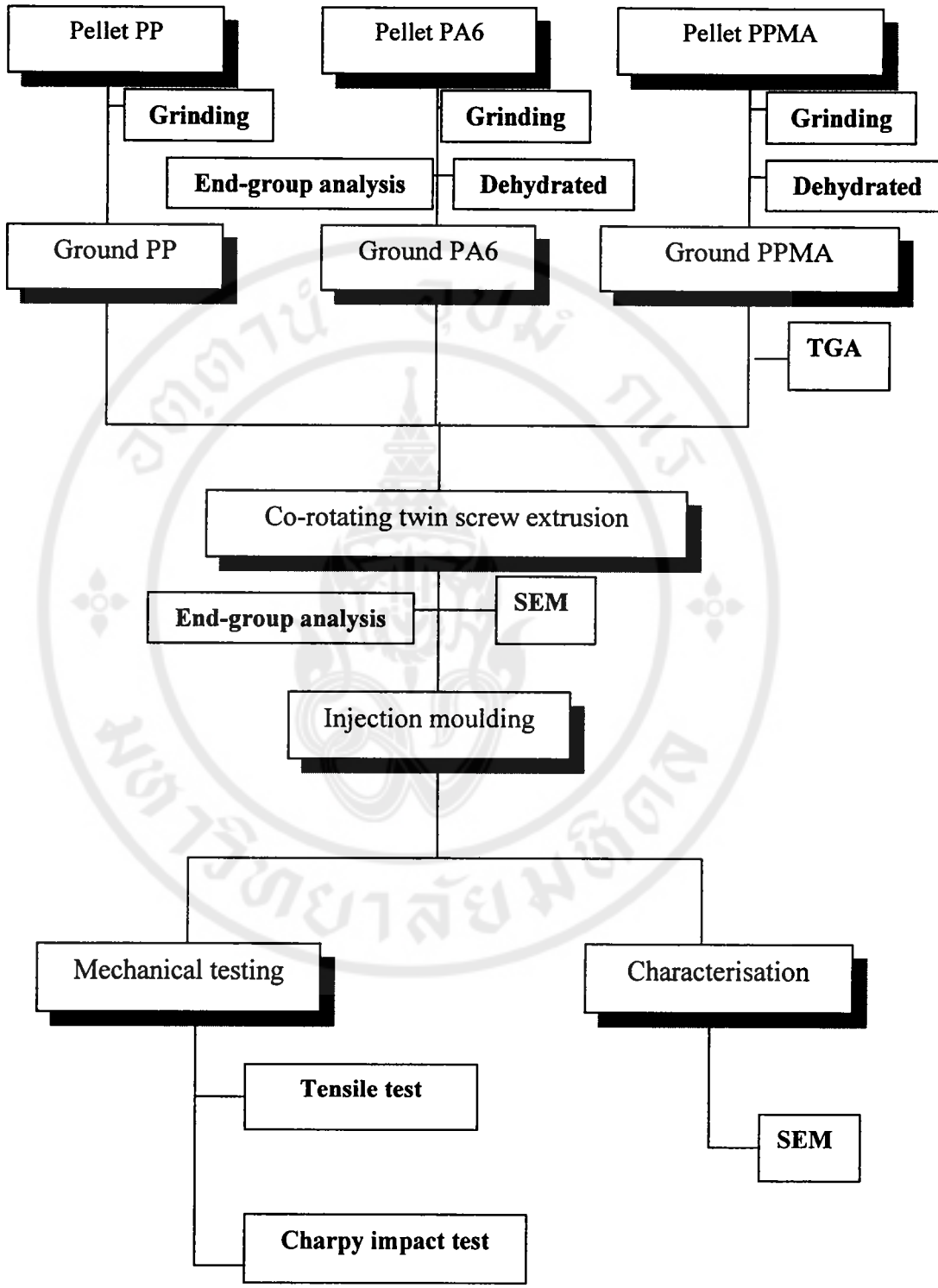

Figure 2.5 Flow chart describing the experiments carried out in the first part

2.2.2 Part II: Non-compatibilised and compatibilised PP/PA6 blends

In the second part, PP/PA6 blends were prepared. Each of blends was coded as follows: S means the extruder screw speed at which the blend was compounded and the following number was its speed, C means compatibiliser content which was applied at the amount of its following number. In addition, the different injection moulder screw speed was operated to prepare the test specimens so H and L at the end of each code mean, respectively, high (170 rpm) and low (50 rpm) injection screw speed. For example, S100C2.5H means this specimen has been compounded at the extrusion screw speed of 100 rpm and the amount of compatibiliser added was experimentally 2.44 vol%, and the injection speed set to shape this specimen was 170 rpm. The experimental formulations of PP/PA6 blends produced in this part are shown as detailed in Table 2.5. The scheme representing the chart diagram shows in Figure 2.6.

Table 2.5 Experimental formulations produced of the PP/PA6 blends prepared in the second part

Code	Polymeric component (PP:PA6:PP-g-MAH) (vol. ratio)	Compatibiliser content (vol%)
$S_{50}C_0$	40:60:0	0.00
$S_{50}C_1$	40:60:1	0.99
$S_{50}C_{2.5}$	40:60:2.5	2.44
$S_{50}C_4$	40:60:4	3.85
$S_{100}C_0$	40:60:0	0.00
$S_{100}C_1$	40:60:1	0.99
$S_{100}C_{2.5}$	40:60:2.5	2.44
$S_{100}C_4$	40:60:4	3.85
$S_{150}C_0$	40:60:0	0.00
$S_{150}C_1$	40:60:1	0.99
$S_{150}C_{2.5}$	40:60:2.5	2.44
$S_{150}C_4$	40:60:4	3.85
$S_{200}C_0$	40:60:0	0.00
$S_{200}C_1$	40:60:1	0.99
$S_{200}C_{2.5}$	40:60:2.5	2.44
$S_{200}C_4$	40:60:4	3.85

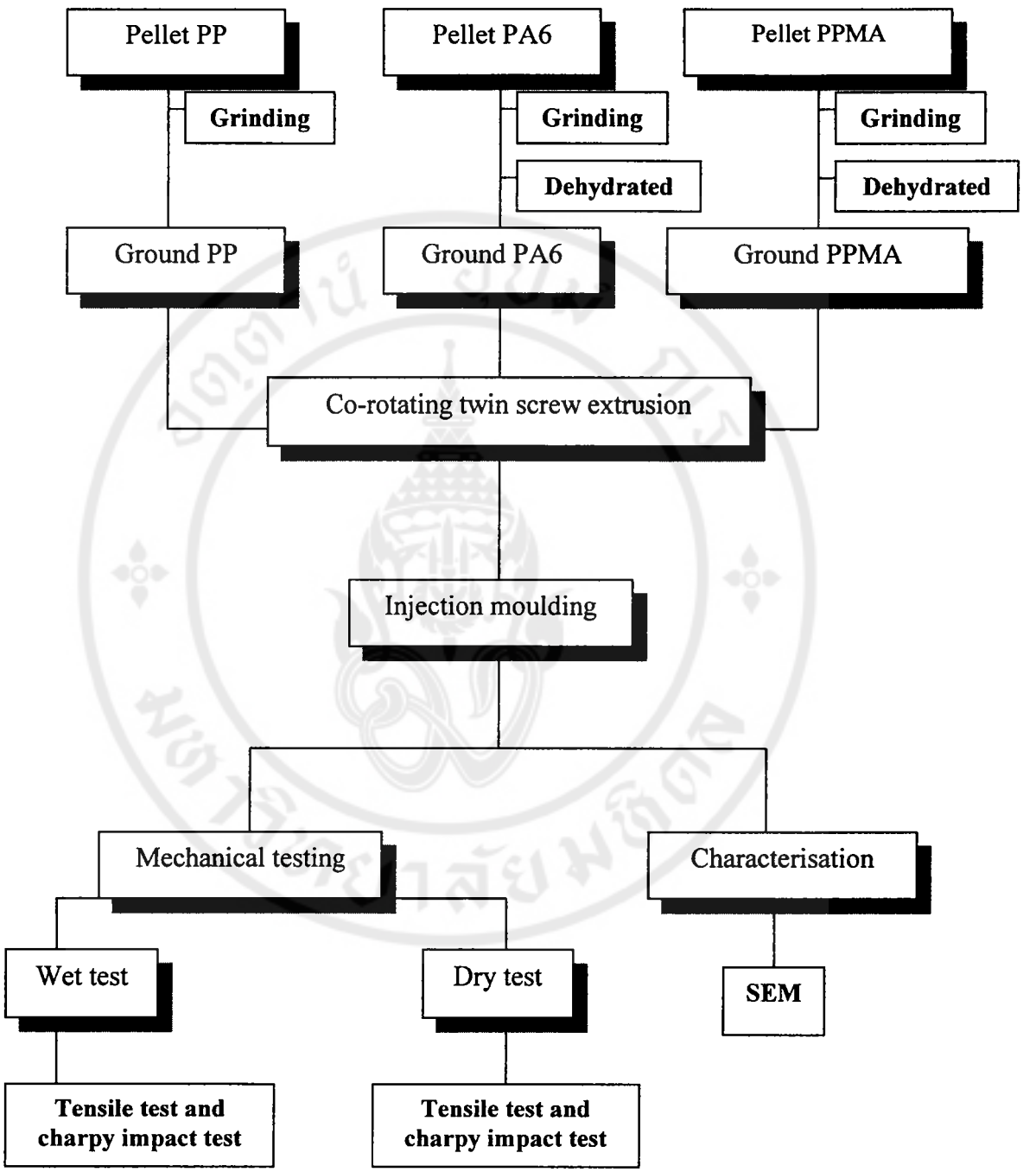

Figure 2.6 Flow chart representing the experiments carried out in the second part

2.3 Characterisation

2.3.1 Phase morphology characterisation

2.3.1.1 Scanning electron microscope (SEM)

Observation of the flattened surfaces was achieved using a Hitachi scanning electron microscope with 15 kV accelerating voltage, using complementary surface preparation techniques; i.e., via etching and staining, to reveal the phase morphology. Before etching or staining, samples were microtomed cryogenically using an RMC MT-7 ultramicrotome equipped with a glass knife at an approximate –50 ^{0}C .

(a) Etching technique

Etching of samples was carried out through the use of boiling Xylene, which selectively dissolves the PP phase, for 3 hours. Afterwards, the whole sample was in a fresh boiling xylene for 1 hour. Methanol was then used to rinse the sample to make sure that xylene was completely washed. Samples were dried and finally sputter coated with Pt-Pd alloy ready for SEM observation.

(b) Staining technique

In order to increase the contrast between the different phases and to minimise the damage of the occlusion morphology caused by etching the sample, a staining technique was chosen. The flattened surfaces were wholly submerged in a solution of ethanol and phosphotungstenic acid (10 % by weight) for 3 days at room temperature, then washed and allowed to dry. To allow for atomic contrast in SEM, the samples were carbon coated using high vacuum thermal evaporation.

2.3.1.2 Image analysis

Measurement of the average diameter of the dispersed phase was accomplished by the use of Image Pro Plus software developed by Media Cybernetics. Number, D_n, and volume, D_v, average diameters were calculated from:

$$D_n = \frac{\sum N_i D_i}{\sum N_i} \qquad (2.2)$$

$$D_v = \frac{\sum D_i V_i}{\sum V_i} \qquad (2.3)$$

Where N_i is the number of particle with diameter D_i

V_i is the total volume of particles with diameter D_i

2.3.1.3 Annealing study

In order to assess the stability of the phase morphology of the PP/PA6 blends in the molten state. An annealing technique was used. Only the specimens 2.4 vol% of compatibiliser were characterised. A small piece of the cut from a tensile specimen was wrapped with aluminium foil and immersed in an oil bath at 230 ^0C for 10 minutes. Afterwards, the small piece was notched and broken using an impact tester under cryogenic temperature. The etching technique was used to prepare the samples before SEM observation.

2.3.2 Mechanical properties

In the first part, the mechanical properties were tested dry, as moulded. In the second part, the mechanical test conditions were divided into 2 methods, namely at dry and wet condition. The dry test was simply accomplished at room temperature, as in the first part. For the wet test, ASTM D-618 (procedure D) was used to condition the specimen. The specimens were prepared by immersion in distilled water with circulating pump operated for 24 hours at $23 \pm 1\ ^{0}C$. The specimens were wiped with a damp cloth, then with a dry cloth, and tested at room temperature. Specimens were only removed from the water, just before the tests were conducted.

2.3.2.1 Tensile properties

The dumbbell specimens of the blends were well kept in desiccators at room temperature for a week to condition them before having their size measured. Shortly after that, the specimens were left overnight at 25 ^{0}C; i.e., under the tensile test conditions. The test conditions were; 20 mm/min crosshead speed with a 5 kN. load cell on an instron 4301 at 25 ^{0}C. The data reported are the mean values from 10 replications.

(a) Yield stress and ultimate tensile stress

Engineering tensile stress at yield and break point were calculated based upon the original cross-sectional area of the test specimen using the following relation:

$$\sigma = \frac{F}{A_0} \qquad (2.4)$$

Where σ is engineering tensile stress (N/m^2)

F is load at yield and break point (N)

A_0 is the initial cross-section area (m^2)

b) Elongation at yield and break

The percentage of elongation at yield and elongation at break were computed in relation to the original gauge length with the following equation:

$$\%Elongation = [\frac{(l - l_0)}{l}]X100 \quad (2.5)$$

Where l is the specimen length at the yield and break point (mm.)

l_0 is the original length (80 mm.)

c) 1 % Secant modulus

Secant modulus is the ratio of stress to corresponding strain, 1% strain, on the stress-strain curve.

$$Secant\ modulus = \frac{stress\ at\ 1\%\ strain}{0.01} \quad (2.6)$$

2.3.2.2 Charpy impact properties

Impact properties were performed in charpy mode. The impact bars were stored at room temperature in a desiccator for one week before having their size measured. The 4 J and 0.5 J hammers were equipped for the unnotched and notched impact testing, respectively. This arbitrary measurement of energy (J) can be converted into

the impact strength (J/m^2) by dividing the total energy dissipated to break the specimen by its cross-sectional area. The data reported are the average values from 10 replications.

2.3.3 Thermal stability

Since the compatibiliser plays a significant role on the blends' properties, its stability throughout the compounding is important. The investigation on the thermal stability of PP-g-MAH was made using a thermal gravimetric analyser (TGA). The pellet form of PP-g-MAH was first dried in a vacuum oven for 3 hours at 80 ^0C and allowed to cool under vacuum. The pellet was then placed in a pan in TGA. The sample was pyrolised and burned from 50 to 700 ^0C at heating rate of 20 ^0C /min under flowing of air while the temperature dependent weight change was simultaneously measured.

2.3.4 Chain-end analysis

About 0.6 g of pure polyamide-6 or blend samples were weighed into the 50 mL round bottom flask and 30 mL of phenol-methanol (70:30 wt%) were added. A water-cooled reflux condensor was attached and the solution was heated on an electric hot plate under flowing nitrogen gas. Only a suitable temperature, at approximate 170 ^0C, to cause gentle reflux of the solvent was required. When the polymer had dissolved, the round bottom flask was removed from the hot plate and the solution was allowed to cool to around 80 ^0C. A few drops of 0.1 percent solution of Thymol blue in water were added. The titrant, 0.02 N aqueous hydrochloric acid, was very

slowly run out from a microburette; the solution was constantly stirred. The walls of the round bottom flask were washed with distilled water. The titration was continued until Thymol blue became a faint pink. The procedure was repeated 2 or 3 times. In addition, pure polyamide-6 was extruded and pelletised. The sample was then prepared in solution and the tritration was also performed. The scheme representing how the amine end-groups are reacted upon the addition of hydrochloric acid in titration is proposed in Figure 2.7.

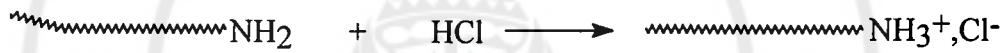

Figure 2.7 The proposed scheme represents the reaction of the amine end group and hydrochloric acid

The amine end-groups of polyamides can react with the maleic anhydride group (MAH) which is grafted onto the polypropylene backbone. Non-reacted amine end-groups can therefore be titrated. Direct titration is the preferred method for general use on account of its rapidity and high accuracy [84].

CHAPTER III

RESULTS AND DISCUSSION

The chapter consists of two parts. In the first part, an experimental design used to investigate the relationships between three independent extrusion variables, namely screw configuration, screw speed, and compatibiliser content upon selected response variables from a PP/PA6 blend is described. In the second part, the effects of three independent variables during sample preparation, namely extruder screw speed, compatibiliser content, and the screw speed of the injection moulder are detailed. In addition, the effects of wet and dry specimen conditioning were reported.

3.1 Part I: Compatibilised PP/PA6 blends

3.1.1 Experimental design

The present study is directed to find the conditions of processing to improve the properties of the compatibilised PP/PA6 blends. *The independent variables* or *independent factors* are the factors that act on the experimental units independently. Three independent factors thought to affect the properties of the PP/PA6 blends are (1) extruder screw speed, (2) the compatibiliser content, and (3) the compounder screw configuration. The factors can be grouped into 2 classes, namely *quantitative factors* and *qualitative factors*. The extruder screw speed and compatibiliser content

are *quantitative factors* whereas the compounder screw configuration is a *qualitative factor*. In addition, there are *response variables*, widely known as *the independent variables*, that change in response to the *level of the independent variables*. Examples include yield stress, tensile modulus, and stress at break. The *levels* of a quantitative factor take numerical values, such as extruder screw speed of 100, 150, and 200 rpm. and compatibiliser content of 1.0, 2.4, and 3.8 vol% while the levels of a qualitative factor are categories of the factor, such as high and low intensity of compounder screw configuration.

3.1.2 Analysis of extrusion

The constituent resins behaved approximately as power law fluids; i.e., $\tau = k\dot{\gamma}^n$. For PP, k = 11.2 kPa·s and n = 0.33, while for PA6, k = 0.7 kPa·s and n = 0.85; τ is the corrected shear stress, n is the non-Newtonian exponent, k is a constant, and $\dot{\gamma}$ is the corrected shear rate. The maximum shear rates were found between the tip of the mixing paddle and the wall of the barrel, whereas the minimum shear rates were in the deepest part of the conveying sections, from the following expression: $\dot{\gamma} = \pi(D - 2h)N/h$; where D is the internal barrel diameter (16 mm), N is screw speed, and h is the distance between the tip of the mixing paddle and the wall of the barrel (0.2 mm) or the channel depth (3.3 mm). The calculated maximum shear rates were 408, 613, and 817 s^{-1} for extruder screw speeds of 100, 150, and 200 rpm, respectively. The minimum shear rates were estimated to be 15, 22, and 30 s^{-1} at extruder screw speeds of 100, 150, and 200 rpm, respectively.

The shear rate in the die opening was estimated from the following equation; $\dot{\gamma} = (4Q_v / \pi r^3)(3n + 1/4n)$, where $n = d\lg\tau / d\lg\dot{\gamma}$, and $Q_v = V_{T,P} m/t$, Q_v is the volumetric melt output rate, $V_{T,P}$ is the specific volume of the melt at temperature, T, and pressure, P, r is the radius of the die orifice (1 mm), m/t is gravimetric output rate, m is mass, and t is time. The shear rate through the circular-section die was around 90 s^{-1}.

3.1.3 Specific mechanical energy (SME)

Specific mechanical energy (SME), given in Table 3.1, during compounding through twin screw extrusion was calculated from $SME = (T/T_{max})(N/N_{max})PQ^{-1}$; the equation is as previously defined in section 2.2. The SME results are derived from the average of ten torque readings. Die pressures during extrusion tabulated here are based on the average of three readings for each sample. Melt temperature, measured by using a direct contact thermocouple, is also included. The standardised Pareto chart was used to determine the standardised effects of the independent variables upon the dependent variables; i.e., the influence of extruder screw speed, screw configuration, and compatibiliser content upon die pressure, SME, and melt temperature.

Table 3.1 Compounding data recorded during the preparation of the PP/PA6 blends through twin screw extrusion, bracketed values report as SD

Run	S	C	N	SME ($kWhrkg^{-1}$)	Die pressure (bar)	Melt temperature (^0C)
1	A	-1	-1	0.032*(0.001)*	13.0*(0.00)*	243.6
2	B	-1	-1	0.061*(0.001)*	13.0*(0.00)*	237.4
3	A	-1	1	0.071*(0.002)*	13.3*(0.50)*	228.1
4	B	-1	1	0.113*(0.003)*	11.0*(0.00)*	242.6
5	A	1	-1	0.036*(0.001)*	15.8*(0.50)*	246.1
6	B	1	-1	0.079*(0.002)*	12.0*(0.00)*	238.6
7	A	1	1	0.069*(0.002)*	17.5*(0.58)*	231.8
8	B	1	1	0.131*(0.003)*	13.8*(0.50)*	248.6
9	A	0	0	0.064*(0.002)*	15.3*(0.50)*	245.0
10	B	0	0	0.112*(0.003)*	11.0*(0.00)*	242.4
11	A	0	0	0.057*(0.002)*	15.0*(0.00)*	243.5
12	B	0	0	0.098*(0.003)*	12.5*(0.58)*	246.2
$\overline{X}^*$				0.061,0.105	15.2,11.8	244.3,244.3
σ^*				0.005,0.010	0.21,1.06	1.06,2.69
$\%CV^{\varphi}$				8.2,9.4	1.4,9.0	0.4,1.1

*, $^{*,\varphi}$ mean, standard deviation, coefficient of variation of centre points, the former is for Run 9 and 11 whereas the latter is for Run 10 and 12. Where S, C, and N define extruder screw configuration, compatibiliser content, and extruder screw speed, respectively

According to the Pareto plot, the dashed line shows the point of 95% confidence below which indicates the insignificant effects of the independent variables upon the dependent variables. As will also be seen, a positive value or a negative value signifies the positive (incremental) and negative (reductive) effect, respectively, of the independent variables on a particular response.

It is seen from Figure 3.1 (a) that the effects of extruder screw configuration and extruder screw speed on SME were significant. This is because the screw speed is proportional directly to SME as expressed in equation 2.1 and screw configuration affected the stress. Therefore, an increase in extruder screw speed and the severity of the extruder screw configuration cause SME to increase. Only extruder screw configuration is found to influence die pressure from a Pareto plot. Increased severity of extruder screw configuration led to a significant decrease of die pressure during extrusion, as illustrated in Figures 3.1 (b) and 3.2.

From Figure 3.3, the combination of high extruder screw speed and severe extruder screw configuration resulted in a significant increase in melt discharge temperature. It may be due to the melt temperatures from the systems were generated from higher viscous heat upon higher shear rates. From the data in Table 3.1, it is found that the melt temperatures of all runs, but Run 3, were higher than the highest temperature set on the electric heater bands on the barrel of the extruder; i.e., 230 ^{o}C. This is because the melt-flow generated heat and caused the temperatures to be increased. In Run 3 and Run 7, the combination of high extruder screw speed and configuration A may have led to a short residence time and low viscous heat dissipation, and hence low melt temperatures.

The samples with even run-numbers were processed with a high intensity twin screw configuration. Compared with the odd run-numbers, which were processed using a low intensity twin screw configuration, the even run-numbers have higher SME. The high intensity compounder screw configuration resulted in higher energy dissipitation during extrusion than the low intensity configuration. The use of a more intense twin screw configuration should generate higher melt temperatures, for example, Run 8, which was prepared using the high intensity configuration had the highest melt temperature.

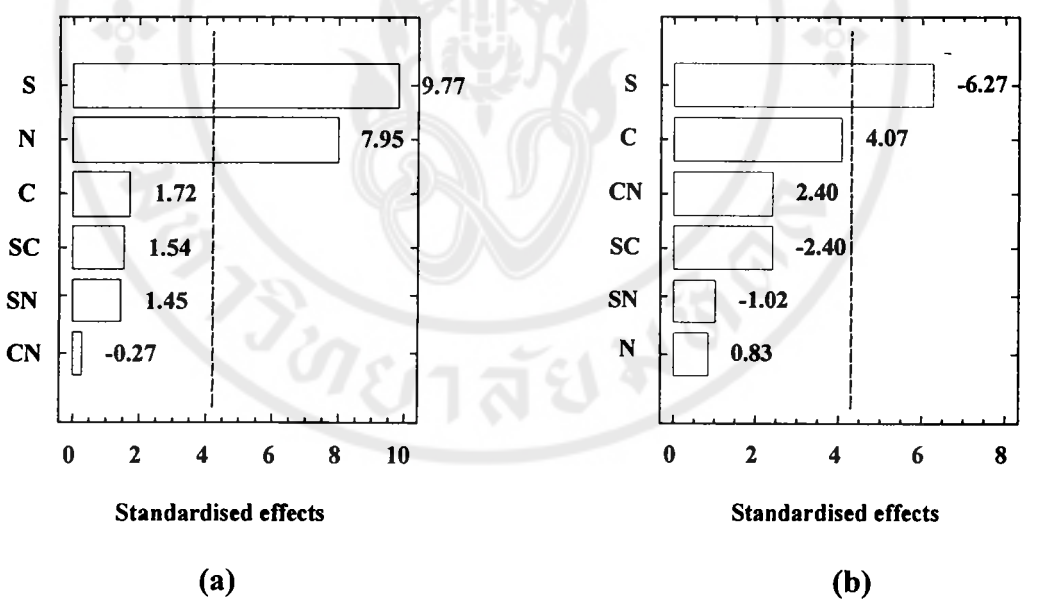

Figure 3.1 Pareto charts for **(a)** SME and **(b)** die pressure of the blends during compounding; S, C, N stand for screw configuration, compatibiliser content, and screw speed, respectively

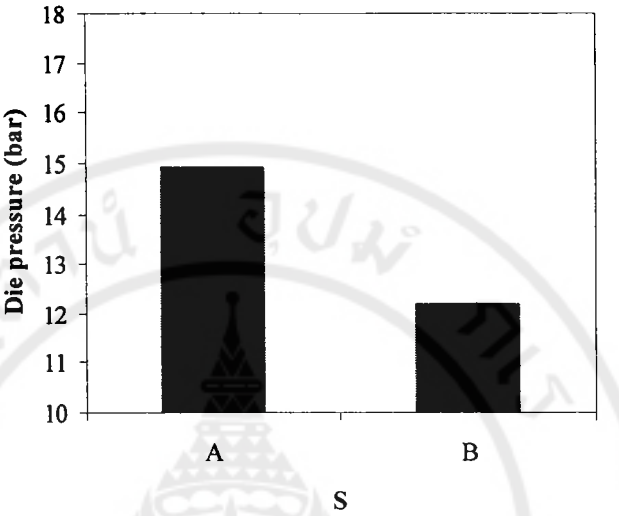

Figure 3.2 The main effects of the independent variables on die pressure; S stands for extruder screw configuration, consisting type A and B

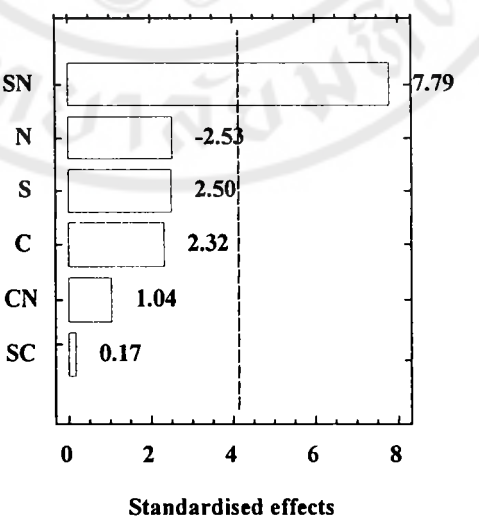

Figure 3.3 A Pareto plot for melt temperature; S, C, N mean screw configuration, compatibiliser content, and screw speed, respectively

3.1.4 Theoretical estimate of melt temperature

In melt processing, solid polymers must be heated to above their melting or softening points. The heat for this purpose comes from two sources. The first is the external heat supplied; i.e., from the electrical heater bands on the barrels of the extruder. The second source is heat generated by viscous dissipitation in a highly viscous fluid being sheared at high shear rates.

The calculation below shows the results of the heat balance analysis during compounding. *Total heat* is the energy absorbed by the blend when the temperature increases by ΔT. *Viscous heat* is the energy of the mechanical work.

The calculated *viscous heat* was used to predict the discharge melt temperature. *Total heat* was estimated from the following equation.

$H_T = W_T \times \text{time}$ (kJ)

$W_T = [(C_{P(PA6)}\,\Delta T) + H_{PA6}]w_{f(PA6)}Q + [(C_{P(PP)}\,\Delta T) + H_{PP}]w_{f(PP)}Q$ ($kJhr^{-1}$)

Where H_T = Total heat

W_T = Total power consumption

$C_{p(j)}$ = Specific heat capacity at constant pressure

ΔT = A change in processing temperature

H_j = Latent heat

$w_{f(j)}$ = weight fraction of j

$w_{f(PP)} = w_{f(PP+PP\text{-}g\text{-}MAH)}$

Q = Output rate

From Appendix A: Specific heat capacity for PA6 and PP are 1.67 and 1.93 $kJkg^{-1}\,{}^{o}C^{-1}$, respectively. While Latent heat of fusion for PA6 and PP are 130 and 100 $kJkg^{-1}$, respectively. An example of the calculation for Run 1 is shown below.

ΔT = Measured discharge melt temperature - Room temperature (30 ^{o}C)

= 243.6 - 30

= 213.6 ^{o}C

Therefore:

Total power PA6 = [(1.67 x 213.6) + 130] x 0.648 x 1.80

= 568 $kJhr^{-1}$

Total power PP = [(1.93 x 213.6) + 100] x 0.352 x 1.80

= 325 $kJhr^{-1}$

Therefore, *total power* used to raise the temperature of solid base polymers from 30 to 243.6 ^{o}C was 568 + 325 $kJhr^{-1}$.

= 893 $kJhr^{-1}$ = 248 W

An example calculation for *viscous heat* is shown below. SME given in Table 3.1 was firstly corrected for the mechanical work consumed through the rotation of the screws alone. Thus, the correction was needed as follows.

$$\text{Corr. SME} = \left(\frac{\left(\frac{T - T_0}{T_{max}}\right)\left(\frac{N}{N_{max}}\right)P_{max}}{Q}\right) \ (kWhrkg^{-1})$$

Where T = Torque on screw during compounding

T_0 = Torque on screw with the barrel empty which was 4.6, 4.9, and 5.0 Nm for an extruder screw speed of 100, 150, and 200 rpm, respectively.

T_{max} = The maximum Torque of the twin screw extruder (24 Nm)

N = Screw speed

N_{max} = The maximum screw speed (300 rpm)

P_{max} = The maximum power of the drive (0.75 kW)

Q = Output rate ($kghr^{-1}$)

Thus, for Run 1:

$$\text{Corr. SME} = \left(\frac{\left(\frac{5.55-4.60}{24}\right)\left(\frac{100}{300}\right)}{1.80} x0.75\right)$$

$$= 0.005 \ kWhrkg^{-1}$$

Viscous heat was therefore estimated using the following equation.

Viscous heat = Corr.SME x Output rate x Time (kJ)

$= 0.005 \times 1.80 \times 3.6 \times 10^3$

= 32.4 kJ (Viscous power = 9 W = 32.4 $kJhr^{-1}$)

It was assumed that there was no transfer of heat due to mechanical work into or out of the melt; i.e., it was an adiabatic process. Hence, viscous heat was assumed only to cause a rise in temperature; i.e., to a temperature that was higher than the set

temperature on the electric heater bands. An increase of temperature, ΔT_0, was calculated from the following equation:

$$W_v = C_{p(PA6)} \times w_{f(PA6)} Q \Delta T_0 + C_{p(PP)} \times w_{f(PP)} Q \Delta T_0$$

$$= (C_{p(PA6)} w_{f(PA6)} + C_{p(PP)} w_{f(PP)}) Q \Delta T_0$$

$$\Delta T_0 = \frac{W_v}{(C_{P(PA6)} w_{f(PA6)} + C_{P(PP)} w_{f(PP)}) Q}$$

Where W_v = Viscous power ($kJhr^{-1}$)

$w_{f(PP)} = w_{f(PP+PP\text{-}g\text{-}MAH)} = 0.352$ ($w_{f(PA6)} = 0.648$)

Thus, melt discharge temperatures were predicted as follows,

$$\Delta T_0 = \frac{32.4}{(1.67 \times 0.648 + 1.93 \times 0.352) 1.80}$$

$$\Delta T_0 = 10.2\ ^{o}C$$

Discharge melt temperature = Barrel temperature + ΔT_0

$$= 230 + 10.2\ ^{o}C$$

$$= 240.2\ ^{o}C$$

Table 3.2 represents the results of the heat balance analysis during compounding.

Table 3.2 The measured and calculated melt-discharge temperatures; the latter assuming that the extrusion process was adiabatic

Run	Measured melt-discharge temp (°C)	ΔT (°C)	Total power ($kJhr^{-1}$)	Corr. SME ($kWhrkg^{-1}$)	Viscous power ($kJhr^{-1}$)	Viscous power to total power (%)	ΔT_0 (°C)	Calculated melt-discharge temp (°C)
1	243.6	213.6	893	0.005	32	3.6	10.2	240.2
2	237.4	207.4	561	0.019	79	14.1	38.8	268.8
3	228.1	198.1	844	0.013	84	10.0	26.6	256.6
4	242.6	212.6	680	0.037	183	27.0	75.6	305.6
5	246.1	216.1	901	0.009	58	6.5	18.4	248.4
6	238.6	208.6	408	0.022	66	16.3	45.0	275.0
7	231.8	201.8	988	0.019	142	14.4	38.8	268.8
8	248.6	218.6	662	0.052	246	37.1	106.3	336.3
9	245.0	215.0	730	0.012	63	8.7	24.5	254.5
10	242.4	212.4	434	0.025	79	18.2	51.1	281.1
11	243.5	213.5	829	0.011	66	8.0	22.5	252.5
12	246.2	216.2	542	0.027	105	19.4	55.2	285.2

From Table 3.2, there are some difference between the measured and the calculated discharge melt temperatures. Nearly all of the calculated values are greater than the measured values. This implies that the extrusion process studied herein was far from adiabatic. *Viscous power* is a minor part in comparison with the *total power* consumption. This specifies that the mixing energy utilitised to melt the constituent

resins results largely from the electric heater bands. Around 5 to 40 % of the power is derived from mechanical work.

In the 16 mm twin screw extruder; i.e., the Prism TSE16, the ratio of surface area to free volume is 0.47 m^2L^{-1}, in comparison with values of 0.31 and 0.16 m^2L^{-1} for the 24 and 48 mm, respectively, with the same centre-line/radius ratio (25/16) of 1.563. Centre-line distance is the distance between the centres of the screws. It was thought that if the surface area to free volume ratio is smaller, the extruder may operate at closer to adiabatic conditions, since there is less area for heat exchange between the melt and the barrel. The viscous heat generated from the samples produced using high severity of extruder screws; i.e., even run-number samples, are higher than those from the samples prepared using low severity.

3.1.5 Phase morphology observation

It was shown in the previous work [89] that the phase inversion point estimated from $\phi_{PP} = (\eta_{PP}\phi_{PA6})/\eta_{PA6}$ using flow data determined at shear rates less than 90 s^{-1} correlated with the observed phase morphology. Where ϕ_{PP} and ϕ_{PA6} are the volume fractions of component PP and PA6, respectively, while η_{PP} and η_{PA6} are the melt viscosities of PP and PA6, respectively. From the expression above, at a shear rate of 38 s^{-1} the predicted phase inversion point was 34 vol% of PA6; the observed co-continuous range was from 30 to 40 vol% PA6. All of the polymer blends analysed in the present work had dispersed phase morphologies with the PA6 forming the continuous phase, or matrix phase, while PP was dispersed. Observed by SEM, the

PA6 phase appears light and the etched PP phase leaves dark holes. The SEM micrographs shown hereafter were shot from two types of specimen, namely lace (taken from the solidified extrudate) and tensile bar specimens (obtained from the core of tensile piece processed through injection moulding). The preparation of these specimens for SEM investigation was as previously stated in 2.3.1.1 (a). The PP domain diameters of the blend samples are displayed in Table 3.3.

The calculation for the number average diameter ($\overline{D}_n$) and volume average diameter ($\overline{D}_v$) of dispersed phase PP was accomplished using equations 2.2 and 2.3, respectively. The PP domain diameters presented in Table 3.3 were calculated from the average of at least 120 particles per position following the work by Ghiam and White [87]. The scale bar used throughout this thesis is 3 μm in length, unless otherwise specified.

Table 3.3 The number ($\overline{D}_n$) and volume ($\overline{D}_v$) average diameters of the domains in the blend samples, the bracketed values are SD

Run	S	C	N	Lace		Tensile bar		Extrusion condition		
				D_n (μm)	D_v (μm)	D_n (μm)	D_v (μm)	Melt temp. (^{0}C)	SME (kWhrkg^{-1})	Die pressure (bar)
1	A	-1	-1	2.51 *(1.00)*	3.80 *(4.80)*	1.55 *(0.76)*	2.81 *(2.44)*	243.6	0.032*(0.001)*	13.0*(0.00)*
2	B	-1	-1	0.43 *(0.31)*	1.04 *(0.32)*	1.05 *(0.56)*	1.93 *(1.17)*	237.4	0.061*(0.001)*	13.0*(0.00)*
3	A	-1	1	0.95 *(0.68)*	3.97 *(1.55)*	1.58 *(0.78)*	2.96 *(2.66)*	228.1	0.071*(0.002)*	13.3*(0.05)*
4	B	-1	1	2 61 *(0.99)*	4.55 *(4.90)*	1.64 *(1.05)*	3.10 *(5.04)*	242.6	0.113*(0.003)*	11.0*(0.00)*
5	A	1	-1	1.26 *(0.65)*	3.97 *(1.70)*	0.74 *(0.45)*	1.38 *(0.69)*	246.1	0.036*(0.001)*	15.8*(0.50)*
6	B	1	-1	0.50 *(0.35)*	1.30 *(0.450)*	0.48 *(0.281)*	0.90 *(0.265)*	238.6	0.079*(0.002)*	12.0*(0.00)*
7	A	1	1	0.49 *(0.283)*	0.93 *(0.26)*	0.45 *(0.29)*	0.79 *(0.29)*	231.8	0.069*(0.002)*	17.5*(0.58)*
8	B	1	1	0.58 *(0.43)*	1.75 *(0.67)*	0.54 *(0.34)*	1.64 *(0.36)*	248.6	0.131*(0.003)*	13.8*(0.50)*
9	A	0	0	1.31 *(0.67)*	2.24 *(2.32)*	0.39 *(0.29)*	1.00 *(0.28)*	245.0	0.064*(0.002)*	15.3*(0.50)*
10	B	0	0	0.96 *(0.97)*	1.78 *(0.97)*	0.60 *(0 35)*	1.06 *(0.38)*	242.4	0.112*(0.003)*	11.0*(0.00)*
11	A	0	0	1 26 *(0.62)*	2.23 *(1.76)*	0 90 *(0 60)*	1.73 *(1.12)*	243.5	0.057*(0.002)*	15.0*(0.00)*
12	B	0	0	0.90 (0.50)	1.85 (1.07)	0.62 (0.37)	1.22 (0.49)	246.2	0.098(0.003)	12.5(0.58)

Table 3.4 Mean, standard deviation, and coefficient of variation of centre points, the former is for Run 9 and 11 whilst the latter is for Run 10 and 12

	Lace		Tensile bar		Extrusion condition		
	D_n (μm)	D_v (μm)	D_n (μm)	D_v (μm)	Melt temp. (^{0}C)	SME ($kW \cdot hr \cdot kg^{-1}$)	Die pressure (bar)
$\bar{X}$	1 29,0.93	2.24,1.82	0.65,0.61	1.37,1.14	244.3,244.3	0.061,0.105	15.2,11.8
σ	0.04,0.04	0.01,0.05	0.36,0.14	0.52,0.11	1.06,2.69	0.005,0.010	0.21,1.06
%CV	2.8,4.6	0.3,2.7	55.9,2.3	37.7,9.9	0.4,1.1	8.2,9.4	1.4,9.0

3.1.6 Effect of independent variables upon dispersed phase size

From the Pareto chart shown in Figure 3.4 (a), the combination of extruder screw configuration and speed significantly increased D_n of the PP domains. The effects of compatibiliser content and extruder screw configuration on D_n of PP the domains was also found to be significant. They considerably decreased D_n of the PP domains. The combination of compatibiliser content and extruder screw speed significantly decreased D_n of the PP domains.

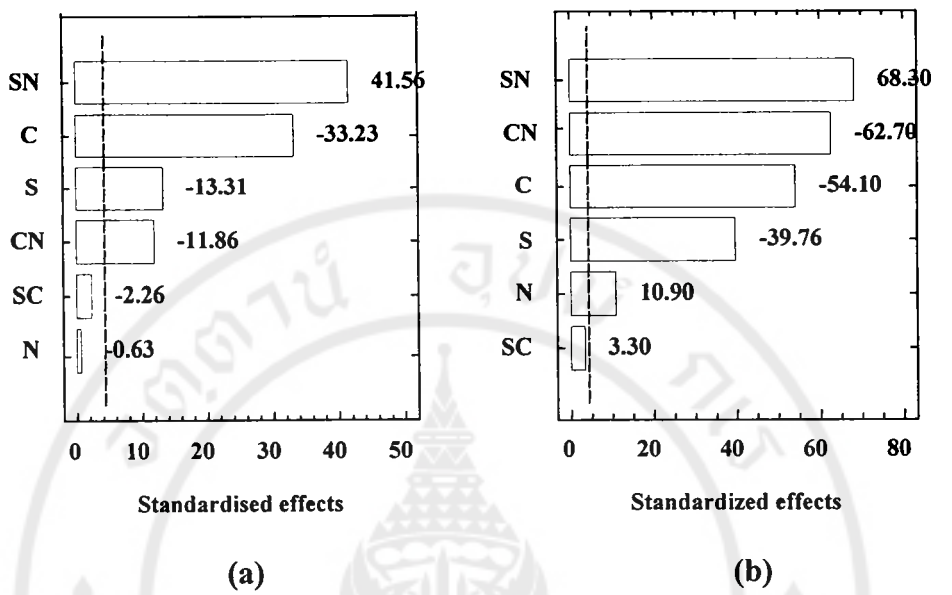

Figure 3.4 A Pareto chart for **(a)** D_n and **(b)** D_v; S, C, N specify screw configuration, compatibiliser content, and screw speed

Some extrudate samples prepared with a 1.0 vol% loading of compatibiliser and high mixing energy had the largest domain sizes. This gave rise to the significant, positive, effect of the combination of S and N upon D_n. An increase in severity of screw configuration resulted in a negative effect upon D_n; i.e, high stress generated during compounding caused the break up of dispersed phase to take place. From Figure 3.4 (a), S and N, due to higher stress, may produce small-sized PP domains but the high interfacial tension between neat PA6 and PP may eventually cause them to coalesce. For example, Run 4 has a number average domain diameter of 2.61 μm.

From Table 3.3, the biggest dispersed phase size, D_n, is shown to be approximately 2.6 μm. Higher amounts of compatibiliser; i.e., 2.4 and 3.8 vol% in the extruded blends led to the smaller domain sizes of below 1.5 μm .

Greater amounts of compatibiliser mean larger quantities of MAH available to react with amine end groups, and hence increase the chance of PP-b-PA6 formation. Therefore, the greater amount of compatibiliser could lead to the smaller dispersed domain size.

From Figure 3.4 (b), extruder screw speed had a significant effect on D_v of the PP domains. The effect of the combination of extruder screw configuration and extruder screw speed was also significant. The combination of extruder screw configuration and extruder screw speed clearly increased D_v of the dispersed domains. In contrast, compatibiliser content, extruder screw configuration, and the combination of compatibiliser content and extruder screw speed reduced D_v of the PP domains.

From the SEM micrographs, displayed in Figure 3.5, the differences in dispersed phase size are shown for the samples produced with the differences in the amount of compatibiliser used during the processing of the blends. Run 1 and Run 4, produced with 1.0 vol% of PP-g-MAH, are clearly found to have bigger dispersed particles; i.e., of around 2.5 μm in diameter in comparison to those of Run 5 and Run 8 whose dispersed domain sizes are 1.26 and 0.58 μm in diameter, respectively. An increase in PP-g-MAH to 3.8 vol% for Runs 5 to 8 led to a reduction in the dispersed phase diameter by almost half.

From Table 3.3, the dispersed phase diameters measured using image analysis software; i.e., both D_n and D_v, declines as the compatibiliser content is higher. Compare Run 1 to Run 5, the dispersed phase size is found to be significantly lower in Run 5 resulting from the difference in compatibiliser content. The other extrusion variables in Run 1 and Run 5 are the same. Recently, it has been reported that the reduction in dispersed phase size was mainly the result from the decrease in interfacial tension [88]. Owing to the reactive maleic anhydride group (MAH) grafted onto PP backbone, the formation of PP-b-PA6 from the reaction between MAH groups and the amine end groups was highly possible [71].

Since PP-g-MAH was, in this case, added during the preparation of the blends, thus the formation of PP-b-PA6 could be also probable. Therefore, the *in-situ* formed PP-b-PA6 might have encouraged the lowering of interfacial tension and enhanced the adhesive strength between the dispersed PP and matrix PA6, and thus led to a reduction in the tendency of the dispersed PP to coalesce.

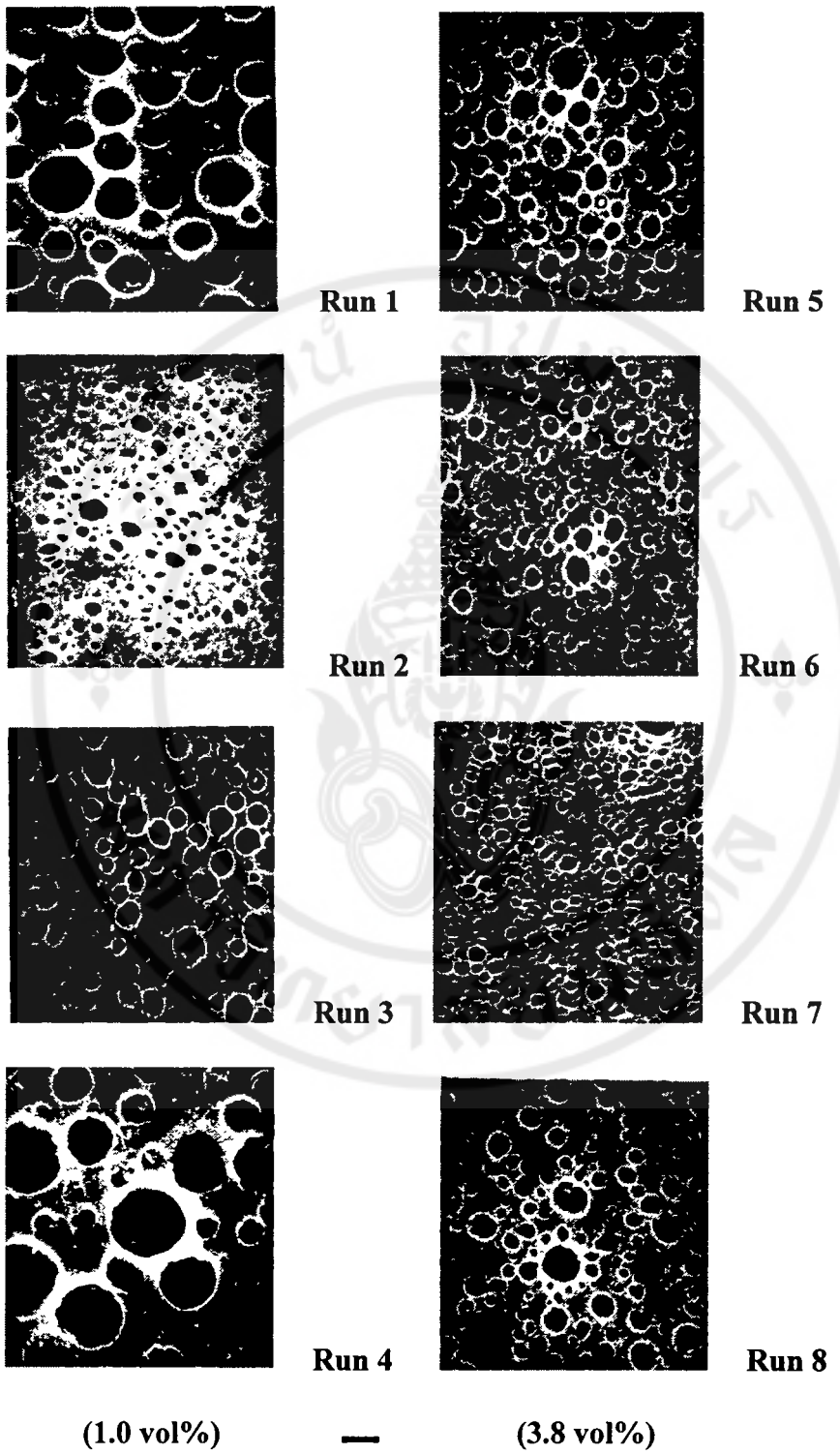

Figure 3.5 The SEM micrographs of etched lace specimens of the blends processed with dissimilar compatibiliser contents

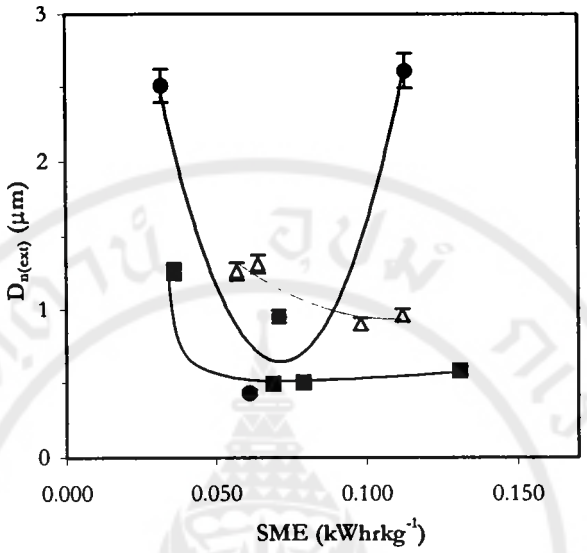

Figure 3.6 The relationship between mean diameter of dispersed domains of the extrudate samples and SME, for samples containing (•) 1.0 vol%, (Δ) 2.4 vol%, and (■) 3.8 vol% PP-g-MAH

Wu [4] reported that the dispersed phase diameters, D_n, of a series of extruded elastomer/PA blends could be described by the following expression: $D_n = 4\Gamma_{1,2}\lambda^{\pm 0.84} / \dot{\gamma}\eta_m$. The model treats the melt flow of the blend as being homogeneous; this is rarely the case. $\Gamma_{1,2}$ is interfacial tension, $\lambda = \eta_d/\eta_m$, $\dot{\gamma}$ is shear rate, η_m is matrix viscosity, and η_d is dispersed phase viscosity. The $\dot{\gamma}\eta_m$ term can be replaced by τ_e, the effective stress during compounding. τ_e may be defined from corr. SME = $((T - T_0)/T_{max})(N/N_{max})PQ^{-1}$, if Q has units of m^3/s and P is in

Watts, an effective stress can be obtained; i.e., corr. SME = τ_e = $W/m^3/s$ = $Nm/s/m^3/s$ = N/m^2 = Pa; thus $D_n \alpha \tau_e^{-1}$ or $D_n \alpha$ corr. SME $^{-1} \alpha SME^{-1}$. $D_{n(ext)}$ the domain diameter in the extrudate is plotted versus SME in Figures 3.6. For compatibiliser contents of 2.4 and 3.8 vol% around mechanical energy inputs of 0.07 $kWhrkg^{-1}$, D_n levels off at even increasing higher SME. For the sample with 1.0 vol% of PP-g-MAH there is a minimum in the $D_{n(ext)}$ versus SME curve around 0.07 $kWhrkg^{-1}$. At higher SME, larger particles are obtained.

S_{ext} is the specific interfacial area between the PP and PA6 phases in the blend; it is related to the number average diameter in the cross-section, D_n, and the volume fraction of the dispersed domains, $\phi_d = V_d/\Sigma V_j$, through these expressions: $V_d = 4\pi nr_v^3/3$, $D_v = 4D_n/\pi$, $r_v = D_v/2$, and hence $S_{ext} = 4\pi nr_v^2$, assuming that the dispersed domains are spheres of uniform size, where r_v is the radius in volume of the domains, n is the number of domains per unit volume, ΣV_j. For example, if D_n = 0.5 μm and ϕ_d = 0.4, then S_{ext} = 4.8 μm^{-1}. The ratio of the interfacial area divided by the volume fraction of compatibiliser in the blend, S_{ext}/ϕ_c, is plotted versus corr. SME in Figure 3.7. From the plot, for the lowest compatibiliser content, the ratio varies by a relatively large amount with corr. SME in comparison to the values for the compounds containing 2.4 and 3.8 vol% of compatibiliser that reach a steady value of approximately $S_{ext}/\phi_c \approx 91\mu m^{-1}$ for corr. SME greater than 0.015 $kWhrkg^{-1}$. That is, the dispersive mixing is largely controlled by the content of compatibiliser at higher SME. The average thickness of the interface, λ, is determined from $\lambda = \phi_I/S_{ext}$,

where ϕ_I is the volume fraction of the interface. Assuming that $\phi_I = \phi_c$, for the samples with 2.4 and 3.8 vol% compatibiliser, $\lambda \approx 11$ nm for corr. SME greater than 0.015 kWhrkg^{-1}. For compatibiliser content of 1.0 vol% there may be insufficient PP-*b*-PA6 formed to cover the surface of the dispersed PP particles and here the interfacial area is unstable.

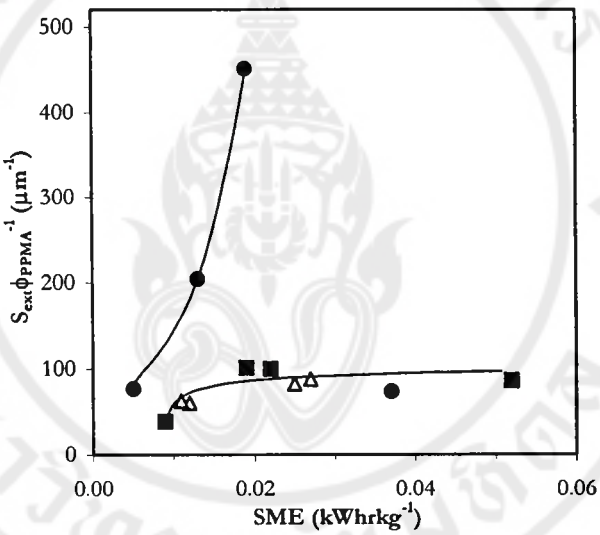

Figure 3.7 A plot of interfacial area of dispersed domains, divided by volume fraction of compatibiliser, versus corr. SME for samples containing (•) 1.0 vol%, (Δ) 2.4 vol%, and (■) 3.8 vol% PP-g-MAH

An estimate of the molecular dimensions of the *in-situ* formed compatibiliser was obtained through the following reasoning. The molecular weight of the PP-g-MAH was estimated through the correlation of MFI with the MFI values of

isotactic polypropylene samples of known $\overline{M}_n$ and $\overline{M}_w$ determined through gel permeation chromatography: ln *MFI* = 2.05lnM_n - 5.99lnM_w + 54.182 [90]. M_w was estimated as 144 kgmol^{-1}. The PP-g-MAH contained 0.45 wt% of MAH; i.e., [MAH] = 4.59 x 10^{-5} molg^{-1} while the average number of anhydride groups per PP chain, f, is thus given by f = [MAH]M_w; f = 6.6. The statistical segment length, b, of isotactic polypropylene in the melt-state at 200 °C is given by b = Rg/Mw$^{1/2}$; b = 34 pm/mol$^{1/2}$, and hence R_g = 12.9 nm [91]. The characteristic ratio, C, for PA6 under theta conditions is 6.35 [92]. The statistical segment length is calculated from b = $(CnL^2/n_s)^{1/2}$, where n is the number of backbone bonds, L is the average bond length in the PA6 backbone (assuming that C-C = 154 pm, CO-N = 133.5 pm and NH-CR = 145.5 pm, L = 150 nm) [93], and n_s is the number of statistical segments, in this case the number of repeat units: $R_g = b(n_s/6)^{1/2}$, and hence R_g = 6.0 nm. The PA6 is assumed to have one amine end-group per molecule; i.e., f = 1. Thus, the reaction of one amine end group with one anhydride functional group of the compatibiliser would result in the formation of a block copolymer with the coil size of the PA6 block around half the size of the PP block. Thus, the estimated average interphase thickness is of comparable size to the radius of gyration of the PP block. The constancy of the ratio S_{ext}/ϕ_c at higher mixing stresses may correspond to saturation of the PA6 dispersed particles with the *in-situ* formed PP-b-PA6. The generation of fresh interface would be achieved only by doing work against the interfacial tension of the 'bare' PA6/PP interface. An experimental value for the PA6/PP interfacial tension is 9.5 mN/m at 260 °C [94].

The power dissipated per unit volume during plasticisation, P, in the injection moulder was taken as $P = \eta(\dot{\gamma}_c)$, where η is the steady shear viscosity at shear rate, $\dot{\gamma}_c$, in the channel of the screw in the metering zone; for injection moulder D, the internal barrel diameter, was 24 mm, N, the screw speed, was 100 rpm, and h, the screw channel depth, was 2 mm. Thus, $\dot{\gamma}_c = 52\ s^{-1}$. Specific mechanical energy (SME) input during plasticisation, SME, was calculated SME = Pt_p, where t_p is the plasticisation time (5 s); SME = 7.5 MJm^{-3} at 230 °C. The shear rate in the nozzle, $\dot{\gamma}_N$, was estimated from the same method used to estimate the shear rate in the extruder die. In this case, Q = $V_{T,P}m/t_I$, where Q is the melt injection rate, m is the short weight (15 g), $V_{T,P}$ is the specific volume of the melt at temperature, T, and injection pressure, P (3.4 MPa), t_I is the injection time (2 s), and r is the radius of the nozzle orifice (1.25 mm): $\dot{\gamma}_N$ = 6,500 s^{-1}, assuming a specific melt volume 1.33 cm^3g^{-1} for melts at 230 °C under 3.4 MPa of pressure. Cooling of the moulding was described by the Fourier equation solved for the bi-direction heat transfer from a flat sheet. Fourier equation is expressed as follows; $\partial T/\partial t = \alpha(\partial^2 T/\partial x^2)$ where T is the temperature, t is time, α is the thermal diffusivity, and x is the distance between the centre of the moulded specimen, and its surface that was in contact with the cooling water at 30 °C. The thermal diffusivity is determined from $\alpha = \kappa/\rho C_P$; κ is the specific thermal conductivity, ρ is the density, and C_p is the specific heat capacity. It was assumed that α was constant over the temperature change. The dimensionless Fourier parameter, F_0, is calculated $F_0 = \alpha t/x^2$. In this case, x is half the moulding

thickness; i.e., 3.2 mm/2. A plot of temperature gradient $\Delta T = (T_{x,t} - T_w)/(T_0 - T_w)$ against F_0 for a cylinder was used to find F_0 at ΔT and hence the time to reach $T_{x,t}$ may be found [95]. T_w is the temperature of the cooling water (30 °C), T_0 is the initial melt temperature (typically 240 °C), $T_{x,t}$ is the temperature at x after time t. $T_{x,t}$ was taken as the estimated temperature where the crystal growth rate of polyamide was a maximum, that is at 180 °C, 40 °C below the melting point of 220 °C, 150 $\mu m min^{-1}$ [96]; $\Delta T = 0.71$, $F_0 = 0.25$, and hence t = 6.4 s. The solidification time was 9.9 s.

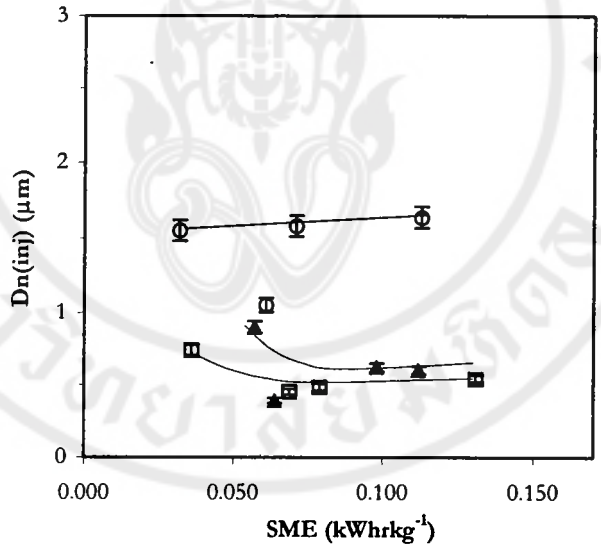

Figure 3.8 The relationship between mean diameter of dispersed domains of moulded tensile bars and SME, for samples (o) 1.0 vol%, (▲) 2.4 vol%, and (□) 3.8 vol% of PP-g-MAH

From a plot between mean diameter of dispersed domains of moulded tensile bar versus SME during compounding in Figure 3.8, it shows that higher concentrations of

PP-g-MAH caused a reduction in dispersed domain dimension. For SME greater than 0.07 $kWhrkg^{-1}$, the dispersed domain diameters tend to reach a stable minimum at a diameter of about 0.5 μm, for the 3.8 vol% PP-g-MAH content.

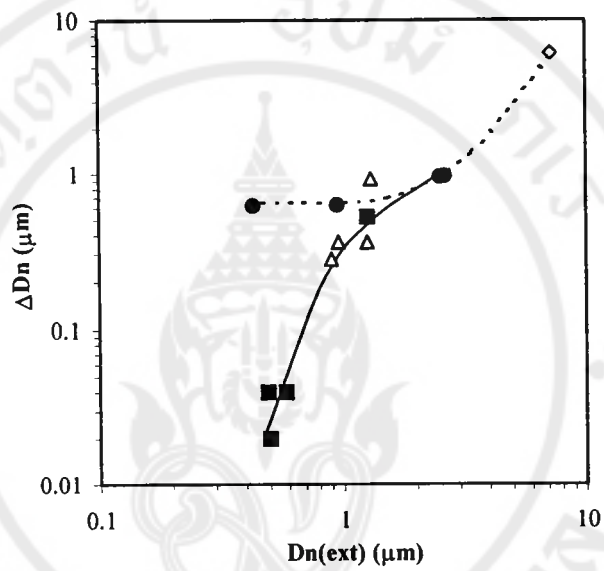

Figure 3.9 A plot of the difference of mean diameter between the extrudate samples and the moulded tensile bars versus mean diameters measured from extrudate laces for samples containing (•) 1.0 vol%, (Δ) 2.4 vol%, (■) 3.8 vol.% PP-g-MAH, and ◊ for the same sample containing no PP-g-MAH taken from ref [89]

The stability of the PP dispersion formed in the extruder during injection moulding was quantified through the difference, ΔD_n, expressed as follows: $\Delta D_n = \left| D_{n(ext)} - D_{n(inj)} \right|$. Figure 3.9 shows a plot of the difference of the measured domain diameters between extrudate and moulded samples against the initial domain

sizes measured from extrudate samples. There is little difference between the domain sizes measured from extrudate and tensile bar for the samples processed with high loading of compatibiliser content of 3.8 vol% and high mixing energies. At a lower compatibiliser content of 2.4 vol%, the difference becomes larger. Figure 3.9 implies that the larger PP domain sizes measured from the extrudate laces tend to be changed the most during injection. Apparently, the flow conditions in the injection moulder were sufficiently vigorous to change the domain dimension of particles of mean diameter of 1 μm and larger. The smallest fraction of particles with mean diameters around 0.5 μm were not greatly altered during injection moulding.

3.1.7 Amine ($-NH_2$) end groups analysis

Since polyamide-6 possesses amine end groups, which can readily be reacted with acid, such as hydrochloric acid, titration provides the possibility to determine the number-average molecular weight ($\overline{M}_n$). Firstly, the results of direct titration of the amine end groups of pure polyamide-6, which was processed differently, was carried out to investigate the influence of processing upon molecular weight. The results are displayed in Table 3.5 (a). The samples were PA6 as received, PA6 as extruded, and PA6 as blended; i.e., the PP/PA6 (40:60 vol/vol) blend without compatibiliser. Table 3.3 (b) shows the results of direct titration of the polymer blend samples; where $[NH_2]$ is the concentration of amine end-group in the PA6, in the units of μmol per gram of PA6.

Table 3.5 (a) Amine end-group concentrations of PA6 determined through titration using HCl

PA-6 sample	$[NH_2]$ ($\mu mol g^{-1}$)	$\overline{M}_n$ ($gmol^{-1}$)
PA-6 as received	49.1*(0.12)*	20,400*(87.10)*
PA-6 as extruded	52.5*(2.66)*	19,000*(968.56)*
PP/PA-6 as blended	51.6*(0.35)*	19,400*(152.68)*

An example of the calculation used was as follows:

0.2125 g of pure PA-6 was dissolved in a phenol-methanol mixture 70:30 w/w (30 mL). The solution was titrated using 0.48 cm^3 of 0.0217 M HCl. The end group concentration of NH_2 was calculated:

$$[NH_2] = \frac{[HCl]V_{titrant}}{1000}$$

$$[NH_2] = \frac{(0.0217 \times 0.48)}{1000} = 1.04 \times 10^{-5} \text{ mol}$$

Therefore,

$$[NH_2]_{gPA6} = \frac{[NH_2]}{M_{PA6}}$$

$$= \frac{1.04 \times 10^{-5}}{0.2125} \qquad = 4.90 \times 10^{-5} \ gmol^{-1}$$

Where M_{PA6} = Mass of PA6

$[NH_2] = (4.90 \times 10^{-5}) \times (1 \times 10^{6}) = 49.0 \quad \mu molg^{-1}$

$$\overline{M}_n = \frac{1}{49.0 \times 10^{-6}} = 20{,}408 \quad gmol^{-1}$$

The pure PA6 has $\overline{M}_n$ of 20,400 $gmol^{-1}$.

Each sample was titrated 2-3 times and the means of these results are listed in Table 3.3 (a). The polyamide-6 (PA6) has a number average molecular weight of 20,400 $gmol^{-1}$ that decreased to around 19,000 $gmol^{-1}$ during extrusion. This may be due to the stress during compounding.

For the blends containing PP-g-MAH compatibiliser, the amine end group is much more reactive with MAH, compared to the amide groups. However, there has been a report that a MAH/amide reaction forming an imide is possible, but less likely. It is believed that the anhydride group grafted onto the polypropylene backbone can preferably react with amine end groups on the polyamide-6. Only the unreacted amine end-groups can therefore be titrated upon addition of hydrochloric acid. The results of amine end-group titrations of the compatibilised blends are shown in Table 3.5 (b).

Table 3.5 (b) The results of amine end-groups titration of the compatibilised PP/PA6 blend samples

Sample (Run)	Weight fraction PP:PA6:PP-g-MAH	Measured residual $[NH_2]$ (B) $(\mu mol\,g^{-1})^{\#}$	Extent of reaction (%)	Calculated residual* $[NH_2]$ (A) – (C) $(\mu mol\,g^{-1})$*	Calculated extent of reaction (%)
1	0.34:0.65:0.01	47.0*(2.33)*	8.9	50.9	1.2
2	0.34:0.65:0.01	50.3*(3.79)*	2.5	50.9	1.2
5	0.33:0.63:0.03	44.5*(0.24)*	13.8	49.2	4.7
11	0.34:0.64:0.02	45.6*(1.16)*	11.6	50.1	2.9

* Assuming that 100% of the available anhydride functional groups react with amine end groups.

per gram of PA6 phase

The calculation used was as follows:

For example, in sample 1, 0.2051 g of the blend was dissolved in a phenol-methanol mixture 70:30 w/w (30 mL).

The weight of PA6 in the blend was calculated from:

Weight of PA6 in the blend, $M_{PA6} = M_{sample}\, w_{PA6}$

$$= \frac{(0.2051 \times 684.92)}{(362.27 + 684.29 + 9.05)} \quad g$$

$= 0.1330$ g

Where w_{PA6} = Weight fraction of PA6

Total NH_2 available for reaction with MAH was thus calculated from:

$$[NH_2] = \frac{0.1330 \times 10^6}{19{,}400\,*} \quad \mu mol$$

$= 6.85$ μmol

The concentration of NH_2 per gram of PA6 was:

$$[NH_2] \text{ per gram of PA6} = \frac{6.85}{0.1330} \quad \mu mol g^{-1}$$

Total $[NH_2]$ per gram of PA6 $= 51.5$ $\mu mol g^{-1}$ (A)

*19,400 $gmol^{-1}$ was used as $\overline{M}_n$ of the extruded PP/PA6 blend without compatibiliser.

0.27 cm^3 of 0.0217 M HCl was consumed to reach the end-point of the titration.

Therefore, mol HCl = mol of unreacted NH_2 after extrusion

$$\text{Unreacted } NH_2 = \frac{0.27 \times 0.0217}{1{,}000} \quad mol$$

$$= \frac{0.27 \times 0.0217}{1{,}000} \times 10^6 \quad \mu mol$$

$= 5.86$ μmol

The concentration of unreacted NH_2 was computed from:

$$= \frac{\text{Unreacted}NH_2}{M_{PA6}}$$

$$= \frac{5.86}{0.1331}$$

$$= 44.0 \qquad \mu mo\,lg^{-1} \qquad (B)$$

The concentration of unreacted NH_2 listed in Table 3.2 (b) was from the average of three titrations, therefore 47.0 $\mu molg^{-1}$ with S.D. 2.33.

The weight of PP-g-MAH in 0.2051 g of the blend was calculated as follows:

$$M_{PP\text{-}g\text{-}MA} = M_{sample}\, w_{PP\text{-}g\text{-}MAH}$$

$$= \frac{0.2051 x 9.05}{(362.27 + 684.29 + 9.05)} \quad g$$

$$= 1.76 \times 10^{-3} \quad g$$

Where $w_{PP\text{-}g\text{-}MAH}$ = Weight fraction of PP-g-MAH

PP-g-MAH has 0.45 %wt. of MAH, thus the weight of MAH was calculated from:

$$M_{MAH} = \frac{(1.76 \times 10^{-3}) x 0.45}{100} \quad g$$

$$= 7.92 \times 10^{-6} \quad g$$

The number of moles of MAH available to react with NH_2 was calculated:

$$= \frac{(7.92 \times 10^{-6}) x (10^{6})}{98.06^{*}} \quad \mu mol$$

$$MAH = 8.08 \times 10^{-2} \quad \mu mol$$

*MW of MAH used in the calculation was 98.06 $gmol^{-1}$.

The maximum extent of reaction that may take place is when 100 % of the MAH groups react with NH_2 in the ratio of 1:1, hence the result was expected;

Mol of unreacted NH_2 = Total mol of NH_2 - mol of MAH

$= (A) - (C)$

$= 6.85 - (8.08 \times 10^{-2})$ μmol

$= 6.77$ μmol

$= \frac{6.77}{0.1330}$ $\mu molg^{-1}$

$= 50.9$ $\mu molg^{-1}$ (C)

In every sample the expected value of the residual amine end-group concentration was slightly greater than the value obtained. That is not all of the remaining [NH_2] was available for reaction during titration. The phase morphology may have hindered dissolution of the polyamide-6. There would have been some polyamide-6 occluded in the polypropylene dispersed phase. The titration results therefore represent only the amine end groups that can be dissolved, but not the total amine end-groups.

This idea is supported by the SEM photomicrograph in Figure 3.10 (a). The features are examined in Figure 3.10 (b). Moreover, the differences between the [NH_2] concentrations of the different runs were of comparable magnitude to the experimental error; thus, the measured differences are not significant.

(a)

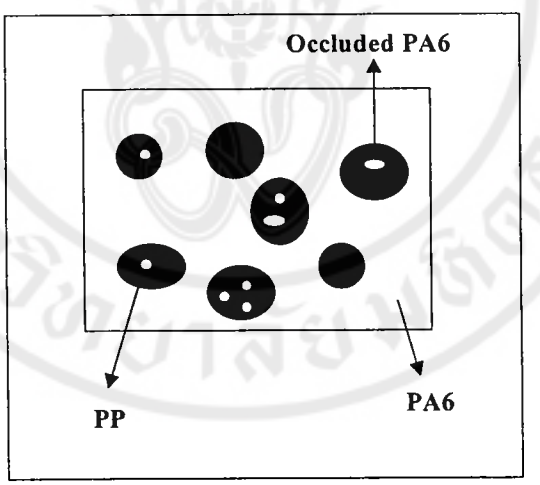

(b)

Figure 3.10 (a) SEM micrograph and **(b)** a schematic representation of the phase morphology of the compatibilised PP/PA6 blends showing occluded PA6 within PP domains that may disturb amine end-groups analysis

3.1.8 Thermal stability of materials used in the study

Maleic anhydride grafted onto polypropylene backbone, PP-g-MAH, was used as the compatibilising agent for the PP/PA6 blends. The properties of polymer blends depend heavily on the amount of compatibiliser added to the blend system. It is also important that the compatibiliser must be stable under the processing conditions. The thermal stabilities of the compatibiliser, PP, and PA6 are shown in Figure 3.11.

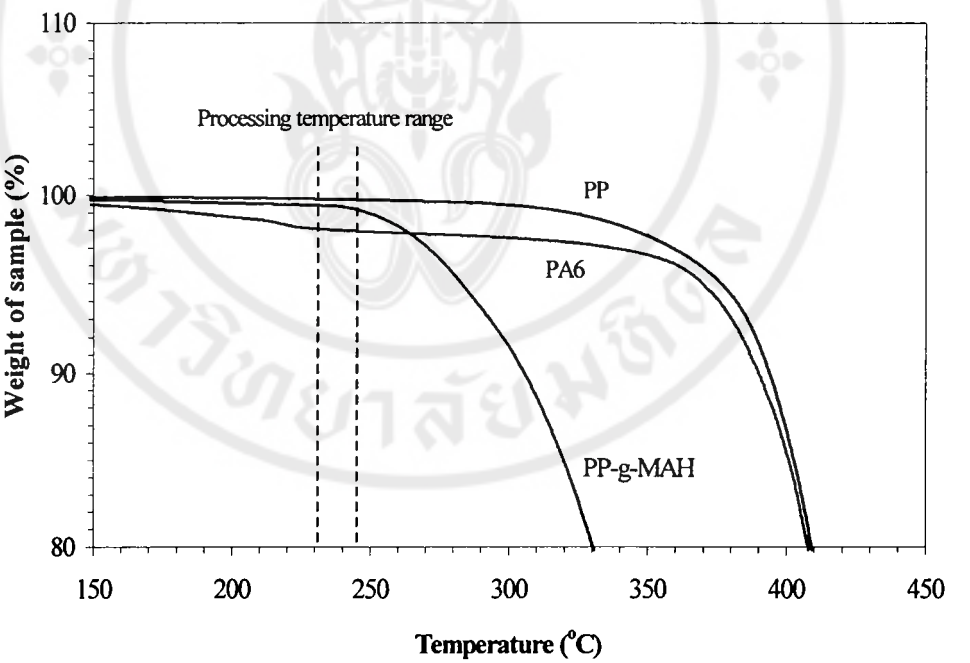

Figure 3.11 The TGA plot indicates the thermal stability in air of the compatibiliser (PP-g-MAH), polypropylene (PP), and polyamide-6 (PA6)

As displayed in Figure 3.11, the weight of PA6 fell by about 2 wt% at around 210 °C. Further increasing of temperature, however, plays an insignificant role in lowering weight of PA6 until 360 °C, whereafter the weight of PA6 sharply drops.

This tendency implies that PA6 can be stable during processing conditions; i.e., temperatures in the range 230-245 °C. Drastic changes in the weight of the compatibiliser and PP are observed at about 250 and 320 °C, respectively. PP is relatively stable but grafting of MAH to form PP-g-MAH worsens its thermal stability. It can thus be concluded that the compatibiliser is the most vulnerable material to higher temperatures during compounding. Within the temperature range employed in this work; i.e., 230-245 °C, the compatibiliser should have adequate stability. However, under high shearing conditions, significant degradation may take place.

3.1.9 Mechanical properties of the blends

The mechanical properties of the polymer blends are presented in Table 3.6. The processing conditions are also included. The following discussion is derived largely from the experimental error of the experimental unit determined from the repetition study of Run 9 to Run 12.

The standardised Pareto plot was used to determine the influence that each variable has on the properties of the blends listed in Table 3.6.

Table 3.6 Mechanical properties of the compatibilised PP/PA6 blends, the bracketed values are SD

Run	S	C	N	Yield stress (MPa)	Yield strain (%)	Strain at break (%)	Initial modulus (MPa)	Secant 1% modulus (MPa)	Notched impact strength (kJ/m^2)	Unnotched impact strength (kJ/m^2)
1	A	-1	-1	52.7*(0.68)*	5.8*(0.16)*	11.8*(0.79)*	1464*(85)*	1721*(89)*	3.75*(0.91)*	65.5*(17.01)*
2	B	-1	-1	54.8*(0.86)*	6.1*(0.19)*	11.1*(0.80)*	1429*(169)*	1603*(122)*	3.74*(0.22)*	76.5 *(5.11)*
3	A	-1	1	55.1*(0.53)*	5.7*(0.20)*	11.0*(0.77)*	1504*(80)*	1758*(51)*	3.74*(0.22)*	84.7 *(7.59)*
4	B	-1	1	54.1*(0.87)*	5.3*(0.34)*	8.6*(1.09)*	1547*(114)*	1773*(65)*	2.97*(0.21)*	54.4 *(8.89)*
5	A	1	-1	53.0*(0.57)*	6.3*(0.28)*	28.9*(11.87)*	1247*(110)*	1492*(169)*	5.29*(0.50)*	N/B
6	B	1	-1	52.7*(0.94)*	5.7*(0.25)*	26.1*(2.90)*	1378*(62)*	1658*(49)*	6.28*(0.74)*	N/B
7	A	1	1	53.5*(0.93)*	5.3*(0.31)*	22.2*(11.81)*	1475*(230)*	1758*(113)*	5.96*(0.96)*	N/B
8	B	1	1	54.9*(0.92)*	5.7*(0.26)*	20.9*(4.73)*	1352*(109)*	1690*(61)*	6.34*(0.63)*	N/B
9	A	0	0	53.1*(0.65)*	5.6*(0.12)*	28.6*(3.57)*	1517*(56)*	1737*(52)*	5.01*(0.34)*	88.0*(10.47)*
10	B	0	0	54.6*(0.86)*	6.1*(0.19)*	22.1*(3.15)*	1338*(181)*	1608*(62)*	6.56*(0.78)*	N/B
11	A	0	0	53.9*(0.75)*	5.8*(0.19)*	28.4*(3.71)*	1406*(59)*	1699*(61)*	5.12*(0.18)*	N/B
12	B	0	0	54.7*(1.30)*	5.8*(0.26)*	24.9*(7.40)*	1380*(107)*	1639*(86)*	5.21*(0.18)*	N/B
13	-	-	-	47.3*(0.50)*	-	6.4*(0.20)*	-	-	3.00*(0.10)*	27.0 *(1.60)*

N/B not broken, sample number 13 was prepared using agitator screw C, no compatibiliser, and a screw speed of 150 rpm

3.1.9.1 σ_y (Yield stress) and ε_y (Yield strain) of samples

The Pareto plot in Figure 3.12 (a) suggests that no independent variable influenced the yield stress of the blends. From Table 3.6, the yield stress is almost unchanged throughout the variation of the independent variables. The yield stress varies from nearly 53 (Run 1) to 55 (Run 3) MPa. While the yield stress of Run 13, containing no compatibiliser as obtained from a previous work of the same blends [89], was only 47.3 MPa.

The Pareto chart displayed in Figure 3.12 (b) also signifies the standardised effect of every independent variable used in this work on yield strain. None of independent variables, however, are found to influence yield strain. As shown in Table 3.6, yield strain varies over the range 5.3% (Run 7) to 6.3% (Run 5). The variation is not significant in comparison with the experimental error.

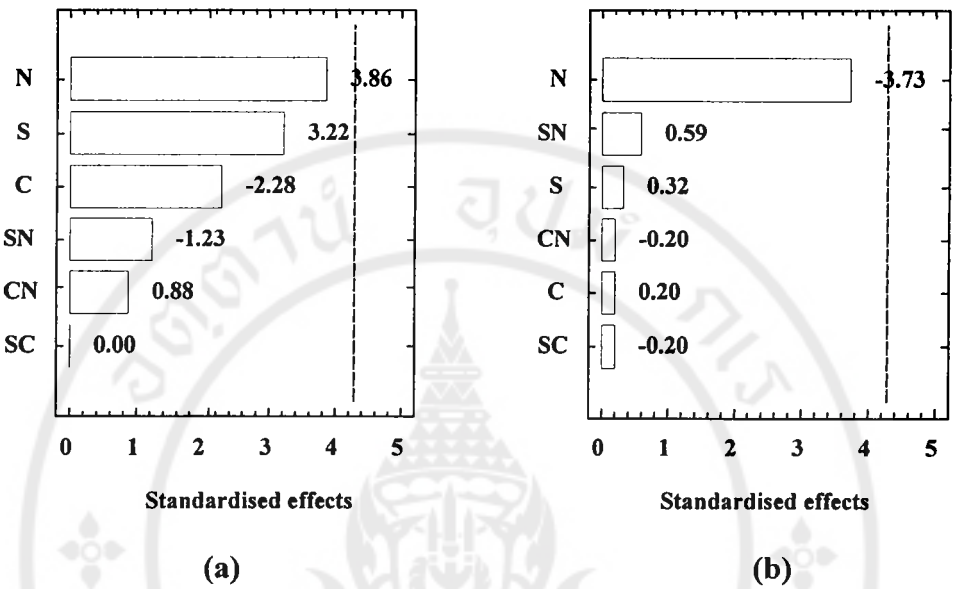

Figure 3.12 The Pareto charts for **(a)** yield stress and **(b)** yield strain

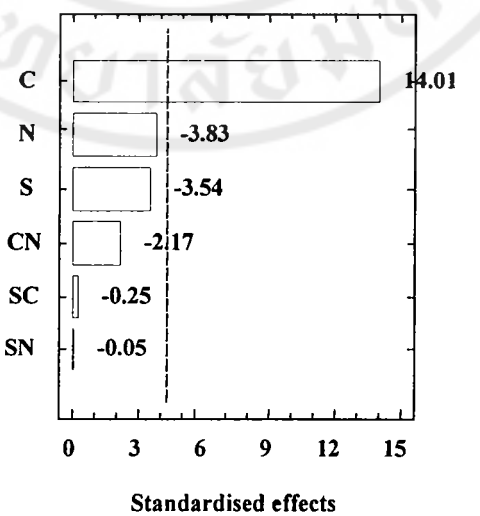

Figure 3.13 The Pareto chart for elongation at break

3.1.9.2 ε_b (Elongation at break)

As displayed in Figure 3.13, the compatibiliser content has the greatest standardised effect on the elongation at break of the blends. Whilst the other variables' effects are found to be of no significance. The ductility of the blends was markedly improved, as shown in Table 3.6, upon the introduction of compatibiliser. The compatibiliser added at 3.8 vol% led to a nearly two-fold improvement in elongation at break, compared with that of the blends with 1.0 vol%. The PP-b-PA6 formation from the reaction of MAH and amine end group may take place. The obtained results, therefore, stem from the *in-situ* formed PP-b-PA6, thereby the interfacial adhesion between the immiscible PP/PA6 components could be strengthened.

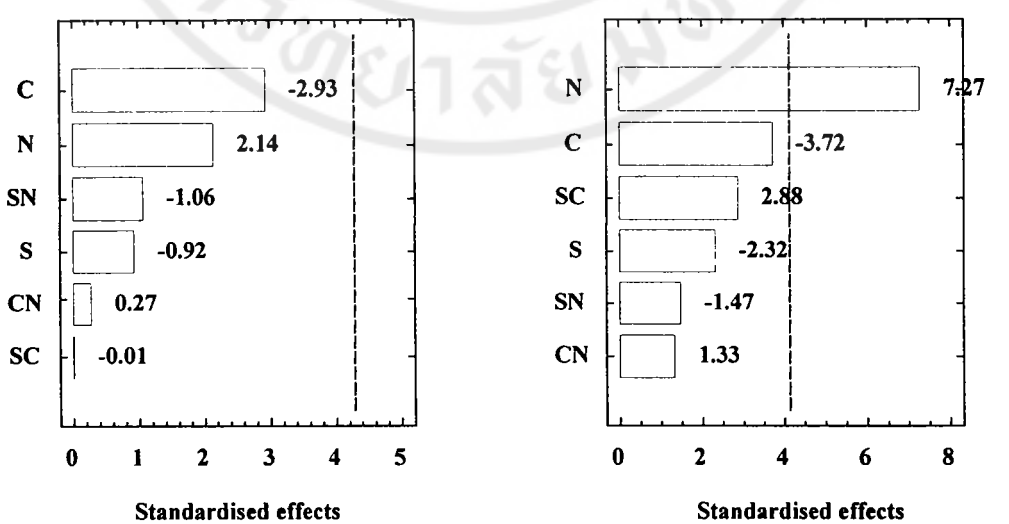

Figure 3.14 The Pareto charts for **(a)** initial and **(b)** secant 1 % modulus

3.1.9.3 Initial and secant 1 % modulus

Pareto plot in Figure 3.14 (a) reveals the insignificant effect of all independent variables on initial modulus. The Pareto plot in Figure 3.14 (b) shows the standardised effects of all independent variables applied in the present study on secant 1% modulus. The positive standardised effect of extruder screw speed is observed, whereas those of the other variables are not significant. From Table 3.6, it is clear that secant 1% modulus of the blends was enhanced significantly at the operation of high-speed extruder screw. Table 3.6 also shows that the secant 1 % modulus varies from 1492 (Run 5) to 1773 (Run 4) MPa for the minimum and maximum value, respectively.

3.1.9.4 Notched and unnotched impact strength

The Pareto plot in Figure 3.15 illustrates the significance of compatibiliser content on the notched Charpy impact strength of the blends. For the unnotched impact strength; specimens containing 2.4 and 3.8 vol% of PP-g-MAH were not broken at the maximum energy of the test (98 kJm^{-2}). Only the uncompatibilised blend and blend compatibilised with 1 vol% of PP-g-MAH were broken.

It is seen from Table 3.6 that the notched and unnotched impact strength was remarkably improved upon the addition of higher compatibiliser contents. The toughness of the blends was markedly improved, as shown in Table 3.6, upon the addition of compatibiliser. The improvement in notched impact strength of those

containing 3.8 vol% of PP-g-MAH was almost two-fold those of the blend containing 1.0 vol% of PP-g-MAH. Unnotched impact strength was also considerably improved by about 100-200 % with 1.0 vol% compatibiliser in comparison with the uncompatbilised blend. Some of the unnotched specimens tested in this study were not broken under the 4 J hammer application. This might be due to the compatibilising effect of PP-g-MAH that toughens the blends.

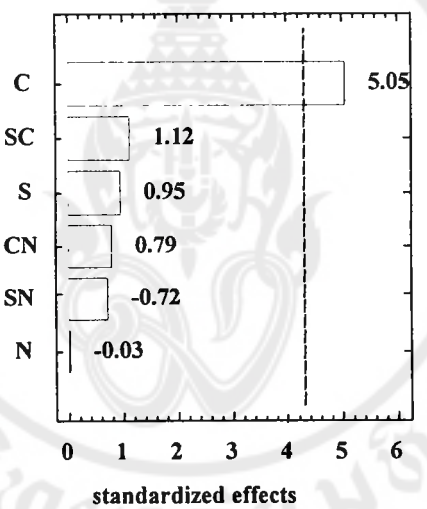

Figure 3.15 The Pareto chart for notched Charpy impact energy

Summary

The effect of independent variables studied in the first part upon the blend's properties could be summarised. Compatibiliser is the key factor that influences the properties of the blends. Extruder screw speed and extruder screw configuration influenced the processing characteristics, namely SME, melt temperature, and die pressure. The amounts of PP-g-MAH of 2.4 and 3.8 vol% were found to combat

coalescence efficiently as evidenced by a 50 % reduction of the dispersed phase diameters from the extruded samples in comparison to the blends prepared with 1.0 vol% compatibiliser. The titration determination suggests the reaction between MAH groups on PP-g-MAH and the amine end groups of PA6 took place. Higher amounts of *in-situ* formed PP-b-PA6 were thought to locate at interphase and stabilise the phase morphology of the blends as described by the insignificant difference between the PP domain diameter measured from the extruded samples and the same sample after injection moulding. The mechanical properties were also improved; i.e., better elongation at break, notched, and unnotched Charpy impact strength were obtained.

3.2 Part II: Non-compatibilised and Compatibilised PP/PA6 blends

The screw configuration type C was used to process the blends throughout the second part. The configuration C was typically designed herein to generate the processing intensity at the level between the configuration type A and B.

3.2.1 Specific mechanical energy (SME)

Specific mechanical energy (SME), given in Table 3.7, during compounding in the second part through twin screw extrusion was computed using equation 2.1. The SME results are based on the average of ten torque readings. Die pressures during extrusion tabulated here are averaged from three readings for each sample. Melt temperature, measured by using a direct contact of thermocouple, is also tabulated.

Given in Figure 3.16, the difference in the amount of PP-g-MAH added during the processing does not greatly influence the SME. This could be evidence that the ranges of PP-g-MAH content added do not greatly affect the viscosity of the blends in the molten state, and thus the SME.

Table 3.7 Compounding data recorded from the preparation of PP/PA6 blends through twin screw extrusion, the codes used here are described in detail in 2.2.2, the bracketed values are SD

Run	SME ($kWhkg^{-1}$)	Die pressure (bar)	Melt temperature (^0C)
$S_{50}C_0$	0.041*(0.001)*	2.0*(0.00)*	226.2
$S_{50}C_1$	0.034*(0.001)*	4.0*(0.00)*	223.6
$S_{50}C_{2.5}$	0.029*(0.001)*	5.0*(0.00)*	233.0
$S_{50}C_4$	0.028*(0.001)*	5.0*(0.00)*	229.1
$S_{100}C_0$	0.043*(0.001)*	4.0*(0.00)*	223.1
$S_{100}C_1$	0.048*(0.002)*	5.0*(0.00)*	235.1
$S_{100}C_{2.5}$	0.053*(0.002)*	6.0*(0.00)*	233.6
$S_{100}C_4$	0.048*(0.002)*	6.0*(0.00)*	238.2
$S_{150}C_0$	0.076*(0.001)*	4.0*(0.00)*	226.1
$S_{150}C_1$	0.068*(0.002)*	6.0*(0.00)*	236.5
$S_{150}C_{2.5}$	0.075*(0.002)*	6.0*(0.00)*	237.7
$S_{150}C_4$	0.082*(0.002)*	6.0*(0.00)*	241.1
$S_{200}C_0$	0.075*(0.002)*	4.0*(0.00)*	233.1
$S_{200}C_1$	0.094*(0.002)*	6.0*(0.00)*	240.1
$S_{200}C_{2.5}$	0.084*(0.002)*	7.0*(0.00)*	237.1
$S_{200}C_4$	0.104*(0.003)*	6.0*(0.00)*	240.6

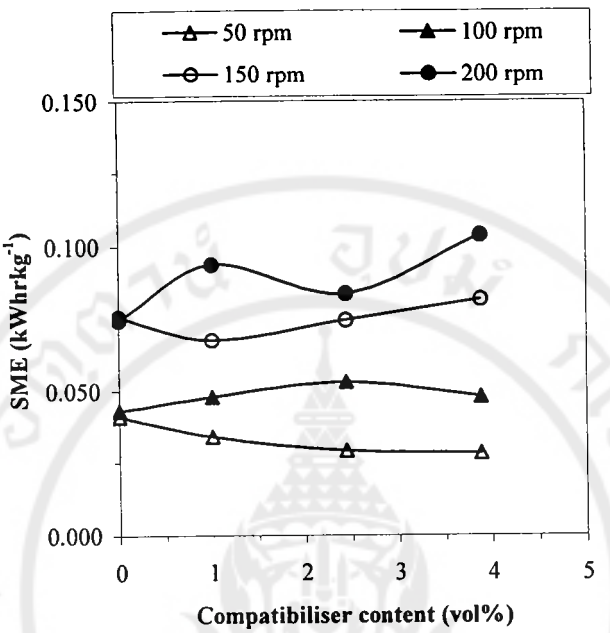

Figure 3.16 The calculated SME of the blends during twin-screw extrusion as a function of compatibiliser content

From Table 3.7, die pressures and melt temperatures are much lower than those recorded in the first part. The lower die pressures were believed to result from the use of a 2 mm diameter die in the first part and the 4 mm diameter die in the second part. While the displayed lower temperatures were thought to stem largely from the lower head pressure.

3.2.2 The determination of the independent variable's influences

Table 3.8 The dependent responses upon the variations of different extruder and injection moulder screw speeds through the *dry test condition*, the bracketed values are SD

Run	N(ext) (rpm)	N(mould) (rpm)	SME ($kWhrkg^{-1}$)	Die pressure (bar)	Yield stress (MPa)	Yield strain (%)	Strain at break (%)	Notched Charpy impact strength (kJ/m^2)
1	50	50	0.057	9	47.79	5.79	43.73	4.77
			(0.002)	*(0.0)*	*(0.41)*	*(0.33)*	*(10.51)*	*(0.45)*
2	200	50	0.146	11	49.58	5.48	58.03	4.95
			(0.005)	*(0.0)*	*(1.21)*	*(0.15)*	*(12 15)*	*(0.56)*
3	50	170	0.059	10	48.06	6.06	47.67	4.76
			(0.002)	*(0.0)*	*(0.31)*	*(0 22)*	*(9.28)*	*(0.42)*
4	200	170	0.146	12	48.40	5.82	54.91	4.64
			(0.003)	*(0.0)*	*(0.58)*	*(0.20)*	*(8.32)*	*(0.28)*
5	125	110	0.111	12	47.78	5.99	46.87	5.24
			(0.002)	*(0.0)*	*(0.28)*	*(0.25)*	*(13.21)*	*(1.30)*
6	125	110	0.074	11	49.31	5.99	41.49	4.92
			(0.002)	*(0.0)*	*(0.47)*	*(0.17)*	*(7.49)*	*(0.54)*
7	125	110	0.105	11	47.36	6.20	63.36	5.18
			(0.004)	*(0.0)*	*(0.24)*	*(0.18)*	*(9.81)*	*(0.03)*
8	125	110	0.089	11	49.11	5.65	57.61	5.30
			(0.002)	*(0.0)*	*(0.63)*	*(0 10)*	*(8.06)*	*(0.62)*
9	125	110	0.103	11	49.02	5.98	63.14	5.36
			(0.003)	*(0.0)*	*(0.65)*	*(0.22)*	*(12.92)*	*(0.53)*
$\bar{X}$ ¥			0.096	11.2	48.52	5.96	54.49	5.20
σ§			0.015	0.45	0.88	0.20	19.88	0.17
%CV£			15.45	3.99	1.82	3.31	18.13	3.27

¥, §, £ mean, standard deviation, coefficient of variation of the centre points; Run 5-9, N(ext) and N(mould) define screw speed of extruder and injection moulder, respectively

Table 3.9 The dependent responses upon the variations of different extruder and injection moulder screw speeds through the *wet test condition*, the bracketed values are SD

Run	N(ext) (rpm)	N(mould) (rpm)	SME ($kWhrkg^{-1}$)	Die pressure (bar)	Yield stress (MPa)	Yield strain (%)	Strain at break (%)	Notched Charpy impact strength (kJ/m^2)
1	50	50	0.057	9	48.53	6.18	60.66	5.84
			(0.002)	*(0.0)*	*(3.69)*	*(0.24)*	*(4.61)*	*(0.32)*
2	200	50	0.146	11	46.13	6.15	57.66	5.88
			(0.005)	*(0.0)*	*(0.79)*	*(0.32)*	*(0.98)*	*(0.23)*
3	50	170	0.059	10	46.18	6.68	57.73	5.51
			(0.002)	*(0.0)*	*(0.41)*	*(0 23)*	*(0.52)*	*(0.25)*
4	200	170	0.146	12	44.61	7.65	55.76	5.67
			(0.003)	*(0.0)*	*(0.33)*	*(0.56)*	*(0.41)*	*(0.20)*
5	125	110	0.111	12	47.61	6.49	59.51	5.70
			(0.002)	*(0.0)*	*(0.38)*	*(0.02)*	*(0.47)*	*(0.46)*
6	125	110	0.074	11	45.60	7.34	57.00	6.13
			(0.002)	*(0.0)*	*(0.54)*	*(0.36)*	*(0.68)*	*(0.47)*
7	125	110	0.105	11	46.92	6.56	58.65	5.91
			(0.004)	*(0.0)*	*(0.51)*	*(0.15)*	*(0.63)*	*(0.46)*
8	125	110	0.089	11	44.63	7.18	55.79	5.40
			(0.002)	*(0.0)*	*(0.54)*	*(0.20)*	*(0.67)*	*(0.30)*
9	125	110	0.103	11	44.35	7.74	55.44	5.89
			(0.003)	*(0.0)*	*(0.37)*	*(0.34)*	*(0.47)*	*(0.59)*
$\bar{X}$ ¥			0.096	11.2	45.83	7.06	57.28	5.81
SD §			0.015	0.45	1.44	0.53	1.77	0.27
%CV£			15.45	3.99	3.13	7.53	3.09	4.71

¥, §, £ mean, standard deviation, coefficient variation of centre points; Run 5-9, N(ext) and N(mould) define screw speed of extruder and injection moulder, respectively

Since the effects of extruder screw speed and injection moulder screw speed may affect the properties of the blends. An experiment was set up whereby a series of PP/PA6 blends was prepared with different extruder and injection moulder screw speeds. The independent variables are extruder screw speed with levels of 50, 125, and 200 rpm and injection moulder screw speed with levels of 50, 110, and 170. The mechanical properties, given in Tables 3.8 and 3.9, are not affected by either of these factors. The extruder screw speed and injection moulder speed do not significantly affect the mechanical properties of the PP/PA6 blends studied. The Pareto chart was employed to determine the influence of those variations of screw speed. However, only the effects of screw speeds on yield stress of the blends are shown.

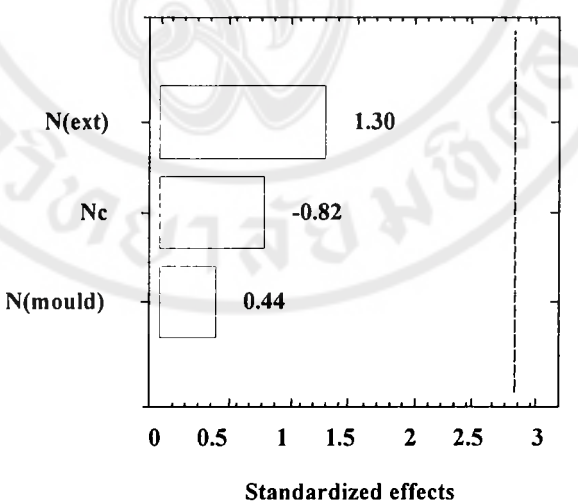

Figure 3.17 Pareto chart of the variations of extruder screw speed, N(ext), injection moulder screw speed, N(mould), and the combination between them, Nc, on tensile stress of the blends (*dry test condition*)

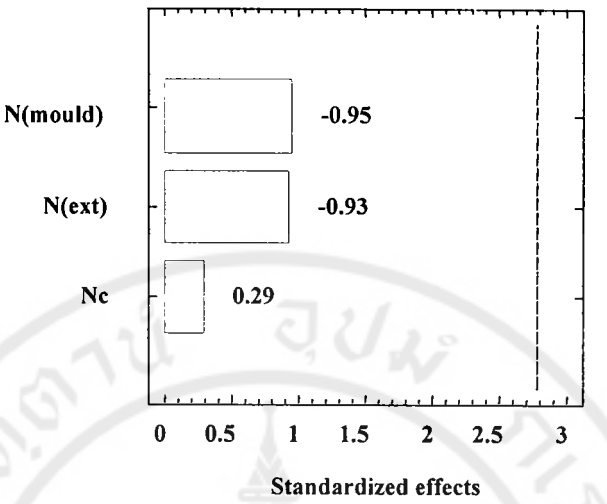

Figure 3.18 Pareto chart of the variations of extruder screw speed, N(ext), injection moulder screw speed, N(mould), and the combination between then, Nc, on tensile stress of the blends (*wet test condition*)

From Figures 3.17 and 3.18, it is found that the variation of extruder screw speed and injection moulder screw speed does not significantly influence the tensile yield stress of the blends. Therefore, tensile properties and impact properties indicated hereafter are only represented for the blend sample prepared with low injection moulder screw speed; i.e., 50 rpm.

3.2.3 Tensile properties of the blends

The tensile data specified in this part are not from section 3.2.2. These data are represented for the blend samples earlier shown in Table 3.6; viz., $S_{50}C_0$ to $S_{200}C_4$.

3.2.3.1 Yield stress for samples moulded with low injection moulder screw speed

The tensile yield stress data are illustrated in Figure 3.19 for four extruder screw speeds and compatibiliser contents. For dry test condition shown in Figure 3.19 (a), incorporation of 1.0 vol% of PP-g-MAH compatibiliser for every extruder screw speed led to a step increase in yield stress in comparison with uncompatibilised blend. Higher compatibiliser contents confer little further change in yield stress, however. Whilst the curves in Figure 3.19 (b) fluctuate, there is a suggestion that the compatibiliser content influences yield stress.

From Figure 3.19 (b), wet test condition, the addition of 2.4 and 3.9 vol% PP-g-MAH led to a great improvement in yield stress at extruder screw speed is seen at extruder screw speed of 100 rpm. Further increasing of extruder screw speed to 150 to 200 rpm caused a little drop in tensile yield stress. This could be summarised from the enclosed data that the 1.0 to 2.4 vol% PP-g-MAH and the extruder screw speed of around 100 to 150 rpm provided the blends with an appreciable tensile yield stress for both test conditions. It is also found that the water absorption of the blends led obviously to a reduction in tensile yield stress.

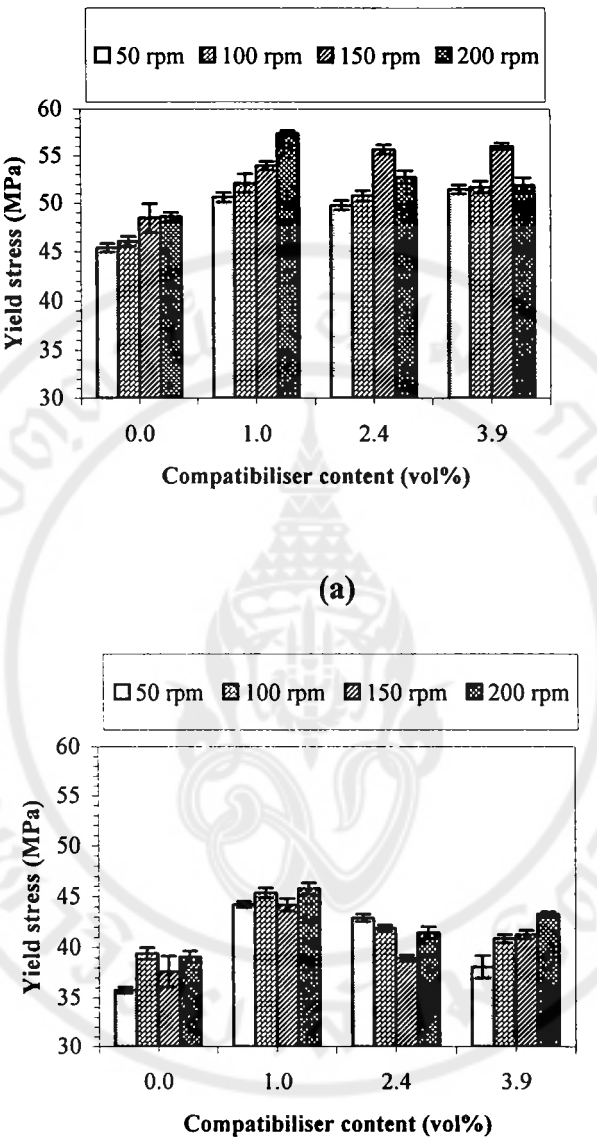

Figure 3.19 Correlations between tensile yield stress of specimens moulded with *low injection moulder screw speed* plotted versus compatibiliser content under **(a)** dry condition and **(b)** wet condition

3.2.3.2 Strain at break for samples prepared with low injection moulder screw speed

Data for strain at break from the tensile tests are shown in Figure 3.20. From Figure 3.20 (a), the dry test condition shows improvements in the ductility of specimens with the addition of compatibiliser in the sequence 0, 1.0, and 2.4 vol% PP-g-MAH compatibiliser. For the highest compatibiliser content; i.e., 3.9 vol%, there is no further increase in ductility. The loss in ductility for the specimens with 3.9 vol% PP-g-MAH is clearly apparent at extruder screw speed of 150 rpm.

The effects of extruder screw speed and compatibiliser content on strain at break of the blends under wet test condition are illustrated in Figure 3.20 (b). The curves for the blends prepared with higher amounts of PP-g-MAH compatibiliser; i.e., 2.4 and 3.9 vol%, are considerably at the same ranges, except for the blend specimens processed with 3.9 vol% PP-g-MAH and the extruder screw speed of 50 rpm which have strain at break around 140%. It is seen that the water absorption is a cause to improve ductility of the blends.

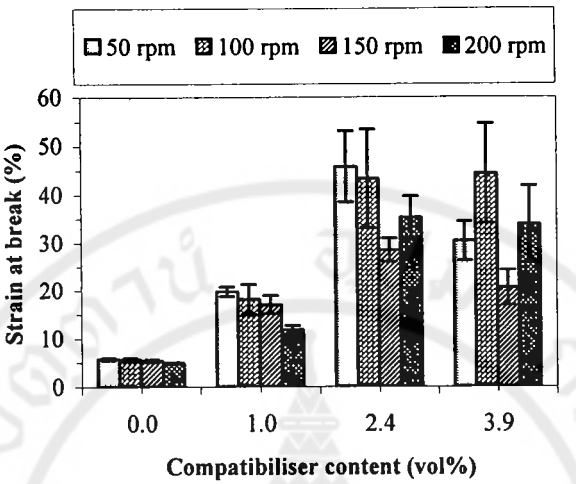

(a)

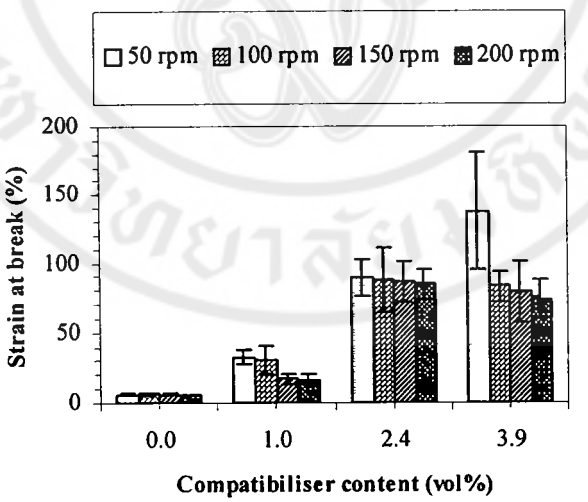

(b)

Figure 3.20 Charts of strain at break of specimens prepared with *low injection moulder screw speed* versus compatibiliser content under **(a)** dry and **(b)** wet condition

3.2.4 Impact properties of the blends

3.2.4.1 Charpy impact strength of notched samples produced using low injection moulder screw speed

Under dry test condition, the impact property data of the blends are shown in Figures 3.21. From the data shown, upon addition of 1.0 vol% PP-g-MAH compatibiliser to the PP/PA6 blend, there is little increase in notched Charpy impact strength, in comparison with the uncompatibilised blend. Upon increasing to 2.4 vol% of PP-g-MAH compatibiliser, notched Charpy impact evidently increases; no further increase is seen at 3.9 vol%.

It is seen that, throughout the range of extruder screw speed but the same amount of PP-g-MAH during the preparation of the PP/PA6 blends, the notched Charpy impact strength changes little. Only the compatibiliser content appreciably affects a change in the notched Charpy impact energy. Greater amounts of PP-g-MAH improved notched Charpy impact strength. For both the blends produced especially with 2.4 and 3.9 vol% of PP-g-MAH cause an increase in notched Charpy impact strength to nearly 6 kJ/m^2. For the wet test condition, the blend specimes were not broken under an application of 0.5 J loading hammer and not included here.

This effect is attributed to PP-b-PA6 formation caused by an anhydride-amine reaction occurring between the two base materials. PP-b-PA6 may act as a compatibiliser to lower interfacial energy, as was inferred previously from the observation that the PP dispersed phase size decreases with addition of PP-g-MAH. In addition, greater amounts of PP-b-PA6 improved notched Charpy impact strength.

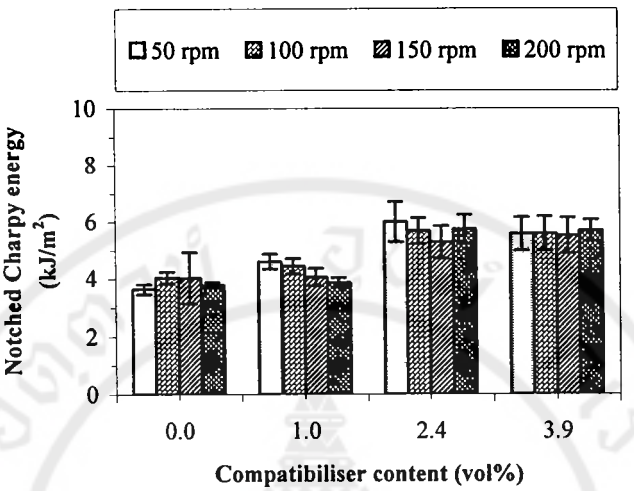

Figure 3.21 Charts show the responses of notched Charpy impact strength of specimens prepared with *low injection moulder screw speed* versus compatibiliser content under dry condition

3.2.4.2 Charpy impact strength of unnotched samples produced using high and low injection moulder screw speed

From Table 3.10, only 1.0 vol% of compatibiliser added to the PP/PA6 blend toughened the specimens more than two-fold, in comparison with the uncompatibilised blend, particularly in specimens processed at the lower extrusion speeds; viz., at 50 and 100 rpm. For higher PP-g-MAH compatibiliser contents, some of the specimens were not broken upon the largest loading available; i.e., of 4 J hammer.

For the specimens produced with 1.0 vol% compatibiliser, impact energy decreases for the highest extruder screw speeds. For the uncompatibilised blends, the

unnotched Charpy impact strength remains unchanged throughout the variation of extruder screw speed; for compatibiliser contents of 2.4 and 3.9 vol%, the specimens were not broken. From a comparison in Table 3.10, it could be concluded that the injection moulding conditions had little effect upon unnotched impact energy.

It is worth emphasising here that although the extruder screw speed and injection moulder speed and injection moulder screw speed do not greatly affect a change in mechanical properties, as evidenced by the Pareto chart. Those screw speeds, however, could be attributed to a change in mixing energy that might lead to a degradation of PP-g-MAH, as evidenced by the TGA traces. Therefore, the poor mechanical properties of the blends might be generated.

Table 3.10 Notched and unnotched Charpy impact strength data of the samples prepared at different injection moulder speeds and extruder screw speeds, the bracketed values represent SD

Sample	Low injection moulder speed		High injection moulder speed	
	Notched Charpy impact strength (kJ/m^2)	Unnotched Charpy impact strength (kJ/m^2)	Notched Charpy impact strength (kJ/m^2)	Unnotched Charpy impact strength (kJ/m^2)
S50C0	3.6*(0.2)*	27.5*(1.6)*	4.4*(0.5)*	27.2*(2.0)*
S50C1	4.6*(0.3)*	102.7*(7.0)*	5.4*(0.3)*	103.0*(5.3)*
S50C2.5	6.0*(0.7)*	N/B	7.0*(0.5)*	N/B
S50C4	5.6*(0.6)*	N/B	7.5*(0.6)*	N/B
S100C0	4.0*(0.2)*	31.1*(1.5)*	5.0*(0.3)*	29.6*(1.3)*
S100C1	4.4*(0.3)*	N/B	5.6*(0.3)*	102.4*(6.8)*
S100C2.5	5.7*(0.5)*	N/B	7.2*(0.7)*	N/B
S100C4	5.6*(0.6)*	N/B	6.7*(0.5)*	N/B
S150C0	4.0*(0.9)*	27.4*(0.7)*	4.6*(0.1)*	27.1*(1.6)*
S150C1	4.1*(0.3)*	87.4*(3.7)*	5.0*(0.2)*	81.7*(7.7)*
S150C2.5	4.1*(0.6)*	N/B	7.0*(0.6)*	N/B
S150C4	5.3*(0.6)*	N/B	6.4*(0.5)*	100.5*(14.7)*
S200C0	3.8*(0.1)*	28.4*(0.8)*	4.5*(0.5)*	28.2 *(1.5)*
S200C1	3.7*(0.2)*	80.4*(5.9)*	4.8*(0.3)*	79.2 *(3.9)*
S200C2.5	5.7*(0.5)*	N/B	7.2*(0.5)*	N/B
S200C4	5.7*(0.4)*	N/B	7.0*(0.7)*	N/B

N/B Samples not broken

3.2.5 Annealing study for the blends prepared with the addition of 2.4 vol% compatibiliser

As specified previously, the blends prepared in this study had dispersed phase morphologies in which PA6 formed the continuous phase while PP phase was dispersed. In order to determine the stability of the phase morphology; selected samples were annealed at 230 °C for 10 minutes under quiescent conditions. Table 3.11 shows the number and volume average disperse phase diameters in the original and annealed specimens.

Table 3.11 The effects of melt-state annealing on the PP dispersed phase particle diameter for the blend samples prepared with 2.4 vol% compatibiliser, the bracketed values show SD

Sample	Average dispersed phase particle diameter (μm)							
	Original specimen				Annealed specimen			
	Low injection moulder screw speed		High injection moulder screw speed		Low injection moulder screw speed		High injection moulder screw speed	
	D_n	D_v	D_n	D_v	D_n	D_v	D_n	D_v
$S_{50}C_{2.5}$	0.44	0.99	0.63	1.21	0.58	1.55	0.50	1.96
	(0.27)	*(0.28)*	*(0.40)*	*(0.54)*	*(0.40)*	*(0.62)*	*(0.49)*	*(0.89)*
$S_{100}C_{2.5}$	0.52	1.00	0.74	1.26	0.86	1.38	0.76	1.46
	(0.30)	*(0.38)*	*(0.36)*	*(0.54)*	*(0.36)*	*(0.62)*	*(0.44)*	*(0.68)*
$S_{150}C_{2.5}$	0.59	1.40	0.45	1.01	0.50	1.49	0.72	1.59
	(0.39)	*(0.57)*	*(0.28)*	*(0.31)*	*(0.43)*	*(0.62)*	*(0.48)*	*(0.85)*
$S_{200}C_{2.5}$	0.42	0.89	0.68	1.61	0.72	2.04	0.80	3.11
	(0.23)	*(0.24)*	*(0.47)*	*(0.77)*	*(0.52)*	*(1.00)*	*(0.76)*	*(2.09)*

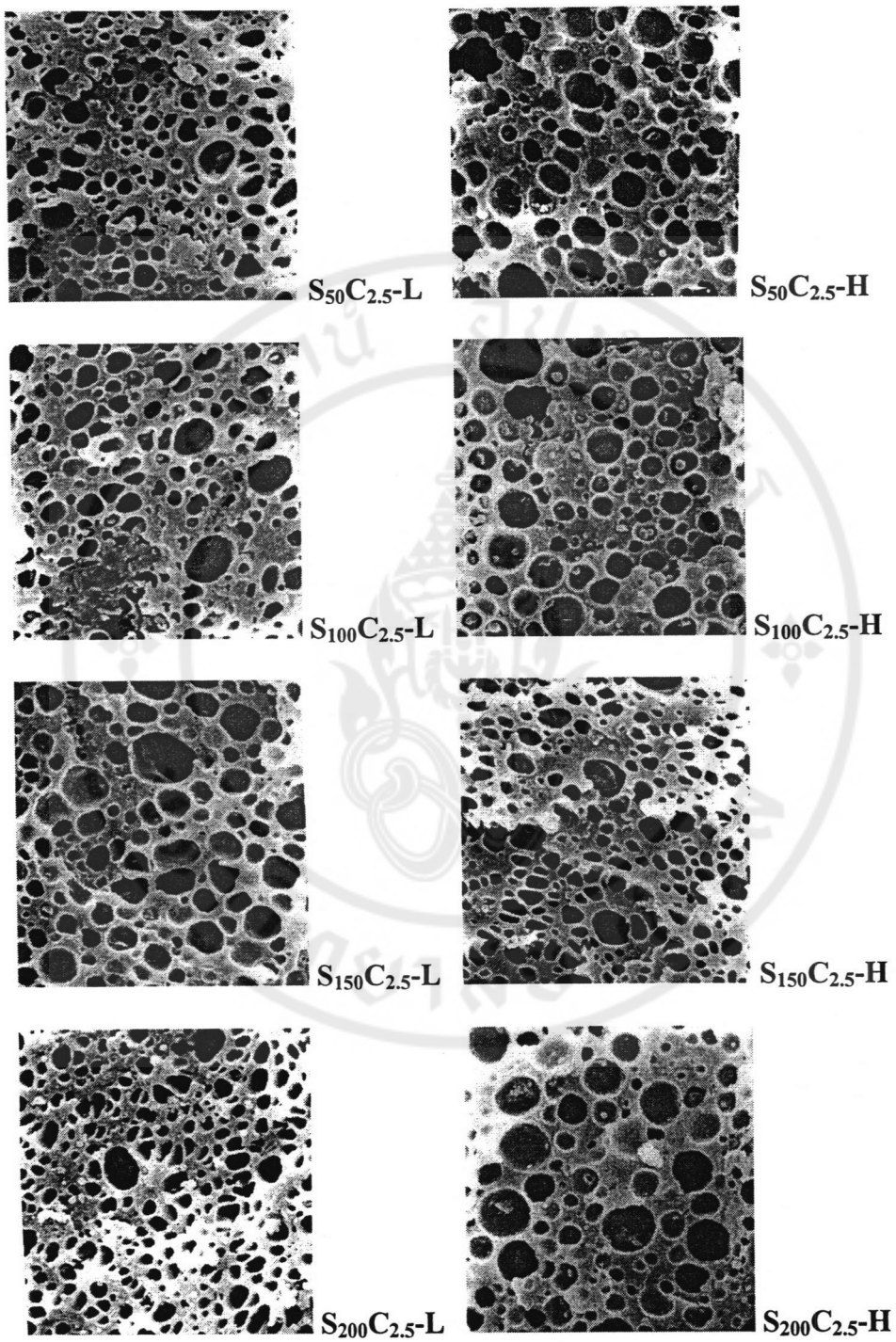

Figure 3.22 The SEM micrographs indicate the effect of injection moulder screw speed upon the PP dispersed particle diameter of PP/PA6 blends

3.2.5.1 Effect of injection moulder screw speed on the PP dispersed phase size

For the original specimen, the dispersed particle diameter changes little with the variation of the injection moulder screw speed as illustrated in Figure 3.22.

3.2.5.2 Effect of annealing on the PP dispersed phase morphology

The tensile bar specimens prepared using low and high injection moulder screw speed were annealed at 230 ^{o}C for 10 minutes under quiescent conditions. It was chosen a period of 10 minutes since it was an approximate residence time for twin-screw extrusion process. The tensile bar specimens produced using high moulder screw speed were also annealed at 230 ^{o}C for 10 minutes. Most annealed blend specimens has dispersed phase morphology with PP dispersed phase size bigger than that of the non-annealed blend specimens. Although the compatibiliser was added to combat coalescence, the increased PP dispersed phase size can be observed, see Table 3.11. For the samples containing 2.4 vol% PP-g-MAH, the dispersed domain dimensions were changed upon a subsequent annealing. However, the change was in the ranges of the domain sizes of not more than 1 μm. This could has proved the compatibilising activity of PP-g-MAH.

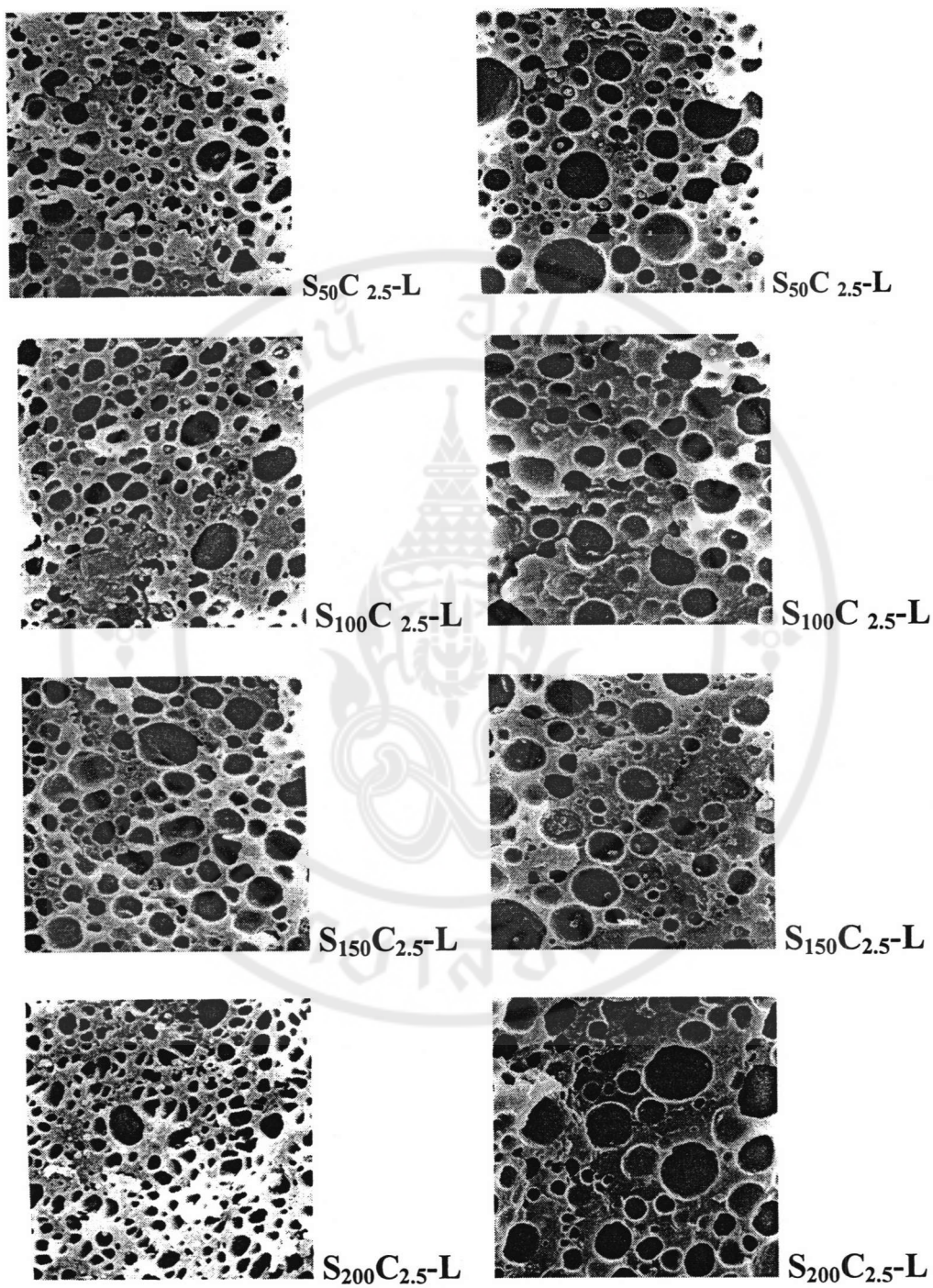

Figure 3.23 The effect of the annealing on the PP dispersed phase size of the tensile bar specimens prepared using *low injection moulder screw speed*

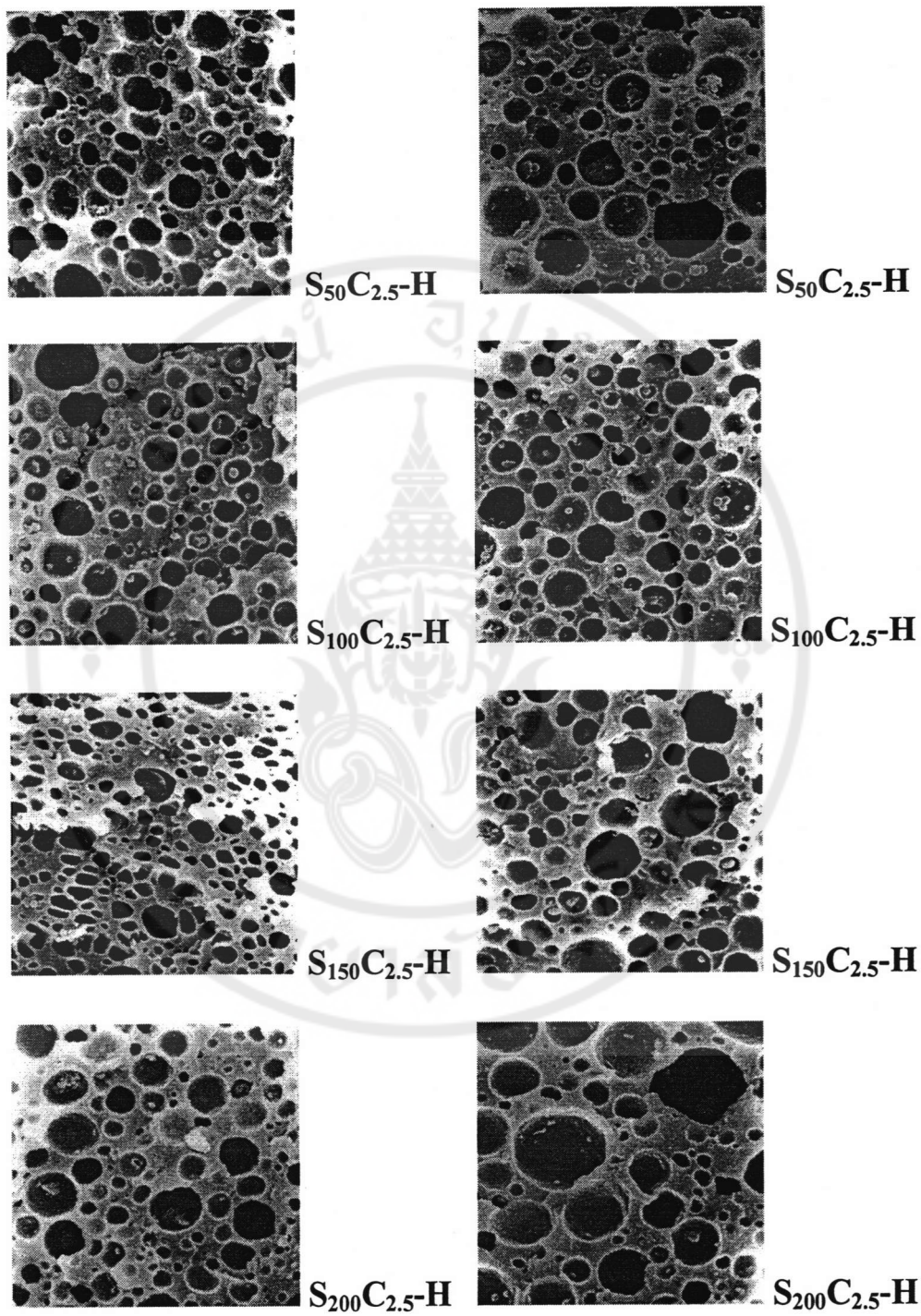

Figure 3.24 The effect of the annealing on the PP dispersed particle size of tensile bar samples prepared with using *high injection moulder screw speed*

CHAPTER IV

CONCLUSIONS

The conclusions, divided into 2 parts, from this work can be drawn as the following:

Part I

1. For compatibiliser contents greater than 2.4 vol% and average compounding stresses greater than 100 MPa the ratio of the specific interfacial area between the PA6 and PP phase reached a constant value of around 90 μm^{-1}. This corresponded to an interfacial thickness of 11 nm. The radius of gyration of the PP block in the *in-situ* formed PP-block-PA6 was estimated to be 12.9 nm, and hence was of comparable size to the interfacial thickness. The mixing was principally controlled by the quantity of *in-situ* formed PP-block-PA6 at the higher mixing stresses. During injection moulding a plasticisation energy of 7.5 MJm^{-3} at a channel shear rate of 52 s^{-1} was used; the nozzle shear rate was around 6,500 s^{-1}. Under these conditions, it was found that the largest domains produced during extrusion underwent the greatest change during injection moudling. For the highest compatibiliser content employed; i.e., 3.8 vol%, at average extrusion stresses greater than

100 MPa, the domain morphology was largely stable under the injection moulding conditions.

2. None of the independent variables have a significant influence on yield stress and yield strain. Increasing amounts of the compatibiliser led to improvement in elongation at break; higher SME led to a decrease. Notched and unnotched Charpy impact strength increased with increasing compatibiliser content. Some of blend samples were not broken under 4 J hammer application; i.e., the largest load available.
3. The number average molecular weight of PA6 quantified through titration was little decreased from 20,400 to 19,000 $gmol^{-1}$ due to the stress during twin-screw extrusion. The amine titration also generated the results of residual unreacted amine end groups left from the reaction with MAH that took place during compounding.
4. The TGA results suggest that significant degradation may take place upon further increasing of temperature. Within the temperature range employed in the current work, all materials, namely PP, PA6, and PP-g-MAH, should have adequate stability.

Part II

1. From annealing experiment, the dispersed phase particle size was very little influenced by a temperature of 230 °C under quiescent conditions. This showed that 2.4 vol% of compatibiliser was sufficient to stabilise the dispersion.

REFERENCES

1. Ajji A, Utracki LA. Compatibilisation of polymer blends. Progress in rubber and plastic technology 1997; 13(3): 153-89.
2. Gleinser W, Braun H, Friedrich C, Cantow HJ. Correlation between rheology and morphology of compatibilised immiscible blends. Polymer 1994; 35 (1): 128-34.
3. Favis BD, Willis JM. Phase size/composition dependence in immiscible blends: Experimental and theoretical considerations. J Polym Sci Part B Polym Phys 1990; 28: 2259-69.
4. Wu S. Formation of dispersed phase in incompatible polymer blends: Interfacial and rheological effects. Polym Eng Sci 1987; 27(5): 335-43.
5. Favis BD, Chalifoux JP. The effect of viscosity ratio on the morphology of polypropylene/polycarbonate blends during processing. Polym Eng Sci 1987; 27(20): 1591-600
6. Thomas S, Groeninckx G. Nylon6/ethylene propylene rubber (EPM) blends: Phase morphology development during processing and comparison with literature data. J Appl Polym Sci 1999; 71: 1405-29.
7. Xiaomin Z, Zhihui Y, Jinhua Y. Binary alloys of Nylon10,10 and ethylene-propylene copolymer: Chemical, morphological, and mechanical anylysis. Polym-Plast Technol Eng 1997; 36(2): 273-83.

8. Tang T, Lei Z, Huang B. Studies on morphology and crystallisation of polypropylene/polyamide-12 blends. Polymer 1996; 37(15): 3219-26.

9. Hermes HE, Higgins JS. Effects of processing conditions and copolymer molecular weight on the mechanical properties and morphology of compatibilised polymer blends. Polym Eng Sci 1998; 38(5): 847-56.

10. Datta S, Lohse DJ. Graft copolymer compatibilisers for blends of isotactic poly propylene and ethene-propene copolymers. 2. Functional polymers approach. Macromolecules 1993; 26: 2064-76.

11. Park DW, Roe RJ. Effect of added block copolymer on the phase-separation kinetics of a polymer blend. 2. Optical microscopic observations. Macromolecules 1991; 24: 5324-29.

12. Majumdar B, Keskkula H, Paul DR. Effect of extruder type on the properties and morphology of reactive blends based on polyamides. J Appl Polym Sci 1994; 54: 339-54.

13. Bouilloux A, Ernst B, Lobbrecht A, Muller R. Rheological and morphological study of the phase inversion in reactive polymer blends. Polymer 1997; 38 (19): 4775-83.

14. Yu ZZ, Lei M, Ou YC, Hu GH. The role of interfacial modifier in toughening of Nylon-6 with a core-shell toughener. J Polym Sci Part B Polym Phys 1999; 37: 2664-72.

15. Favis BD. The effect of processing parameters on the morphology of an immiscible binary blend. J Appl Polym Sci 1990; 39: 285-300.

16. Serpe G, Jarrin J, Dawans F. Morphology-processing relationship in polyethylene-polyamide blends. Polym Eng Sci 1990; 30(9): 553-65.

17. Majumdar B, Paul DR, Oshinski AJ. Evolution of morphology in compatibilised vs uncompatibilised polyamide blends. Polymer 1997; 38(8): 1787-808.

18. Valsamis LN, Canedo EL. Compounding glass-reinforced plastics using novel mixing sections. Plast Eng 1997; April: 37-39.

19. Sundararaj U, Macosko CW. Drop breakup and coalescence in polymer blends: The effects of concentration and compatibilisation. Macromolecules 1995; 28: 2647-57.

20. Roland CM, Boehm GGA. Shear-induced coalescence in two-phase polymeric systems. I. Determination from small-angle neutron scattering measurements. J Polym Sci Polym Phys Edn 1984; 22: 79-93.

21. Francis M, Mirabella JR. Phase separation and the kinetics of phase coarsening in commercial impact polypropylene copolymers. J Polym Sci Part B Polym Phys 1994; 32: 1205-16.

22. Angola JC, Fujita Y, Sakai T, Inoue T. Compatibiliser-aided toughening in polymer blends consisting of brittle polymer particles dispersed in a ductile polymer matrix. J Polym Sci Part B Polym Phys 1988; 26: 807-16.

23. Guégan P, Macosko CW, Ishizone T, Hirao A, Nakahama S. Kinetics of chain coupling at melt interfaces. Macromolecules 1994; 27: 4993-97.

24. Leibler L. Theory of microphase separation in block copolymers. Macromolecules 1980; 13: 1602-17.

25. Odian G. Principles of polymerisation. 3rd ed. John Wiley & Sons, Inc. 1991; 147.

26. de la Cruz MO, Sanchez IC, Theory of microphase separation in graft and star copolymers. Macromolecules 1986; 19: 2501-08.

27. Spontak RJ, Zielinski JM. Dependence of the interphase thickness on chain length in block copolymers: Revisited. Macromolecules 1993; 26: 396-97.

28. Green PF, Russell TP. Segregation of low molecular weight symmetric di-block copolymers at the interface of high molecular weight homopolymers. Macromolecules 1991; 24: 2931-35.

29. Hong KM, Noolandi J. Theory of unsymmetric polymer-polymer interfaces in the presence of solvent. Macromolecules 1980; 13: 964-69.

30. Leibler L. Theory of phase equilibria in mixtures of copolymers and homopolymers. 2. Interfaces near the consolute point. Macromolecules 1982; 15: 1283-90.

31. Park CP.Cingerman GP. Compatibilising PE-PS blends with ethylene-styrene copolymers. Plast Eng 1997; March: 97-99.

32. Fayt R, Jérôme R, Teyssié P. Molecular Design of multicomponent polymer systems. III. Comparative behaviour of pure and tapered block copolymers in emulsification of blends of low-density polyethylene and polystyrene. J Polym Sci Polym Phys Ed 1982; 20: 2209-17.

33. Banaszak M, Whitmore MD. Mean field theory of the phase behaviuor of ternary block copolymer-homopolymer blends. Macromolecules 1992; 25: 249-60.

34. Rigby D, Roe RJ. Small-angle X-ray scattering study of micelle formation in mixtures of butadiene homopolymer and styrene-butadiene block copolymer. 2. Effects of block lengths. Macromolecules 1986; 19: 721-28.

35. Lindsey CR, Paul DR, Barlow JW, Mechanical properties of HDPE-PS-SEBS blends. J Appl Polym Sci 1981; 26: 1-8.

36. Anatasiadis SH, Gancarz I, Koberstein JT. Compatibilising effect of block copolymers added to the polymer/polymer interface. Macromolecules 1989; 22: 1449-53.

37. Favis BD. Phase size/interface relationships in polymer blends: the emulsification curve. Polymer 1994; 35(7): 1552-55.

38. Lee MS, Lodge TP, Macosko CW. Can random copolymers serve as effective polymeric compatibilisers?. J Polym Sci Part B Polym Phys 1997; 35: 2835-42.

39. Cho K, Brown HR, Miller DC. Effect of a block copolymer on the adhesion between incompatible polymers. I. Symmetric tests. J Polym Sci Part B Polym Phys 1990; 28: 1699-718.

40. Russell TP et al. Width of homopolymer interfaces in the presence of symmetric di-block copolymers. Macromolecules 1991; 24: 5721-26.

41. Kressler J et al. Study of polymer-polymer interfaces: A comparison of ellipsometric and TEM data of PMMA/PS and PMMA/SAN systems. Macromolecules 1993; 26: 2090-94.

42. Yukioka S, Inoue T. Ellipsometric analysis of polymer-polymer interface. Polym Comm 1991; 32(1): 17-19.

43. Tanaka H, Hashimoto T. Thermal concentration fluctuations of block polymer/homopolymer mixtures in the disprdered state. 1. Binary mixtures of SI/HS. Macromolecules 1991; 24: 5398-407.

44. Loewenhaupt B, Steurer A, Hellmann GP, Gallot Y. Microphases and macrophases in polymer blends with a di-block copolymer. Macromolecules 1994; 27: 908-16.

45. Taha M, Frerejean V. Morphology development of LDPE-PS blend compatibilisation. J Appl Polym Sci 1996; 61: 969-79.

46. Jin DW, Shon KH, Kim BK, Jeong HM. Compatibility enhancement of ABS/PVC blends. J Appl Polym Sci 1998; 70: 705-9.

47. Siqueira DF, Nunes SP. Morphology of block copolymers in a selective environment. Polymer 1994; 35(3): 490-95.

48. Getlichermann M, David C. Morphology of polyethylene blends: 3. Blend films of polyethylene with styrene-butadiene or styrene-isoprene copolymers obtained by extrusion-blowing. Polymer 1994; 35(12): 2542-48.

49. Srinivasan KR, Gupta AK. Mechanical properties and morphology of PP/SEBS/PC blends. J Appl Polym Sci 1994; 53: 1-17.

50. Chen HL. Miscibility and crystallisation behaviuor of poly(ethylene terephtahlate)/ poly(ether imide) blends. Macromolecules 1995; 28: 2845-51.

51. Bensason S, Nazarenko S, Chum S, Hiltner A, Baer E. Blends of homogeneous ethylene-octene copolymers. Polymer 1997; 38(14): 3513-20.

52. Bensason S et al. Classification of homogeneous ethylene-octene copolymers based on comonomer content. J Polym Sci Part B Polym Phys 1996; 34: 1301-15.

53. Ho RM, Su AC, Wu CH, Chen SI. Functionalisation of polypropylene via melt mixing. Polymer 1993; 34(15): 3264-69.

54. Kelar K, Jurkowski B. Preparation of functionalised low-density polyethylene by reactive extrusion and its blend with polyamide6. Polymer 2000; 41: 1055-62.

55. Yu J, He J, Crystallisation kinetics of maleic anhydride grafted polypropylene ionomers. Polymer 2000; 41: 891-98.

56. Yukioka S, Inoue T. Ellipsometric analysis on the *in-situ* reactive compatibilisation of immiscible polymer blends. Polymer 1994; 35(6): 1182-86.

57. Scott CE, Macosko CW. Model experiments for the interfacial reaction between polymers during reactive polymer blending. J Polym Sci Part B Polym Phys 1994; 32: 205-13.

58. Sundararaj U, Macosko CW, Rolando RJ, Chan HT. Morphology development in polymer blends. Polym Eng Sci 1992; 32(24): 1814-23.

59. Scott CE, Macosko CW. Morphology development during the initial stages of polymer-polymer blending. Polymer 1995; 36(3): 461-70.

60. Scott CE, Macosko CW. Model experiments concerning morphology development during the initial stages of polymer blending. Polym Bull 1991; 26: 341-48.

61. Fellahi S, Favis BD, Fisa B. Morphological stability in injection-moulded high-density polyethylene/polyamide-6 blends. Polymer 1996; 37(13): 2615-26.

62. Lee Y, Char K. Enhancement of interfacial adhesion between amorphous polyamide and polystyrene by *in-situ* copolymer formation at the interface. Macromolecules 1994; 27: 2603-6.

63. McCullagh CM, Blackwell J, Jamieson AM. Transesterification in blends of wholly aromatic thermotropic copolyesters. Macromolecules 1994; 27: 2996-3001.

64. Porter RS et al. Polyester II: A review of phase behaviour in binary blends: Amorphous, Crystalline, Liquid crystalline and on transreaction. Polym Eng Sci 1989; 29(1): 55-61.

65. Yoon H, Feng Y, Qiu Y, Han CC. Structural stabilisation of phase separating PC/polyester blends through interfacial modification by transesterification reaction. J Polym Sci Part B Polym Phys 1994; 32: 1485-92.

66. Golovoy A, Cheung MF, Carduner KR, Rokosz MJ. Control of transesterification in polyester blends. Polym Eng Sci 1989; 29(18): 1226-31.

67. Yanovsky YG. Polymer rheology: Theory and practice. 1st ed. London Chapman & Hall. 1993; 298.

68. Utracki LA, Sammut P. Rheological evaluation of polystyrene/polyethylene blends. Polym Eng Sci 1988; 28(21): 1405-15.

69. Huitric J, Médéric P, Moan M, Jarrin J. Influence of composition and morphology on rheological properties of polyethylene/polyamide blends. Polymer 1998; 39(20): 4849-56.

70. Kim GM, Michler GH, Gahleitner M, Fiebig J. Relationship between morphology and micromechanical toughening mechanisms in modified polypropylenes. J Appl Polym Sci 1996; 60: 1391-403.

71. Duvall J et al. Effect of compatibilisation on the properties of polypropylene/polyamide-6,6 (75/25 wt/wt) blends. J Appl Polym Sci 1994; 52: 195-206.

72. Kudva RA, Keskkuka H. Morphology and mechanical properties of compatibilised nylon6/polyethylene blends. Polymer 1999; 40: 6003-21.

73. Bana-Hani M, Banu D, Campanelli J, Feldman D. Highly filled polyolefin plastomer formulations for possible PVC replacement in flooring. J Appl Polym Sci 1999; 74: 1156-68.

74. Minick K, Moet A, Bear E. Morphology of HDPE/LDPE blends with different thermal histories. Polymer 1995; 36(10): 1923-32.

75. Zhou Z, Lu X, Brown N. The effect of blending high-density and linear low-density polyethylenes on slow crack growth. Polymer 1993; 34(12): 2520-23.

76. González-Montiel A, Keskukula H, Paul DR. Impact-modified nylon6/polypropylene blends: 1. Morphology-property relationships. Polymer 1995; 36(24): 4587-603.

77. González-Montiel A, Keskukula H, Pual DR. Impact-modified nylon6/polypropylene blends: 2.Effect of reactive functionality on morphology and mechanical properties. Polymer 1995; 36(24): 4605-20.

78. González-Montiel A, Keskukula H, Pual DR. Impact-modified nylon6/polypropylene blends: 3. Deformation mechanisms. Polymer 1995; 36(24): 4621-37.

79. Gheluwe PV, Favis BD, Chalifoux JP. Morphological and mechanical properties of extruded polypropylene/nylon-6 blends. J Mat Sci 1998; 23: 3910-20.

80. Dagli SS, Xanthos M, Biesenberger JA. Kinetic studies and process analysis of the reactive compatibilisation of nylon6/polypropylene blends. Polym Eng Sci 1994; 34(23): 1720-30.

81. Li H, Chiba T, Higashida N, Yang Y, Inoue T. Polymer-polymer interface in polypropylene/polyamide blends by reactive processing. Polymer 1997; 38 (15): 3921-25.

82. Xiaomin Z, Zhihui Y, Tainhai N, Jinghua Y. Morphology, mechanical properties and interfacial behaviour of PA10,10/PP/PP-g-GMA ternary blends. Polymer 1997; 38(24): 5905-12.

83. Jannerfeldt G, Boogh L. Månson JAE. Influence of hyperbranched polymers on the interfacial tension of polypropylene/polyamide-6 blends. J Polym Sci Part B Polym Phys 1999; 37: 2069-77.

84. Allen PW. Techniques of polymer characterization. London Butterworths Scientific Publicationtions. 1959, 220-3.

85. Wu S. Phase structure and adhesion in polymer blends: A criterion for rubber toughening. Polymer 1985; 26: 1855-63.

86. Sundararaj U, Macosko CW, Nakayama A, Inoue. Milligrames to kilograms: An evaluation of mixers for reactive polymer blending. Polym Eng Sci 1995; 35 (1): 100-14.

87. Ghiam F, White JL. Phase morphology of injection-molded blends of nylon-6 and polyethylene and comparison with compression molding. Polym Eng Sci 1991; 31(2): 76-83.

88. Venables RA. Course note in: Polymer blends SCCH 665 MSc in Polymer Science. Mahidol University 1997-1998.

89. Kaihirun M. The effect of filler upon the phase morphology and properties of polypropylene/polyamide blends [M.Sc. Thesis in Polymer Science] Bangkok: Faculty of Graduate Studies, Mahidol University, 2000.

90. Aldrich®. Catalog Handbook of Fine Chemicals 1998-1999; 1387.

91. Ballard DGH, Cheshire P, Longman G, Schelten J. Polymer 1978; 19: 379.

92. Bicrerano J. Prediction of polymer properties, Marcel Dekker, New York 1996.

93. Atkins PW. Physical chemistry; 5th ed., 1985.

94. Pionteck J. Proceedings of polymer blends towards 2000, Kasetsart Univ. Bangkok, 18 Aug. 1997; 2.

95. Crawford RJ. Plastics Engineering; 2nd ed., Pergamon Press, Oxford, 1987.

96. Progelhof RC, Throne JL. Polymer Engineering Principles, Hanser Publishers, Munich, 1993.

APPENDICES

APPENDIX A: Thermal properties of polymers

Polymer	Specific heat ($kJkg^{-1}\,^{o}C^{-1}$)	Latent heat of fusion ($kJkg^{-1}$)	Process temp (^{o}C)	Total heat to process ($kJkg^{-1}$)
ABS	1.47	-	225	300
Acetal copol	1.47	163	225	465
PMMA	1.47	-	225	300
Nylon 6,6	1.67	130	280	570
Polycarbonate	1.26	-	300	350
HDPE	2.30	209	240	720
PP	1.93	100	250	550
PS	1.34	-	200	240
uPVC	1.00	-	180	160
Cellulose acetate	1.51	-	195	260
PPO	1.34	-	310	390

BIOGRAPHY

NAME Mr. Adisakdi Chatathanom

DATE OF BIRTH 12 February 1974

PLACE OF BIRTH Surin, Thailand

INSTITUTION ATTENDED Khon Kaen University, 1992-1996:
Bachelor of Science (Chemistry)
Mahidol University, 1997-2000:
Master of Science (Polymer Science)

RESEARCH GRANTS Research Assistant Scholarship
Faculty of Graduate Studies,
Mahidol University; 1998-1999
Teaching assistant Scholarship
Faculty of Science,
Mahidol University; 1997-2000